Cone Beam CT and 3D Imaging

Giacomo Garlaschi

Cone Beam CT and 3D Imaging

Pietro Caruso · Enzo Silvestri
Luca Maria Sconfienza
Editors

Cone Beam CT and 3D Imaging

A Practical Guide

Foreword by Giacomo Garlaschi

Editors
Pietro Caruso
Enzo Silvestri
Radiology Unit
Ospedale Evangelico Internazionale
Genoa
Italy

Luca Maria Sconfienza
Radiology Unit
IRCCS Policlinico San Donato
SciBiS, Università degli Studi di Milano
San Donato Milanese
Milan
Italy

Foreword

Writing the foreword of a book generally represents a moment of joy and satisfaction. These feelings are made even greater as my personal professional consideration and fondness for the Authors of this volume is highly remarkable. In this setting, I like to remember the words of a master of our discipline, Prof. Adelfio Elio Cardinale, who thought that a new book represents "a small lantern that is lit up within the endless roads of science".

The ongoing increase of clinical and physiopathological knowledge, associated to the turbulent improvement of technology, allowed for a greater diffusion of new diagnostic tools, such as the cone-beam computed tomography. This system was able to revolutionize dental and maxillar radiology, both in terms of radiation dose reduction and of dedicated software allowing for multiplanar, three-dimensional reformat.

This textbook is divided into three separate sections in which the principal anatomical, technological, and clinical issues are treated. The chapters are very detailed, also thanks to rich iconography and precise legends. The detailed correlation between clinical and radiological findings makes this book ideal for dentists, radiologists, and radiology technicians. First, dentists may use this book to understand the technical potential of this new system in detail , thus being more confident in interpreting radiological images and reports. Then, radiologists could increase their knowledge of pathological aspects, being able to provide more focused reports, thus also confirming their crucial role of clinical physicians. Finally, technicians could benefit from a detailed description of technical application of these new system, thus improving their professional skills.

In the end, I would like to congratulate and to thank wholeheartedly Drs. Caruso, Silvestri, and Sconfienza who, with their effort, contributed to enforce the prestige of the Radiological School at University of Genova School of Medicine, having been able to conjugate in a single book technology, radiology, and clinical applications.

Prof. Giacomo Garlaschi
Chief, 1st University Department of Radiology
Director, Specialization School in Radiodiagnostics
President, Degree Course in Dentistry
University of Genova School of Medicine

Contents

CBCT Systems and Imaging Technology

Tito Luminati and Eugenio Tagliafico

Radiology is essential in dentistry for determining the presence and extent of disease. It also has a role in treatment planning, monitoring disease progression and in assessing treatment efficacy.

As explained in the following chapters, the jaw comprises two complex bony structures: the mandible and maxilla. Their curved configuration makes radiographic imaging difficult. Furthermore, the superimposition of dense teeth and roots may obscure underlying tissues, and streak artifacts from dental restorations often degrade computed tomography (CT) images.

Recently, dental CT reformatting programs, that use thin transverse images of the jaw to reformat multiple panoramic and cross-sectional views, were developed. Since images are reformatted, streak artifacts that degrade bone visualization at direct coronal CT are projected over the crowns of the teeth, allowing for optimal viewing of bone. As a result, these programs have been successfully used to evaluate implants, cysts, tumors, and surgical procedures. This software created not only a new modality for viewing the jaw but also a new partnership between dentists and radiologists. These programs are useful as they provide accurate information about the height and width of the jaw, as well as information about the location of vital structures, such as the mandibular canal, mental foramen, mandibular foramen, incisive foramen, and maxillary sinuses.

In addition, detailed information about internal anatomy of jaws and the relationship between lesions and the cortical margins and roots of the teeth can be established. Furthermore, streak artifact induced by previous dental restorations

T. Luminati (✉) · E. Tagliafico
Ospedale Evangelico Internazionale—Unit of Radiology,
Corso Solferino 1, Genoa, Italy 16100, Italy
e-mail: tluminati@oeige.org

E. Tagliafico
e-mail: tagliafico.eugenio@oeige.org

can be significantly reduced. These programs are optimally used as an adjunct to, rather than a substitute for, conventional dental radiography.

At any rate, CT administers high amount of ionizing radiations to patients. The advent of cone beam CT (CBCT) represented an enormous advance in dental imaging for low radiation dose it used.

Dental implants are another relevant issue when imaging the teeth. Implants are metallic cylinders that are surgically imbedded into the edentulous jaw to provide attachment for a dental prosthesis. In this way, patients can have artificial teeth that are fixed in the jaw, which provide an attractive alternative to the standard removable dentures.

Dentists and oral surgeons were experiencing difficulty with the use of conventional radiographs to determine whether there was sufficient bone in the jaw to accommodate these implants. They also found it difficult to determine the exact location of the mandibular nerve and other important structures. As a result, dentists soon began to work with their colleagues in radiology, and a dental CT reformatting program was developed to resolve these issues.

Radiographic evaluation is crucial for assessing bony support for endosseous dental implants. Several intraoral and extraoral radiographic methods such as periapical, occlusal, panoramic, and motion tomography are commonly available for evaluation of the implant recipient site, but the information is based on bidimensional geometric projections. Some of the drawbacks of these techniques include superimposition, poor visualization of other anatomic structures, and distortion. There might be discrepancies in measurements compared with those from volumetric methods such as multi-slice computed tomography (MSCT) or CBCT, especially if the area to be evaluated is less than 15 mm thick.

CBCT images are virtually comparable with MSCT images in assessing the enamel, dentin, pulp chamber, lamina dura, periodontal space and spongy bone. With regard to soft tissues, CBCT produces lower-quality images compared with MSCT. It should be noted that MSCT images are more heavily affected by beam-hardening artefacts due to dental-care materials and implants compared with CBCT images.

1.1   Notes on the Use of Ionizing Radiations

X-rays are a type of electromagnetic (EM) radiation. EM radiations also include visible light, radio waves, microwaves, cosmic radiation, and several other varieties of waves (Fig. 1.1). They can be considered as 'packages' of energy, called photons, which have wave properties, most importantly a wavelength and frequency. The importance of this is that small wavelengths mean high energy, deeper penetration though matter and high energy transfer to the matter. When X-rays hit atoms this energy can be transferred, producing ionisation of atoms. All ionising radiations have the capability cause harm to the organs and tissues of the body of exposed persons.
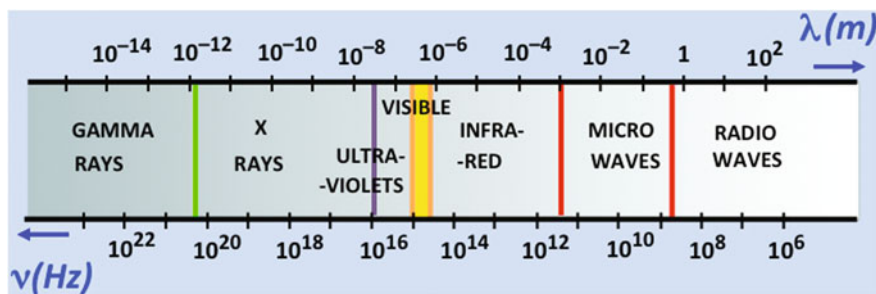
Fig. 1.1 Electromagnetic spectrum

When patients undergo examinations involving the use of X-rays, billions of photons pass through their bodies. These can damage any molecule by ionisation, but damage to the DNA in the chromosomes is of paramount importance. Most DNA damage is repaired immediately, but occasionally a portion of a chromosome may be permanently altered (a mutation). This may lead ultimately to the formation of a tumour. The latent period between exposure to X-rays and the clinical diagnosis of a tumour may be many years.

The effects described above are believed to have no real threshold and they can be considered as casual (i.e., stochastic) effects, in which the magnitude of the risk, though not the severity of the effect, is proportional to the radiation dose. There are other known damaging effects of radiation, such as cataract formation, skin erythema and effects on fertility, which definitely have threshold doses below which they will not occur. These threshold doses vary in size, but all are of a magnitude far greater than those administered in dental imaging. Thus, except in extraordinary circumstances, these deterministic effects are given no further consideration.

The "dose" may be measured for particular tissues or organs (e.g. skin, eye, bone marrow) or for the whole body, while "exposure" usually refers to equipment technical parameters. In this book, however, radiation dose is expressed as the *effective dose*, measured in units of energy absorption per unit mass (joules/kg) called the Sievert (more usually the microSievert, μSv, representing one millionth of a Sievert). Effective dose is calculated for any X-ray technique by measuring the energy absorption in a number of "key" organs/tissues in the body (Fig. 1.2).

All examinations involving the use of ionizing radiations must be justified on an individual basis by demonstrating that the potential benefits to the patient outweigh the potential risks. A detailed record of the justification process must be maintained for each patient. The use of most imaging examinations involving ionizing radiations—and CBCT in particular—should be carefully weighted before being performed. In this setting, routine or screening imaging is unacceptable.

When referring a patient for CBCT examination, the dentist must supply sufficient clinical information (results of a history and clinical examination) to justify the CBCT to be performed.
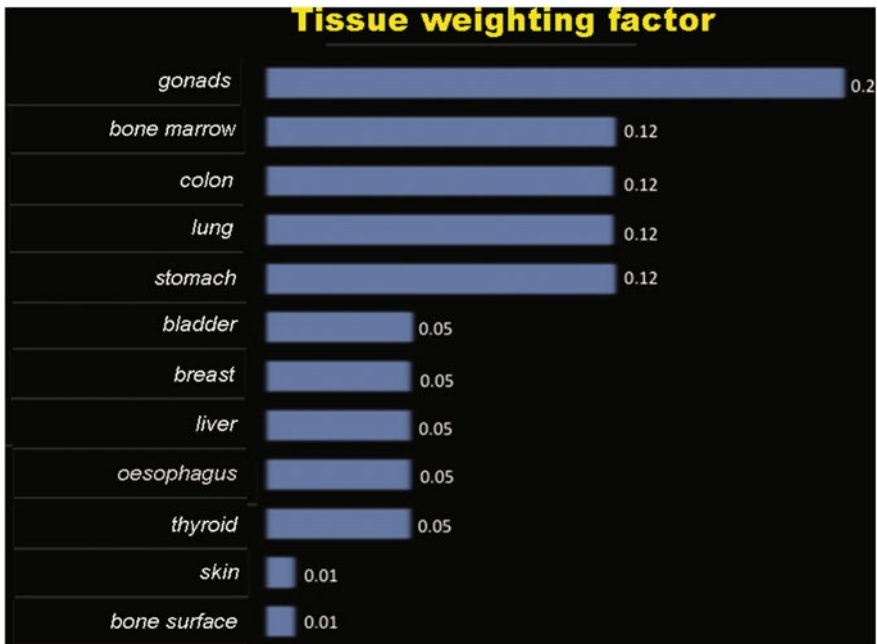
Fig. 1.2 Tissue weighting factor for absorbed energy

CBCT delivered markedly lower doses than did MSCT; compared with OPT, the effective dose was approximately twice as high (0.11 mSv).

The absorbed dose is a physical quantity defined as the amount of energy per unit mass absorbed by a tissue as a result of exposure to radiation; the absorbed dose is measured in gray (symbol Gy) in the International System, where 1 Gy is 1 J of radiation absorbed by 1 kg of mass.

Organ doses were all higher, in fact the salivary glands adsorb a dose ranging from 1.35 to 1.78 mGy; the higher dose delivered by OPT—ranging from 2.01 to 2.57 mGy—is due to the fact that the salivary glands are included in the primary beam (Table 1.1).

Table 1.1 Examination methods and effective doses

Examination	Effective dose (μSv)
Intraoral radiography	<1.5
Panoramic radiograph	2.7–24.3
Cephalometric radiograph	<6
MSCT	280–1410
CBCT	36–846

In summary, the radiation doses (and hence risks) from dental CBCT are generally higher than conventional dental radiography (intraoral and panoramic) but lower than MSCT scans of the dental area.

1.2 CBCT

CBCT is rapidly becoming the standard in 3D dental imaging.

First generation CBCT was first used in 1982 (Mayo Clinic Biodynamics Research Laboratory) to perform angiography. Hence, CBCT system was extended to other medical section, finding its best application in dentistry and maxilla-facial region study.

Although the CBCT principle has been in use for almost 2 decades, only recently—with the development of inexpensive x-ray tubes, high-quality detector systems and powerful personal computers—have affordable systems become commercially available.

CBCT is a compact, faster and safer version of conventional CT. Using a cone-shaped X-ray beam, the size of the scanner, radiation dosage and time needed for scanning are all dramatically reduced.

CBCT scanners are systems that are able to provide 3D reconstructions that are based on the reformat of 2D images. The scan is performed with a single 360° scan in which the x-ray source and a reciprocating area detector synchronously move around the patient's head, which is stabilized by a head holder (Fig. 1.3).

Fig. 1.3 Cone beam CT

At certain degree intervals, single projection images, known as "basis" images, are acquired. These are similar to lateral cephalometric radiographic images, each slightly offset from one another. This series basis projection images is referred to as the projection data.

Dental CBCT units are equipped with digital detectors, which are able to capture x-rays that crossed the patient and to form the image. Spatial and contrast resolution are important aspects of CBCT detectors which influence image quality.

Two types of digital detectors have been used for dental CBCT units. The first type involves conventional image intensifiers (IIs). They consist of an input window, input phosphor, photocathode, vacuum and electron optics, output phosphor and output window. The input phosphor converts the X-rays to optical photons, which then are converted to electrons within the photocathode. The electrons are accelerated and focused by a series of electrodes and then strike the output phosphor which converts the electrons to light photons which are then captured by various imaging devices. Most modern IIs have cesium iodide as the input phosphor because it is a very efficient material in absorbing X-rays. Substantial advantages are low cost, good sensitivity and wide surface; disadvantages are high weight and mass, need of geometric calibration, and the fact that they can be influenced by magnetic field.

The second type, flat panel detectors (FPDs), are composed of an X-ray detection layer and an active matrix array (AMA) of thin film transistors (TFT). The X-ray detector consists of a phosphor layer such as caesium iodide which converts the X-ray photons to light photons. The intensity of the light emitted by the phosphor is a measure of the intensity of the incident X-ray beam. The AMA has a photosensitive element, which produces electrons proportional to the intensity of the incident photons. This electrical charge is stored in the matrix until it is read out and it is converted into digital data sent to the image processor.

FPDs have greater sensitivity to X-rays than IIs and therefore have the potential to reduce patient dose. They have higher spatial and contrast resolution and fewer artefacts than IIs but, in general, IIs are cheaper than FPDs.

The detector is an important element of the imaging chain. In this setting, the optimisation of the detector contributes to dose reduction.

Other relevant parameters for a CBCT are kilovoltage (kV) and milliAmpere per second (mAs), that represent the amount of energy that is provided to the equipment to produce the X-ray beam. Modulating kV and mAs, X-rays with different features can be obtained.

The field of view (FOV) represent the size of the images that can be acquired by a CBCT. FOVs may vary from a few centimetres in height and diameter to a full head reconstruction. Different CBCT systems may be provided with a range of FOV, while a fixed FOV may be provided on others. Of note, the larger the FOV size, the higher the radiation dose administered. However, larger FOVs may allow providing information about surrounding structures, such as the temporomandibular joint (TMJ). This joint is rather a difficult area to investigate radiographically. A number of imaging techniques have been developed over the years; however, there is still no single technique that provides accurate imaging of all the

components of the complex anatomy of the joint. Modern imaging modalities, such as MRI and CT, are now being used more frequently for radiographic examination of the TMJ. MRI is considered as one of the most useful investigations since it provides images of both soft tissue and bony components. However, the contraindications for certain types of patients and a few other disadvantages of MRI, such as long scanning time and restricted availability of the equipment, should be taken into consideration. CBCT provides images of the bony components only. However, in most cases this can be sufficient for the final diagnosis in a number of pathological conditions, like formation of osteophytes, erosion, fractures, ankylosis, developmental abnormalities, as well as the position of the condyle in the fossa in open and closed-mouth conditions.

The rotation of the X-ray tube and the detector around the patient's head produces multiple projection images. The total number of acquired projections depends on the rotation time, frame rate (number of projections acquired per second), and on the completeness of the trajectory arc. A high number of projections is associated with increased radiation dose to the patient, higher spatial resolution and greater contrast resolution. Increasing the number of projections does not influence the linear accuracy of CBCT. Reducing the number of projections, while maintaining a clinically acceptable image quality, results in patient dose reduction through a reduction in exposure (mAs).

Shielding devices could be used to reduce doses to the thyroid gland, as it lies close to the primary beam. Care is needed in patient's positioning so that no repeated exposure is needed.

Motion artifacts can relevantly affect the images and may represent a problem especially in younger patients. Adequate technical parameters may help to reduce these artefacts.

CBCT systems are provided with specific softwares, developed for dental clinicians, that help to enhance the capabilities of these equipments. Multiplanar, three-dimensional, and curvilinear reconstructions can be obtained.

1.3 Others Radiological Techniques

Other imaging modalities are traditionally available to assess dental pathology.

1.3.1 Intraoral Radiography

Intraoral radiography is still the most common radiographic technique used by dentists. Using an x-ray generator and intraoral detector, a projection radiograph is obtained of a small region (1–3 teeth) in the dento-alveolar process.

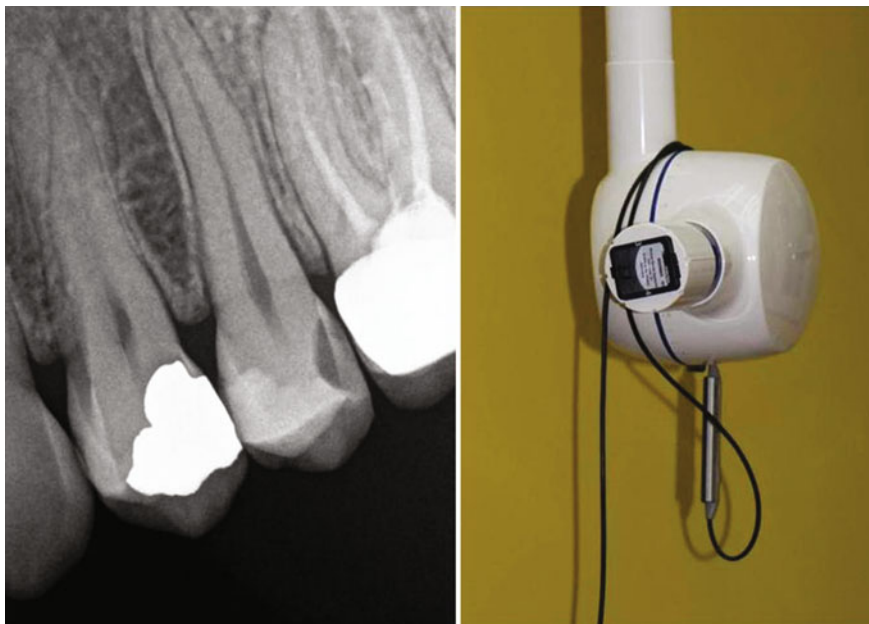Three configurations are usually performed: periapical, bitewing and occlusal radiographs.

Fig. 1.4 Intraoral radiography

Occlusal radiographs are obtained with larger receptors (approximately 7×5 cm), positioned between the occlusal teeth surfaces. X-ray tube positioning is critical for adequate image quality (Fig. 1.4).

Intraoral radiographs provide dentists with information concerning the bony contour around a tooth, internal anatomy and associated pathology, which cannot be derived from the clinical examination alone. The major limitation of intraoral radiography is its two dimensional nature with overlapping anatomical structures.

1.3.2 Extraoral Radiography

Extraoral dental imaging generates diagnostic images of the larger craniofacial complex and can be subdivided into extraoral projection radiography and tomographic imaging.

1.3.3 Orthopantomogram

Orthopantomogram (OPG) or dental panoramic radiography (DPR), also known as a "panorex", is a panoramic scanning X-ray of the upper and lower jaws. It shows a two-dimensional view of a half-circle from ear to ear.

DPR equipment consists of a horizontal rotating arm which holds an X-ray source and a moving film mechanism (carrying a film) arranged at opposed extremities. The patient's skull stands between the X-ray generator and the film. The X-ray source is collimated toward the film, to give a beam shaped as a vertical blade having a width of 4–7 mm on the film after crossing the patient's skull. Also the height of that beam covers the mandibles and the maxilla regions. The arm moves and its movement may be described as a rotation around an instant center which shifts on a dedicated trajectory.

DPR provide a broad overview of the orofacial region including jaws, teeth, sinuses and TMJ (Fig. 1.5).
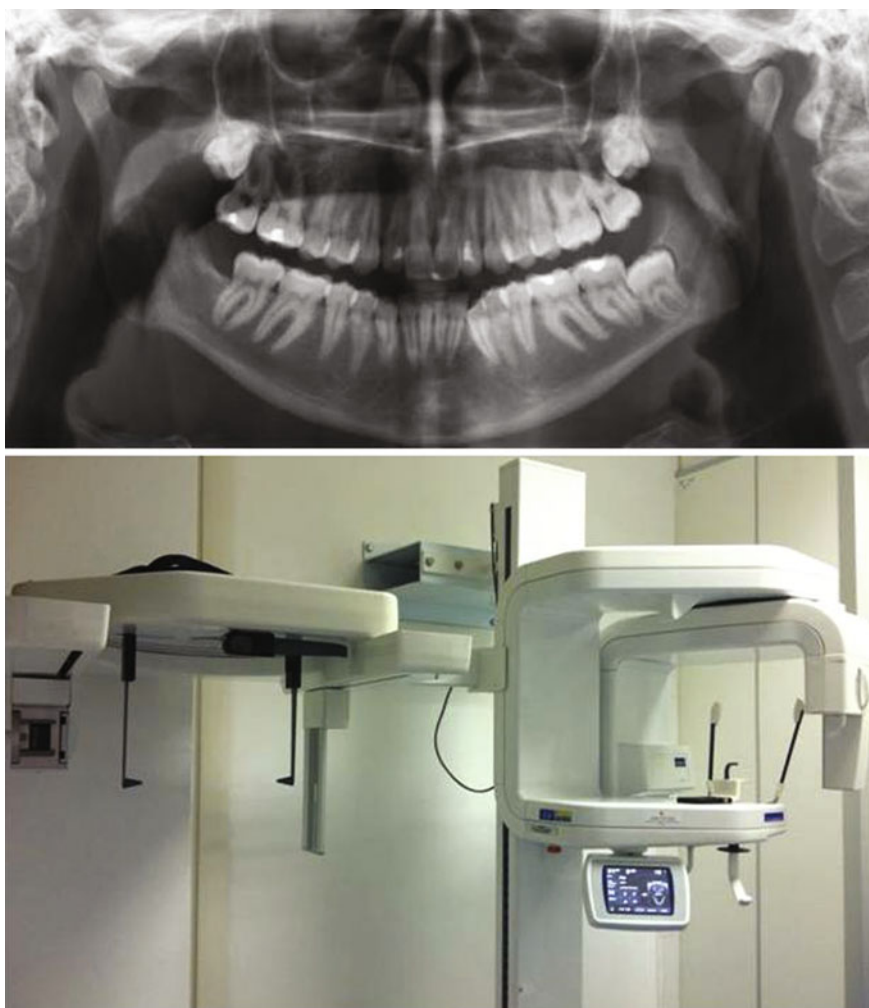
Fig. 1.5 Dental panoramic radiograph

They are especially useful in showing dental development stages or anomalies, or as an initial examination for generalised disease or multiple problems. It can reveal inflammatory or traumatic bony lesions. For heavily mutilated or edentulous patients, DPR is thus the preferred initial examination. Although panoramic screening for occult diseases should be discouraged, dentists must be aware of possible additional findings.

DPR systems are cheaper than systems that are used to obtain 3D imaging and are easily accessible for dentists, but major disadvantages are the presence of magnification and distortion of 3D anatomical structures onto a 2D plane with overlapping of tooth surfaces or other important landmarks.

The thin image layer makes patient positioning a crucial issue to properly visualise both dental arches. Asymmetrical positioning may lead structures to fall out of the image layer and cause asymmetrical distortion. DPR spatial resolution is lower than that of intraoral radiographs, hampering detection of minor or nascent lesions. DPR are thus not recommended for diagnosis of periapical lesions, caries or marginal bone loss without additional intraoral radiographs.

1.3.4 MSCT

CT scanning technology was first introduced in 1972 by G. Hounsfield. CT can be divided into two categories based on acquisition x-ray beam geometry, namely cone beam (see above) and fan beam. In fan-beam scanners, an x-ray source and solid-state detectors are mounted on a rotating gantry. Data are acquired using a narrow fan-shaped x-ray beam transmitted through the patient. Modern MSCT systems use a widened fan-shaped beam and a two-dimensional array detector (Fig. 1.6). Submillimetre imaging (as small as 0.5 mm) can now be accomplished with sub-second rotation times. Nevertheless, even with 64 detector rows, multiple rotations are necessary to image the dento-maxillo-facial complex, leading to an elevate radiation dose to the patient.

The patient is imaged slice-by-slice, usually in the axial plane, and interpretation of the images is achieved by stacking the slices to obtain multiple 2D representations. The linear array of detector elements used in conventional helical fan-beam CT scanners is actually a multi-detector array. This configuration allows multidetector CT scanners for acquiring up to 64 slices simultaneously, considerably reducing the scanning time compared with single-slice systems and allowing for generating 3D images at substantially lower doses of radiation than single detector fan-beam CT arrays. These application in dentistry has been limited because of costs, availability and radiation dose.

Fig. 1.6 Multi-detector tomograph

References

Abrahams JJ (1993) Anatomy of the jaw revisited with a dental CT software program: pictorial essay. AJNR Am J Neuroradiol 14:979–990

Alexiou K, Stamatakis H, Tsiklakis K (2009) Evaluation of the severity of temporomandibular joint osteoarthritic changes related to age using cone beam computed tomography. Dentomaxillofac Radiol 38:141–147

Carrafiello G, Dizonno M, Colli V, Strocchi S, Pozzi Taubert S, Leonardi A, Giorgianni A, Barresi M, Macchi A, Bracchi E, Conte L, Fugazzola C (2010) Comparative study of jaws with multislice computed tomography and cone-beam computed tomography. Radiol Med 115(4):600–611

Carter L, Farman AG, Geist J, Scarfe WC, Angelopoulos C, Nair MK, Hildebolt CF, Tyndall D, Shrout M, American Academy of Oral and Maxillofacial Radiology (2008) American Academy of Oral and Maxillofacial Radiology executive opinion statement on performing and interpreting diagnostic cone beam computed tomography. Oral Surg Oral Med Oral Pathol Oral Radiol Endo 106:561–562

Honda K, Bjørmland T (2006) Image guided puncture technique for the superior temporomandibular joint space: value of cone beam computed tomography (CBCT). Oral Surg Oral Med Oral Pathol Oral Radiol Endo 102:281–286

Horner K, Islam M, Flygare L, Tsiklakis K, Whaites E (2009) Basic principles for use of dental cone beam computed tomography: consensus guidelines of the European Academy of Dental and Maxillofacial Radiology. Dentomaxillofac Radiol 38:187–195

Lam EW, Ruprecht A, Yang J (1995) Comparison of two dimensional orthoradially reformatted computed tomography and panoramic radiography for dental implant treatment planning. J Prosthet Dent 74(1):42–46

Matteson SR, Deahl ST, Alder ME, Nummikoski PV (1996) Advanced imaging methods. Crit Rev Oral Biol Med 7(4):346–395

Meng JH, Zhang WL, Liu DG, Zhao YP, Ma XC (2007) Diagnostic evaluation of the temporomandibular joint osteoarthritis using cone beam computed tomography compared with conventional radiographic technology. Beijing Da Xue Xue Bao 39:26–29

Rothman SLG, Chaftez N, Rhodes ML, Schwartz MS (1988) CT in the preoperative assessment of the mandible and maxilla for endosseous implant surgery. Radiology 168:171–175

Schwarz MS, Rothman SLG, Rhodes ML, Chafetz N (1987a) Computed tomography. I. Preoperative assessment of the mandible for endosseous implant surgery. Int J Oral Maxillofac Implants 2:137–141

Schwarz MS, Rothman SLG, Rhodes ML, Chafetz N (1987b) Computed tomography. II. Preoperative assessment of the maxilla for endosseous implant surgery. Int J Oral Maxillofac Implants 2:143–148

SedentextCT Project (2009) Radiation protection: cone beam CT for dental and maxillofacial radiology. Provisional guidelines. http://www.sedentexct.eu/guidelines. Accessed 14 Oct 2009

Tsiklakis K, Syriopoulos K, Stamatakis HC (2004) Radiographic examination of the temporomandibular joint using cone beam computed tomography. Dentomaxillofac Radiol 33:196–201

Clinical Indications

2

Alice Arcidiacono and Alessandra Schiroli

The field of application of CBCT technology continuously includes new perspectives and clinical indications. Its utility in dental and maxillofacial practice is already widely accepted in different types of pathological conditions which can be systematically summarized as follows:

- *implant dentistry*: it allows for a global evaluation of the available bone volume, predicting possible reasons of failure; likewise it is fundamental in postimplant evaluation.
- *dental anomalies*: it has proven to be unique in planning surgical extraction of impacted, ectopic, or supernumerary teeth, both in adults and in pediatric age.
- *inflammatory* and *degenerative diseases*: it represents an important diagnostic tool for evaluating periodontal and endodontal diseases, providing informations on the associated periapical lesions and the pulpal inflammations. The CBCT images also allow for differentiating between internal and external root resorptions, the visualization of root canals and the detection of root fractures.
- *cysts* and *tumors* (*odontogenic* and *non odontogenic*): CBCT is able to provide essential information about the extent of expansive lesions and the proximity to other noble anatomical structures.

A. Arcidiacono (✉)
Post-Graduate School of Radiodiagnostic, University of Genoa,
L.B Alberti 4, 16100 Genoa, Italy
e-mail: alice.arcidiacono@hotmail.com

A. Schiroli
Private Practitioner, C.so Mentana 3, 16128 Genoa, Italy
e-mail: schiroli.a@libero.it

- ***temporomandibular joint imaging***: it illustrates the morphological changes of the articular space and the bony defects that may affect the condyle and the mandibular fossa.
- ***paranasal sinuses disorders***: the natural contrast of nasal and paranasal cavity, delimited by osseous walls containing air spaces, is useful in diagnosing many diseases which can involve the first tract of the airways, primarily or secondarily (extension of odontogenic pathology).
- ***maxillofacial surgery***: it gives elucidation of congenital and developmental malformations and traumatic injuries of the osteocartilaginous structures of the craniofacial area.

The high-spatial resolution, the possibility to obtain multiplanar images, the clear anatomical representation in three-dimensional reconstructions, the short scanning times, and the low dose supplied to the patient during each exam, have contributed to spread CBCT use in clinical practice (even in pediatrics). This technology has recently been affirmed as a first-level approach in several clinical conditions.

However, CBCT imaging is not always able to replace other imaging modalities and remains complementary in respect to them. This consideration is valid, in particular, in case of characterization of indeterminate lesions (unlike conventional CT, CBCT does not allow a direct measurement of density of the tissues passed by X-rays), or when a detailed study of craniofacial soft tissues is needed (soft tissue tumors, extension of intraosseous tumors into surrounding soft tissues, position of the disc in temporomandibular joint) in which magnetic resonance (MR) is undoubtedly superior.

In this chapter, we discuss the main odontoiatric pathologies in which CBCT is able to express its best potential.

2.1   Implant Dentistry

The CBCT imaging has acquired an increasing role especially in implant dentistry not only because it allows for a better preoperative implant planning, optimizing the surgical phase, but also because it is extremely useful in postoperative evaluation of patients who underwent treatment of dental implant placement.

In preliminary study of patients designated of having traditional or advanced rehabilitation implant procedures, the use of a multiplanar and high-definition imaging is recommended, in particular in implant planning, in which reference values are measured in millimeters or less. Conventional X-rays, panoramic and endoral radiographs are insufficient to satisfy these requirements and the use of CBCT units has become mandatory.

Thanks to the possibility to get multiplanar, high-quality images and three-dimensional reconstructions, CBCT easily allows for acquiring essential information to assess implant feasibility, place and type of implant, and the possible impingement with adjacent anatomical structures, like mandibular nerve and maxillary sinuses.

More precisely, CBCT allows for defining with elevated accuracy the quality (cortical/medullar ratio) and the quantity (height and thickness) of bone available for the implant, providing the essential information of performing or not a pre-implant bony graft.

Coronal and sagittal oblique images of alveolar processes of mandible and maxilla allows for a precise measurement of spatial relationships among alveolar crest, sinus cavity, nasal cavity, mental foramen, and mandibular canal. On the other hand, axial scans are more useful to identify vestibulo-lingual thickness and the residual spaces.

With two quick measurements, also using three-dimensional reconstructions, it is possible to calculate the implant dimensions (height and diameter) and establish its tilting angle.

The identification of morphological variations of mandible and maxilla and maxillary sinus recesses is crucial to realize appropriate surgical guides in order to minimize the risk of damaging vital anatomical structures. The presence of any coexisting pathology constitutes an important additional information for the surgeon and CBCT is able to identify and partially characterize them.

Due to the capability of accurately visualize bony structures, the additional advantage of this technology is the opportunity to evaluate, even thanks to the postprocessing phase, pre-implantological procedures such as maxillary sinus osteointegration and osteodistraction.

As previously mentioned, CBCT has been progressively considered as the standard technology even for bony implant placement evaluation and follow-up. Compared to conventional CT, CBCT administers a significant lower dose to patients considering similar exposure parameters and FOV. This issue is crucial, especially considering the necessity to perform consecutive exams to evaluate interventional outcomes even after months. In addition, CBCT allows for

minimizing the dose by setting a smaller FOV correlating with the region to examine. Furthermore, it results in a low rate of metal artifacts (dental implants), which significantly affect quality of CT images.

For these reasons CBCT can be effectively performed either for short-term evaluations to understand whether the implant is correctly positioned and to rule out possible premature complications or for long-term evaluation to assess the entity of the implant osteointegration process, and therefore the placement success.

Case

- 64-year-old female.
- Clinical notes: affected by hypertension.
- Need to restore chewing function of superior dental arch.
- CBCT required for preoperative dental implant planning and for evaluation of bone vertical dimension.
- Six dental implants placed in the site 1.6, 1.5, 1.4, 2.3, 2.5, 2.6, loaded with porcelain-fused-to-metal bridges.
- Subsequently rejected implant in site of 1.5 (Figs. 2.1, 2.2, 2.3, 2.4, 2.5a–c and 2.6).
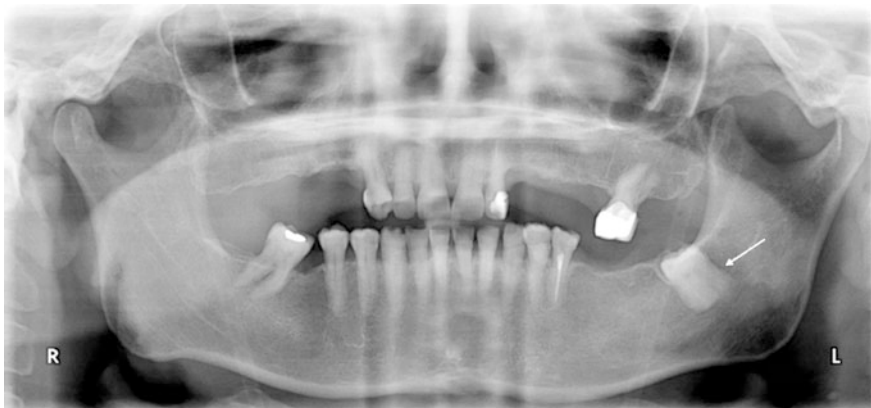
Fig. 2.1 Preoperative orthopantomography: 3.8 is impacted and dysodontiasic (*arrow*); restorative treatment in tooth 4.7, partially edentulous dental arches
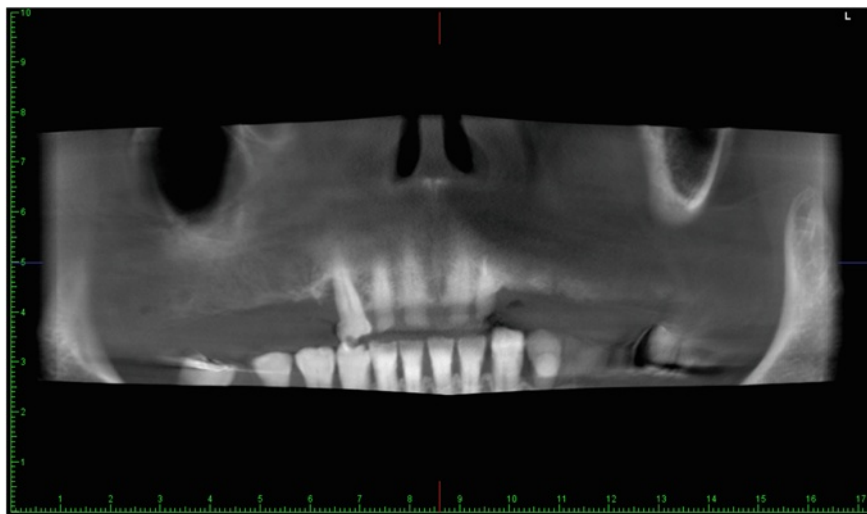
Fig. 2.2 Preoperative panorex CBCT
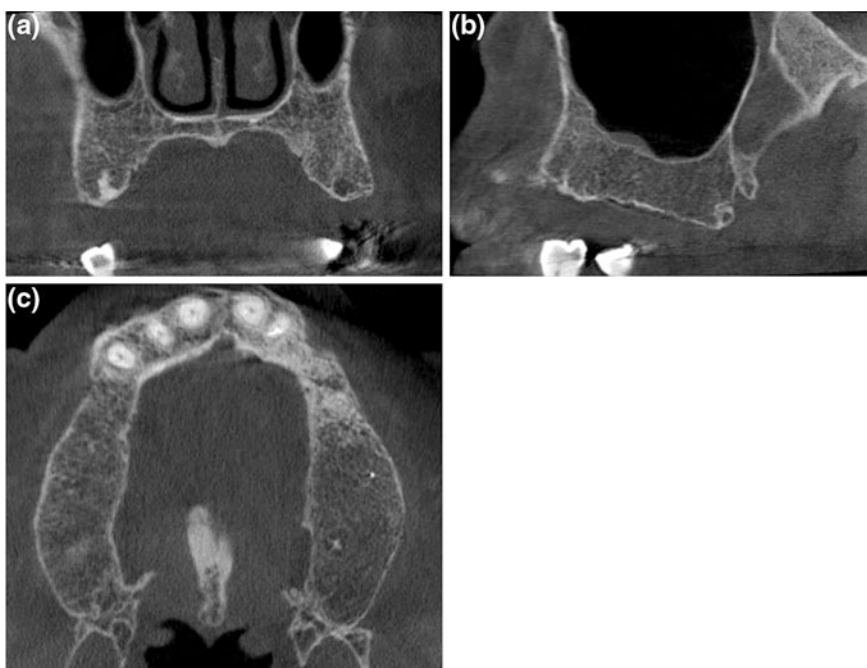
Fig. 2.3 Preoperative CBCT: coronal (**a**), sagittal (**b**) and axial (**c**) scans showing partially edentulous maxilla
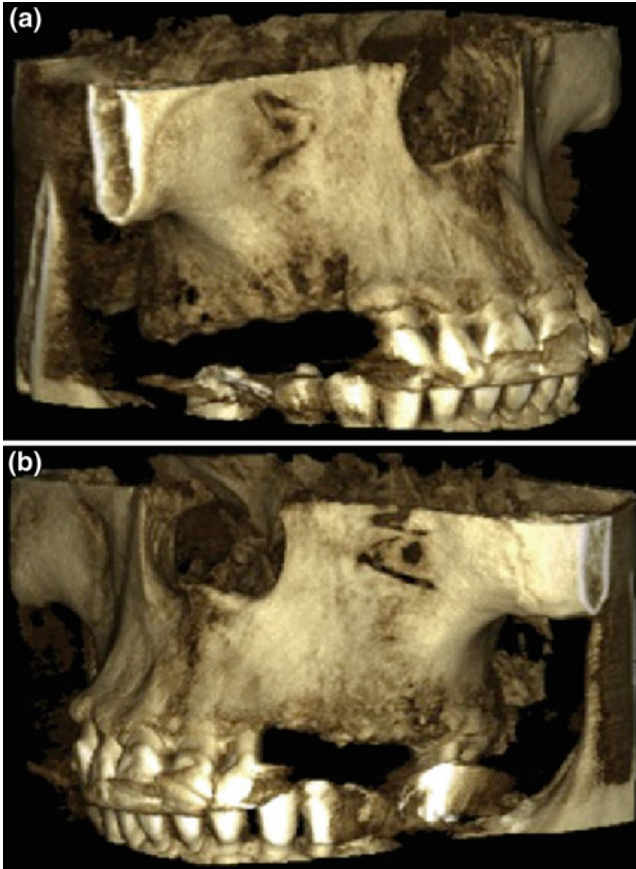
Fig. 2.4 Preoperative CBCT: 3D reconstruction of right (**a**) and left (**b**) edentulous maxillary emiarch

Fig. 2.5 Posttreatment extraoral photographs (**a**, **b**, **c**): frontal and lateral views of *upper* and *lower* arches
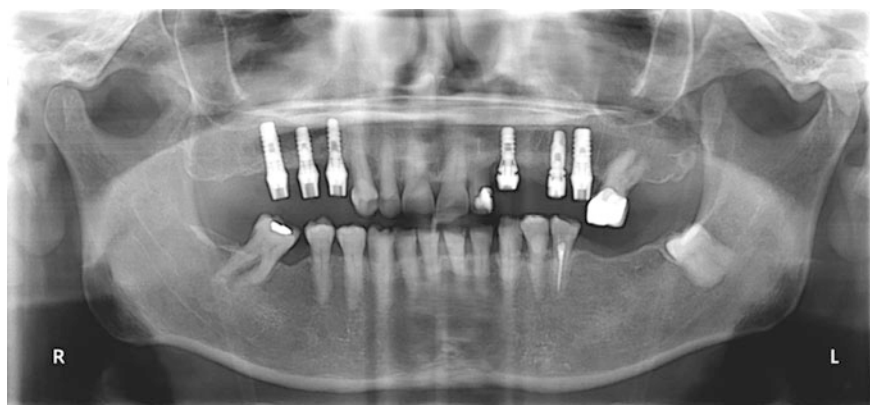
Fig. 2.6 Post-treatment orthopantomography: implant screws are placed correctly in the site of 1.4, 1.5, 1.6, 2.3, 2.5, 2.6

Preoperative CBCT examination with accurate volumetric images allows for a precise evaluation of paranasal sinuses anatomy and an estimation of buccal and palatal bone volume in the surgical interest area.

2.2   Dental Anomalies

Dental anomalies represent a very extensive subject which include *number anomalies* (hyperodontia, hypodontia)*, volume anomalies* (macrodontia, microdontia)*, shape anomalies* (dental fusions, root variations)*, structural anomalies* (hereditary and acquired), and *position anomalies* (dysodontiasis, ectopic and heterotopic teeth).

The most common anomaly is **dysodontiasis** that is eruption difficulty due to the lack of appropriate space within dental arch or the teeth wrong orientation.

Dentoalveolar surgery for impacted teeth is very common in dental clinical practice. The third inferior molars, followed by superior canines, central superior incisors, inferior canines, first and second superior premolars, are the most frequently involved teeth in abnormal eruption. Even deciduous teeth could present with dysodontiasis diseases.

Generally eruption defects cause tooth entrapment in correspondence of the alveolar fossa, sometimes it could determine an ectopic location at the level of the palatine bone, of the chin or of other deeper bony regions. For example, most of the times the third inferior molar (most frequently affected by dysodontiasis) has a mesial orientation, with its crown close to the second molar's roots; less commonly it results impacted onto the mandibular rising branch.

Radiological imaging is very important not only to confirm the presence of impacted teeth but also to evaluate their precise position, their location in respect to the occlusal plane, their orientation (position of the tooth long axis compared with adjacent teeth long axis), and their relationship with surrounding anatomical structures, allowing for an accurate presurgical plane.

Conventional 2D radiographs (periapicals, occlusals, panoramics) can be sufficient to identify an impacted tooth, even if the dentist have to perform several radiographs in order to understand the real tooth location administering a significant radiation dose to the patient. Further, plain films often results globally superficial to determine those elements essential for an appropriate presurgical planning.

CBCT technology is particularly indicated for the diagnosis of impacted teeth because it allows for a better analysis of the dental arches: each tooth does not undergo dimensional and perspective alterations, and superimposition of anatomical structures are eliminated with consequent improved definition of bony landmarks, also minimizing measurement errors. The use of 3D reconstructions also allows for a more comprehensive visual picture for the treating dentist to provide proper vectors of tooth movement.

CBCT not only provides precise information on the impacted tooth location, but also allows for an accurate measurement of the distance from adjacent teeth roots; this information is critical for determining the biomechanics treatment plan needed to bring the impacted tooth into the arch without damaging adjacent teeth.

Location of the mandibular canal, in which omonimous nerve and vessels run, and its close contact to the third molar root structures are risk factors in dento-alveolar surgery. However, the mandibular canal, in some cases, may follow a tortuous path, and may not be reliably interpreted on a 2D image.

Multiplanar views obtained from a CBCT are useful not only in tracking the canal, but also in assessing a bifurcated or trifurcated canal. In addition, knowledge of the location of the canal allows the surgeon for establishing a safer surgical plan without complications, related to the access to the tooth and root elevation.

Ankylosis of impacted teeth is another potential complication in dentoalveolar surgery. Plain films are not reliable in revealing ankylosis of teeth.

In conclusion, compared to panoramic radiography, CBCT images allow for better risk assessment of third molar removal and optimization of the surgical times facilitating postsurgical course.

The use of CBCT imaging by now is essential also in planning surgical extraction of impacted maxillary canines as periapical and panoramic radiographs are often inadequate to locate them and to identify their relationship to the roots of the lateral incisors.

In the end, it is essential to highlight that CBCT offers significant advantages even in pediatrics; the acquisition of a small volume in children is sufficient to enclose the whole dental arches and to perfectly localize impacted teeth with dose saving; above all it is possible to minimize the exposure reducing the field of view and performing an examination on a single tooth or a limited group of teeth of clinical concern.

Case
- 41-year-old female.
- CBCT required for extraction of the mandibular third molars 3.8, 4.8 (Figs. 2.7, 2.8, 2.9, 2.10).

Fig. 2.7 Extraoral photograph: frontal view of upper and lower arches
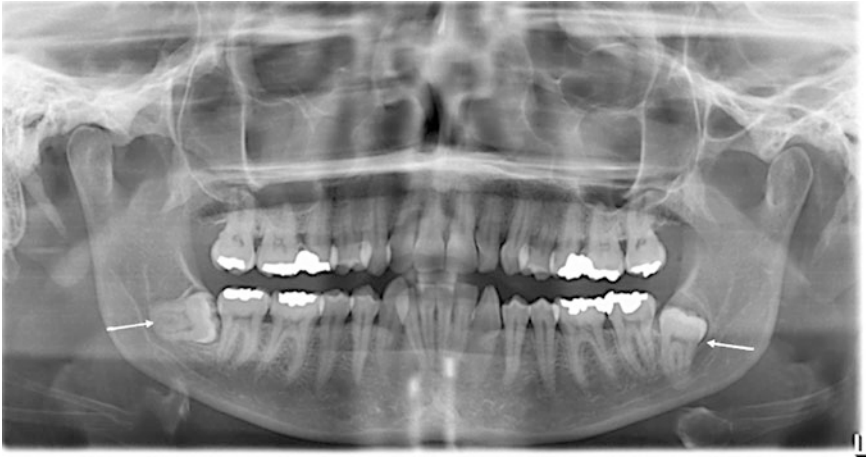
Fig. 2.8 Preoperative orthopantomography: restorations in tooth 1.6, 1.7, 2.6, 2.7, 3.6, 3.7, 4.6, 4.7; mandibular third molars are impacted and dysodontiasic (*arrows*)
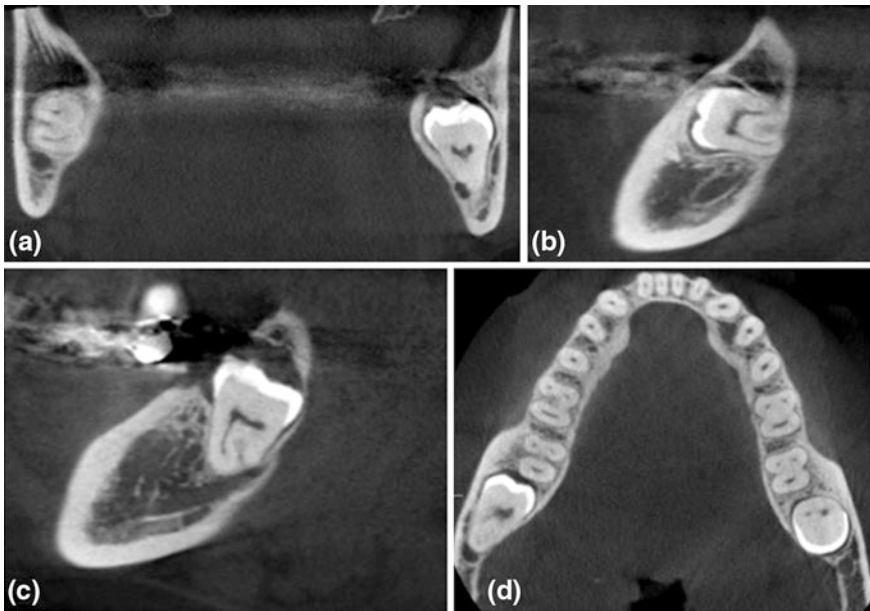
Fig. 2.9 CBCT: coronal (**a**), sagittal (**b**, **c**) and axial (**d**) scans of 3.8, 4.8; mandibular third molars are impacted and dysodontiasic; 4.8 (**b**) moves mesially and is in relation with the superior wall of the mandibular canal; 3.8 (**c**) surrounds the vestibular wall of the mandibular canal that is therefore median-palatal to the root of the tooth
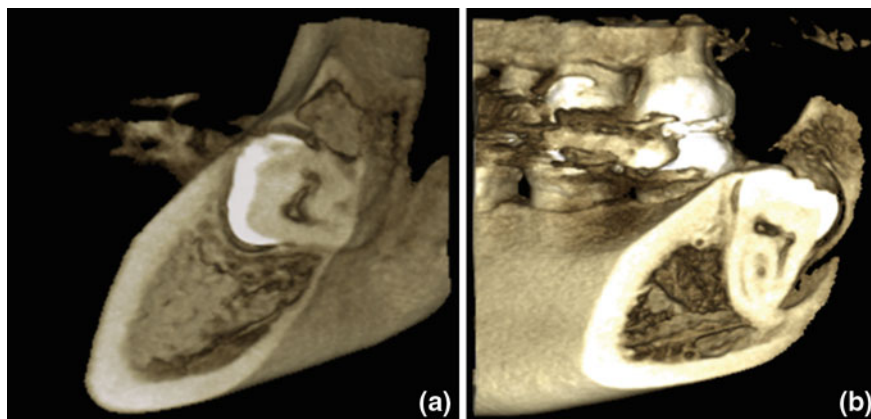
Fig. 2.10 CBCT 3D reconstruction of mandibular *right* (**a**) and *left* (**b**) third molar

2.3 Inflammatory and Degenerative Diseases

Inflammatory and degenerative disorders affecting the dental arches can be distinguished, on the basis of their localization, in *periodontal* (they primarily involve the gums, the alveolar bone, the periodontal ligament and the cementum) and *endodontic pathologies* (that arise from the dental pulp).

Although clinical diagnosis is essential, in **periodontal diseases** (both inflammatories and degeneratives) the radiological examination has a central role in the diagnostic and treatment–outcome evaluation of these patients, being capable of detecting, characterizing, and quantifying contingent defects of the adjacent alveolar bone. This may result in rarefaction (in acute inflammatory and degenerative conditions) or sclerosis phenomena (especially in chronic inflammations) or both aspects.

Panoramic and intraoral radiographs often result inadequate in discriminating fine anatomical details that are necessary for a clear visualization of the small structures surrounding the teeth; they also often underestimate the real extent of bone destruction (early lesions could not generate significant radiopacity changes). Furthermore, some bony defects, located on the vestibular or lingual side of the teeth or covered by superimposed structures, can be difficult to interpret with 2D images.

CBCT system has overcome these limitations. Compared to digital- and film-based conventional radiography, it shows significantly higher accuracy in early detection of periodontal bone disorders, which could lead to better treatment outcomes. Multiplanar views provide detailed information on the periodontal conditions, illustrate the location and extension of the bone destruction, differentiating local from generalized forms, and accurately define the possible involvement of the vestibular or lingual cortical plate.

As for periodontal disease, CBCT technology promises to be superior to 2D imaging for the characterization of **endodontic pathologies**, giving considerable advantages both in diagnostic phase and in posttreatment follow-up.

CBCT imaging achieves a more accurate evaluation of specific morphological features in 3D in comparison to 2D. CBCT provides essential information on:

- *teeth morphology*, including pulp chamber size and degree of calcification;
- *location and number of root canals*: as the success of endodontic treatments depends on the identification of all root canals (so that they can be accessed, cleaned, shaped, and obturated), the use of CBCT systems is certainly recommended. Unlike conventional radiographic techniques, in which the superimposition of anatomic structures hinders the detection of small components, CBCT is able to identify not only each root canal, but also the possible presence of a second mesiobuccal canal in maxillary first molars;
- *characteristics of periapical lesions*: CBCT sensitivity is significantly higher than that of radiographs in detecting periapical osteolytic areas. The high-quality and anatomically detailed CBCT images are unique in the early evaluation of small structural density changes and the differentiation between internal (IRR) and external root resorptions (ERR). Moreover, precisely quantifying IRR and ERR could not be done prior to the introduction of CBCT imaging because of distortion and magnification on 2D radiographs;

- *vertical and horizontal root fractures*: visualizing these fractures with conventional radiographs can be difficult as the beam must be in parallel alignment to the axis of the fracture. The diagnosis of root fractures has found particular application in CBCT imaging, in which these features are well observable;
- *secondary involvement of maxillary sinus*: as the most common inflammatory diseases affecting the paranasal sinus are often of odontogenic origin, identifying the condition of the maxillary sinuses is important. CBCT has a crucial role in providing diagnostic informations on the possible extension of periapical lesions into the maxillary sinuses and in characterizing the associated sinusitic process;
- *complications*: in adverse cases, acute infections can be complicated by periapical abscesses, more frequently located in the posterior side of the mandibular body, rarely in the maxillary bone; the extention of the inflammatory process to the adjacent bone marrow can determine osteomyelitis. On the other hand, chronic infections frequently result in periapical granuloma.

Monitoring the healing of apical lesions and the possible associated complications are important aspects of postoperative assessment in endodontics. Many evidences address the ability of CBCT images for the long-term evaluation of the treatment success.

Case
- 60-year-old female.
- Clinical notes: severe and diffuse periodontal disease; supra and subgingival tartar and plaque, oral hygiene at home has to improve; periodontal pocket depths no greater than 4–5 mm; tooth mobility of second and third degree of upper molars (I e II quadrants).
- CBCT required for preoperative planning of implant placement in edentulous areas in III and IV quadrants and possible extraction of the elements with mobility in I and II quadrants (Figs. 2.11a, b, 2.12, 2.13, 2.14).
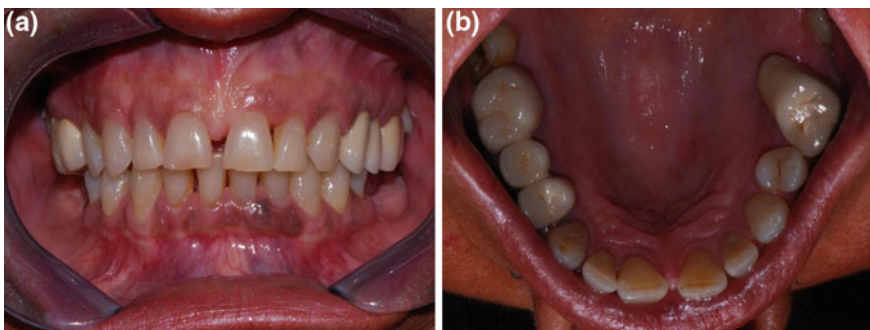
Fig. 2.11 Extraoral and intraoral photographs (**a**, **b**): frontal view of dental arches and occlusal view of upper arch
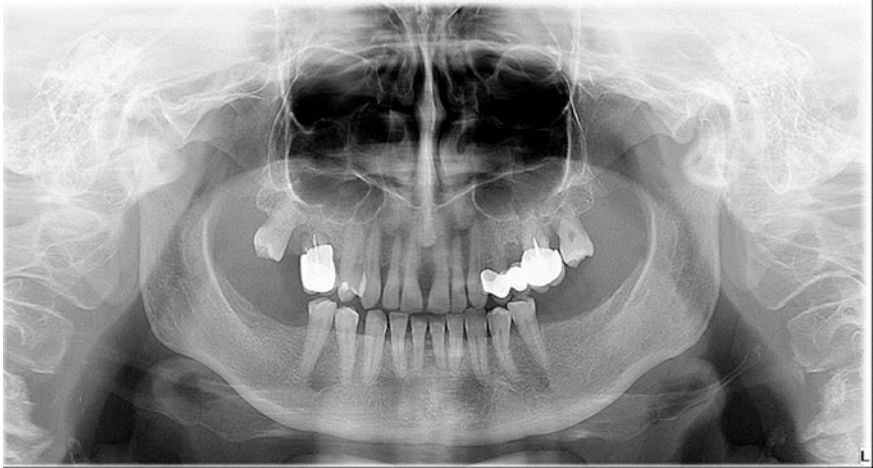
Fig. 2.12 Orthopantomography: radiograph signs of severe periodontitis; restorations in tooth 1.5, 2.4, 2.5, 2.6

Fig. 2.13 Endoral radiography at the level of 2.6: note the periapical bone radiolucency
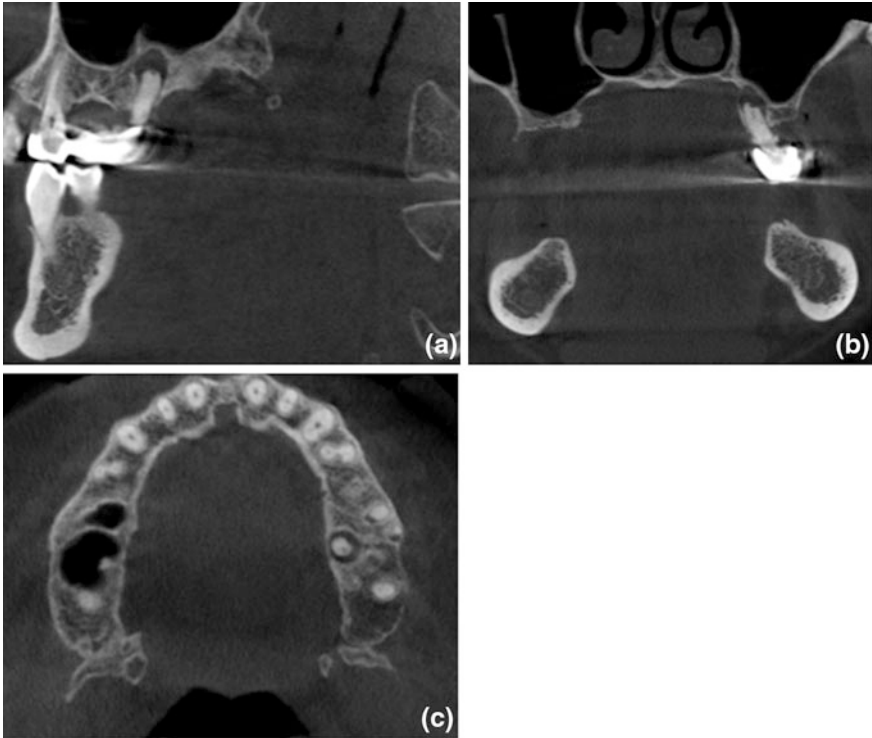
Fig. 2.14 CBCT: coronal (**a**), sagittal (**b**), and axial (**c**) scans showing a radiolucent periradicular area dependent to the element 2.6

Orthopantomography has not clearly showed areas of periradicular periodontitis, suspected in endoral radiograpy. Conversely, CBCT scans provided details in three dimensions for precise location.

2.4   Tumors

The tumor pathology affecting the maxillofacial inferior region includes a wide set of lesions, as reported in the following table (Table 2.1). The aim of this paragraph is to distinguish *benign* from *malignant lesions*, and in each class, *odontogenic* from *non odontogenic tumors*, the firsts originate from odontogenic apparatus, the seconds are of ectodermal and mixed ectodermal-mesodermal origin.

In evaluating **cysts** and **benign tumors**, information achieved by intraoral and panoramic radiographs are extremely limited. Because of their planar view, they only show the two dimensions of a lesion; observation of the third dimension, for example the buccolingual extension of a neoplasia, often requires additional radiographs obtained at 90 degrees from the original view, with an increased radiation exposure not entirely justifiable in respect to the low-quality images. Because of the superimposition of large tissue volumes, extraoral plain film radiographs often cannot provide reliable information on the internal structure of a lesion; furthermore, information on the spatial relationship of the lesion with other anatomical landmarks on such images are limited and often difficult to interpret.

Multiplanar CBCT sections and 3D reconstructions allow for identifying the location, the origin (odontogenic, non odontogenic) of a lesion and to provide precise information of its size, recording all three dimensions. Compared to panoramic radiographs, not reliable for size measurements due to variable magnification errors, CBCT scans are undistorted and without magnification so that measurements, obtained from three different orthogonal planes (axial, coronal, sagittal), and angulations made from them have negligible errors.

The high-spatial resolution-CBCT images can also be used to obtain an adequate evaluation of the bony margins of a lesion (smooth and clear) and its internal architecture, the presence and extent of bone resorption, the sclerosis of neighboring bone, the state of cortical bone (usually not involved), and the proximity to other adjacent anatomical structures for a better surgical planning. CBCT is also helpful in postsurgical follow-up of the margins of lesions that may have a high recurrence rate.

The reported limitations of conventional radiography are also encountered in diagnosing **malignant tumors**, especially in depicting the margins of these lesions that is an essential element for a correct diagnostic and therapeutic overview. Compared to well-defined margins of cysts and benign lesions, the margins of malignant tumors are irregular and ill-defined. For this reason the use of sectional techniques with high-spatial resolution images are highly recommended. Besides the ability to demonstrate the site, the origin, the morphology of the lesion, and the state of the surrounding bone, CBCT images can identify such irregular margins and provide crucial information in the early stages of a malignant lesion.

Since irregular margins are common radiographic features even of other type of disorders, such as chronic osteomyelitis, the examination of the cortical and periosteal bone is necessary for an accurate differential diagnosis.

Table 2.1 Barnes classification, Lyon 2005

BENIGN TUMORS	MALIGNANT TUMORS
Odontogenic epithelium with mature, fibrosus stroma without odontogenicectomesenchyme	*Odontogenic carcinomas*
	Malignant ameloblastoma
Ameloblastoma, solid/multicystic type	Ameloblastic carcinoma
Ameloblastoma, extraosseous/peripheral type	– primary type
Ameloblastoma, desmoplastic type	– secondary type (intraosseus)
Ameloblastoma, unicystic type	– third type (peripheral)
Squamous odontogenic tumor	Intraosseus squamous cell carcinoma
Calcifying epithelial odontogenic tumor	– solid type
Adenomatoid odontogenic tumor	– derived from odontogenic
Keratocystic odontogenic tumor	– derived from odontogenic cysts
Odontogenic epithelium with odontogenic ectomesenchyme with or without hard tissue formation	Clear cell odontogenic carcinoma
	Ghost cell odontogenic carcinoma
Ameloblastic fibroma	*Odontogenic sarcomas*
Ameloblastic fibrodentinoma	Ameloblastic fibrosarcoma
Ameloblastic fibro-odontoma complex/compound type	Ameloblastic fibrodentino- and Odontoma, fibroodonto-sarcoma
Odontoameloblastoma	
Calcifying cystic odontogenic tumor	
Dentinogenic ghost cell tumor	
Mesenchyme and/or odontogenic Ectomesenchyme with or without Odontogenic epithelium	
Odonotgenic fibroma	
Odontogenic mixoma/myxofibroma	
Cementoblastoma	
Bone-related lesions	
Ossifying fibroma	
Fibrosus dysplasia	
Osseous dysplasia	
Simple and aneurysmal bone cysts	

The highly detailed tomographic CB images are able to characterize even a minimal cortical destruction (typical of malignant tumors) and a very thin periosteal reaction (chronic osteomyelitis frequently results in development of a new layer of periosteal bone), differentiating in this way two radiographically similar lesions of different prognosis.

CBCT systems are mostly a tool for diagnosing diseases of the bony structures but they are not helpful to assess soft tissue lesions. Currently, neither multi-detector CT (MDCT) nor CBCT can replace MRI when soft tissue diagnosis is the primary aim. Thus MRI is undoubtedly necessary for an adequate presurgical evaluation of the extentsion of intraosseous tumors into surrounding soft tissues.

However, it is important to highlight that subsequent examinations using CBCT, MDCT, MRI, or nuclear medicine are usually needed for a complete diagnostic work-up of a patient with a malignant lesion.

Case

- 76-year-old female.
- Clinical notes: affected by hypertension, osteoporosis, gallstones and thyroid disease in therapy.
- CBCT required to evaluate the vertical bone thickness in III and IV quadrants, radiopaque lesions in right and left branch of the mandible (Figs. 2.15a, b, 2.16, 2.17, 2.18).
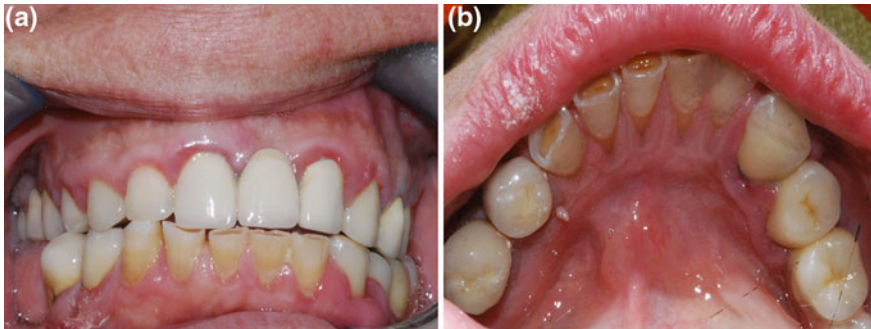
Fig. 2.15 Extraoral and intraoral photographs (**a**, **b**): frontal view of dental arches and occlusal view of lower arch
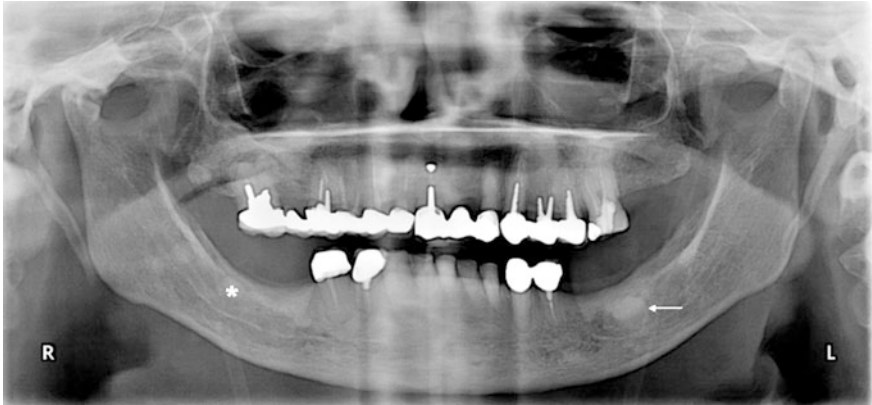
Fig. 2.16 Orthopantomography: sign of endodontic treatment and partially edentulous lower arch. Note the well-defined ovalar radiopaque lesions in the region of *right* (*asterisk*) and *left* (*arrow*) mandibular molars
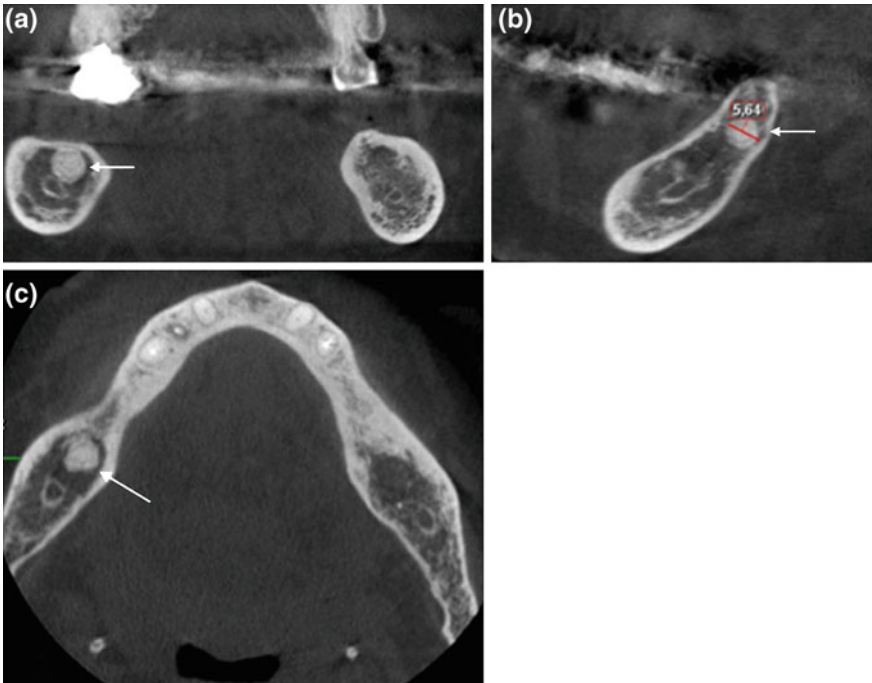
Fig. 2.17 CBCT coronal (**a**), sagittal (**b**), and axial (**c**) scans showing in the region of right mandibular molars an well-defined dishomogeneous hyperdense lesion (*arrows*) with maximum diameter of 5,6 mm without alteration of cortical bone
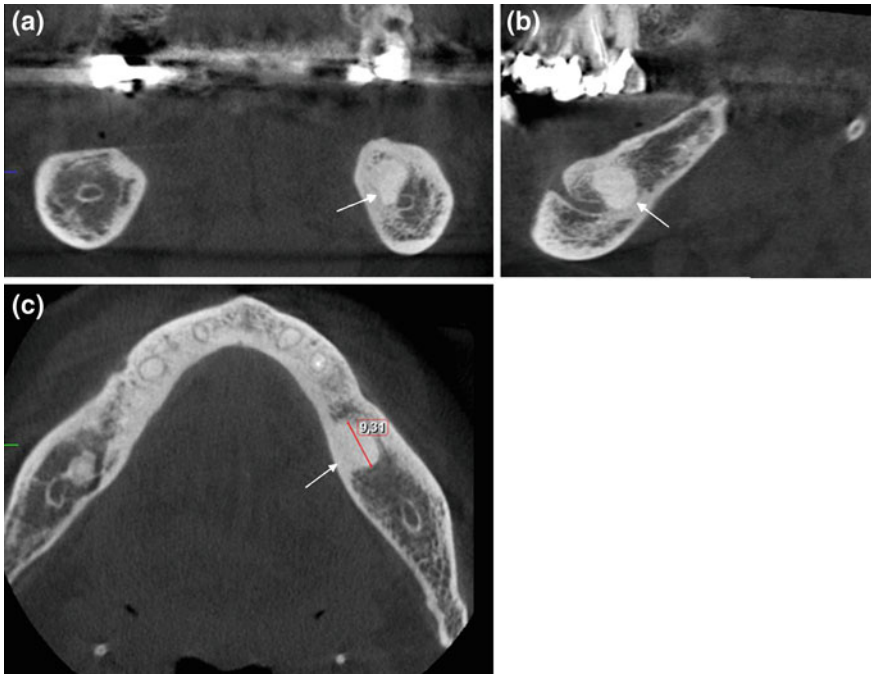
Fig. 2.18 CBCT coronal (**a**), sagittal (**b**) and axial (**c**) scans showing in the region of left mandibular molars an ovalar well-defined lesion (*arrows*) more radiopaque than the precedent one with maximum diameter of 9 mm. Note there are not alteration of cortical bone. The radiological signs directs to a florid cemento-osseous dysplasia

2.5   Temporomandibular Joint Imaging

Thanks to the capability of providing multiplanar views and three-dimensional representations of the maxillofacial skeleton without distortion, the development and commercialization of CBCT technology has seen rapid increase, looking for new emerging clinical indications.

CBCT technique has recently been focused on potential applications for an analytic imaging of temporomandibular joint (TMJ) disorders. Temporomandibular joints can be affected by primitive pathological conditions or can show dysfunctions resulting from odontogenic diseases that modify the chewing process.

Conventional radiographs, performed with opportune lateral-oblique transcranial projection (Schuller projection), and *dedicated digital orthopantomography*, open- and close-mouthed, are still used for joint *motility analysis*, identifying possible abnormalities of condylar movements.

On the other hand, **CBCT systems** have mainly inspired research in TMJ *morphological changes*. High-diagnostic-quality CBCT images provide accurate and detailed information on all pathological processes modifying the structure or the shape of joint surfaces, both on the mandibular and maxillary side. In particular, CBCT is the method of choice in detection of congenital and developmental malformations, traumatic bony injuries, degenerative changes (resorptions, sclerotic reactions, osteophytes), periarticular bony defects associated with arthritis (periarticular erosions, osteolytic focuces, ankylosis), joint remodeling after diskectomy and tumors.

Moreover, the CBCT three-dimensional view facilitate, in a number of clinical situations, the assessment of mechanical impingements and joint space changes (reduction or contact improvement between condyle and mandibular fossa).

CBCT technology is unable to provide images of soft tissues, because, as previously mentioned, is well suited for clearly imaging highly contrasted structures.

Soft tissues are better displayed on MRI which is still superior in illustrating menisci and capsular components: its ability to visualize intra-articular structures (position of the disc and conditions of the joint capsule) and chewing muscles insertions, has contributed to make MRI the gold standard method especially in evaluating phlogistic disorders and condylar in-coordination pathologies.

Case
- 32-year-old female.
- Clinical notes: the patient presents with a restricted mouth opening after a traumatic event (Figs. 2.19, 2.20).
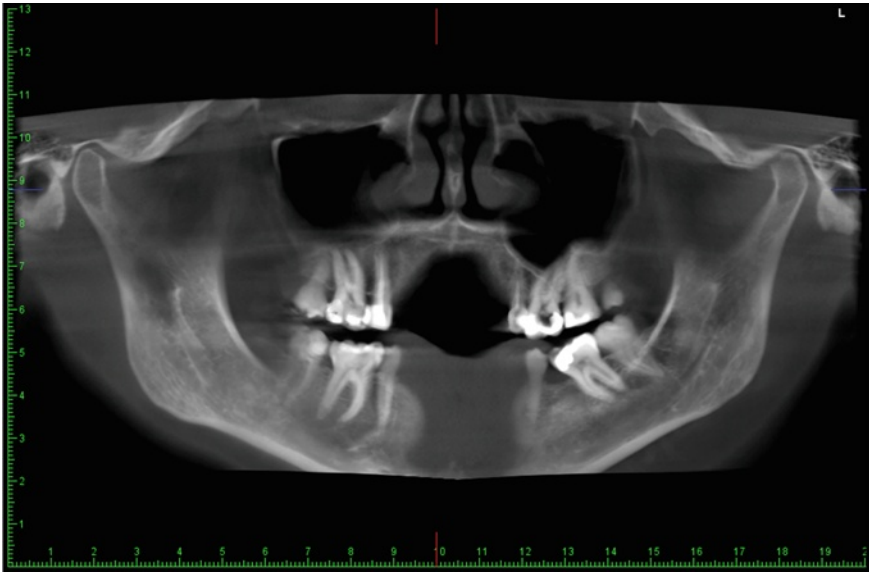
Fig. 2.19 CBCT panorex

Fig. 2.20 CBCT coronal (**a**) e sagittal (**b** and **c**) scans: regular for shape and position the *right* TMJ; the *left* condylar head has an irregularity in antero-superior cortical margin (*arrow*); note the reduction of intra-articular-space. Based on clinical information of restricted mouth opening, is suspected, but not viewable, a displacement of joint disc in this cortical indentation

2.6   Paranasal Sinuses Disorders

The increasing diffusion of CBCT units has continuously intensified the interest in new possible intraoperative and diagnostic applications of this cross-sectional method, beyond the sole examination of the dental arches.

The intrinsic fine anatomical detail of osseous structures, the high isotropic spatial resolution, and the relatively low-dosing requirements of CBCT imaging, when compared with conventional CT, have open the way for new perspectives in its application for paranasal sinuses disorders.

Therefore, in particular maxillary sinuses analysis acquire considerable importance for orthodontists, not only in implantology (it is fundamental to identify if an implant is displaced into the sinus), but also because odontogenic diseases can extent to contiguous sinus cavities, simulating a primitive affection of them, and, on the contrary, sinus cavity pathologies can involve dental elements, simulating odontogenic pathologies.

An accurate analytic study of nasal and paranasal sinuses, using CBCT technology, allows for narrowing all the potential diseases affecting this region of the maxillofacial skeleton.

Undoubtedly, the most common pathological condition that can be encountered in this area is **sinusitis**, most commonly chronic rather than acute (chronicization process is frequent because of secretions stasis due to ostuim obstruction). CBCT is able to identify and localize entity and extension of mucoperiosteal thickening typical of inflammatory changes, calcified materials that often accumulate in fungal sinusitis (this materials can be easily differentiated from the fluid component of the phlogosis), and, at the same time, sclerosis reactions or osteolysis focuses.

CBCT evaluation of the ostiomeatal complex anatomy is certainly an essential element in characterizing inflammatory phatologies escpecially for an adequate treatment planning: particulary coronal scans allow for visualizing possible ostium blockages that may orient in favor of a surgical treatment (functional endoscopic sinus surgery), instead of medical therapy. Moreover, recent studies suggested that CBCT may be suited for specific imaging tasks in the context of intraoperative and perioperative bony structural evaluations; this translates into refinement of surgical strategy, with the additional possibility to exactly guide stent placement, and better visualization of possible residual bony partitions.

Providing a global view of nasal and paranasal cavities, CBCT technique is also indicated to identify possible conditions predisposing ostium blockage, such as nasal septum deviation and concha bullosa (pneumatized cavity within the middle turbinate), and also the presence of other pathological conditions related to the inflammation such as turbinate hypertrophia, mucous retention cysts, mucoceles, antral and sinonasal polyposis.

Tumors are less frequent than inflammatory conditions; CBCT imaging represents an accurate and reliable tool in diagnosing, treatment planning, and also treatment-outcomes assessing of this type of affection. The ability of this sectional

method in visualizing and localizing a neoplastic lesion, characterizing its margins, and relathionship with neighboring anatomical structures has already been widely demonstrated.

It is important to point out that MDCT with contrast medium and MRI result superior to CBCT systems for an accurate definition of the nature of a neoplastic lesion and for a precise extension balance.

Finally, CBCT images can be also used in identifying, qualitative (asymmetries) and quantitative (hypoplasia, aplasia, hyperplasia) **sinus malformations** and in pre and post-surgical evaluation of **traumatic lesions**.

Case
- 31-year-old female.
- Clinical information: breathing difficulty, hyposmia, occasional rhinorrhea, and pressure-like pain in sub-orbital and zygomatic areas (Fig. 2.21).
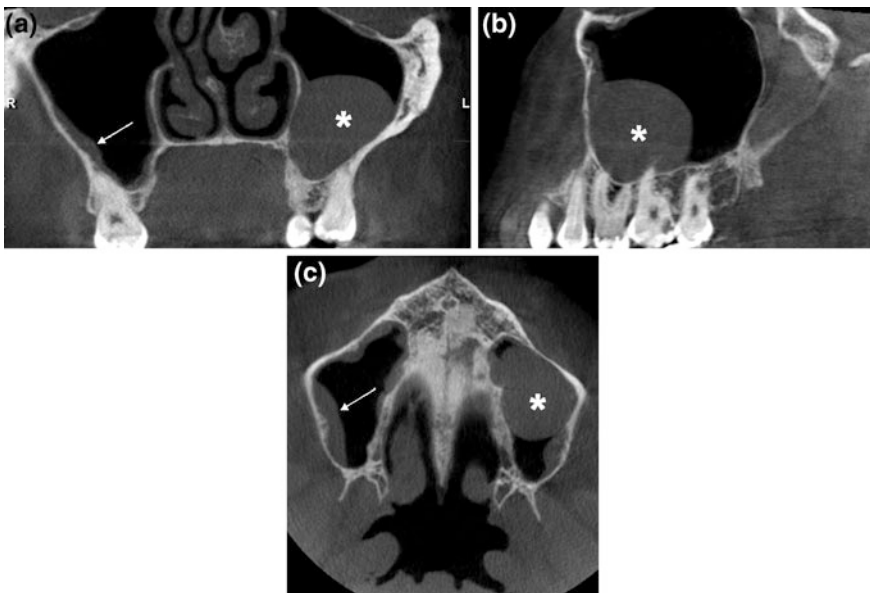
Fig. 2.21 CBCT coronal (**a**), sagittal (**b**) and axial (**c**) scans of maxillar sinuses: mucosal thickening on the *left* sinus floor that appears like an antral mucosal pseudocysts, also called mucoceles (*asterisk*); mucosal thickening on the *right* side (*arrow*)

Further Readings

Ahmad M, Jenny J, Downie M (2012) Application of cone beam computed tomography in oral and maxillofacial surgery. Aust Dent J 57(1 Suppl):82–94

Tyndall DA, Rathore S (2008) Cone-beam CT diagnostic applications: caries, periodontal bone assessment and endodontic applications. Dent Clin N Am 52:825–841

Miracle AC, Mukherji SK (2009) Conebeam CT of the head and neck, part 2: clinical applications. AJNR Am J Neuroradiol 30:1285–1292

Nervina JM (2012) Cone beam computed tomography use in orthodontics. Aust Dent J 57(1 Suppl):95–102

Scarfe WC, Levin MD, David G, Farman Allan G (2009) Use of cone beam computed tomography in endodontics. Int J Dent 2009:634567

The American Dental Association Council on Scientific Affairs (2012) The use of cone-beam computed tomography in dentistry: an advisory statement from the American dental association council on scientific affairs. JADA 143(8):899–902

Scarfe WC, Farman AG, Sukovic P (2006) Clinical applications of cone-beam computed tomography in dental practice. J Can Dent Assoc 72(1):75–80

Basic CBCT Anatomy

3

Angelo Corazza and Luca Maria Sconfienza

3.1 The Skull: Overview

The skull is a bony complex that can be subdivided into two main regions: the neurocranium and the splanchnocranium (Fig. 3.1).

The cranium encloses the brain and could be subdivided into an inferior part—called base—and a superior part—called vault or calvarium. Cranial bones (Fig. 3.2) are occipital, frontal, parietal, temporal, ethmoid, and sphenoid bones. The last two bones also contribute to the constitution of the *splanchnocranium*, together with the maxilla, zygomatic, lacrimal, nasal, palatine bones, inferior nasal conchae, vomer, and mandible. Those structures are connected together by means of immovable joints to compose the cranium; the only exception is represented by the mandible, which bilaterally is connected with temporal bones through a diarthrosis. Some bones of the skull form or contain into their structure air-filled cavities called nasal cavities and paranasal sinuses. In this chapter, anatomical structures that can be of interest in odontostomatologic field will be discussed. A systematic description of cranial and facial bones is beyond the scopes of the present text.

A. Corazza (✉)
Post-Graduate School of Radiodiagnostic, University of Genoa, L.B Alberti 4,
16100, Genoa, Italy
e-mail: angelcoraz@libero.it

L. M. Sconfienza
IRCCS Policlinico San Donato—SciBiS, Università degli Studi di Milano, Piazza Malan 2,
San Donato Milanese 20097, Italy
e-mail: io@lucasconfienza.it

Fig. 3.1 The skull: cranial and facial divisions
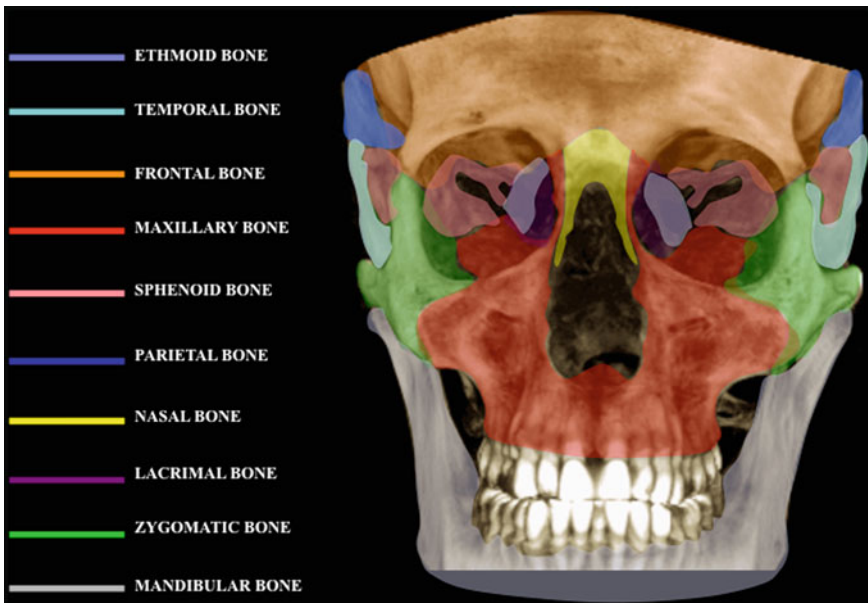
Fig. 3.2 Skull: anterior view

3.2   The Skull Base: Exocranial Aspect

The external aspect of cranial base could be described and distincted into three regions: anterior or facial region, middle or jugular region, and posterior or occipital region. From anterior to posterior, the intermaxillary suture, the ethmoidal perpendicular plate, and the sphenoidal body's external surface can be seen on the midline. From medial to lateral, cribriform plates, ethmoidal cells, and orbital fossae can be seen. Posteriorly, the body of the sphenoid bone can be seen with the rostrum, the crest, the pterygoid processes and fossa, and the greater and lesser wings of the sphenoid delimiting the superior orbital fissure. The optic canal and foramen teres lay in the medial part of the lesser and the greater wings, respectively. Jugular region is occupied by the base of the occipital bone and the petromastoid portion of temporal bone. The occipital base is constituted on midline by the pharyngeal tuberculum and, laterally, by the petrous-occipital joint (delimiting jugular foramen on the anterior side). The petromastoid portion of the temporal bone is formed from medial to lateral by the external foramen of the carotid canal, the petrous fossa, the jugular fossa, the styloid process, and the stylomastoid foramen. The foramen lacerum results from the junction of the
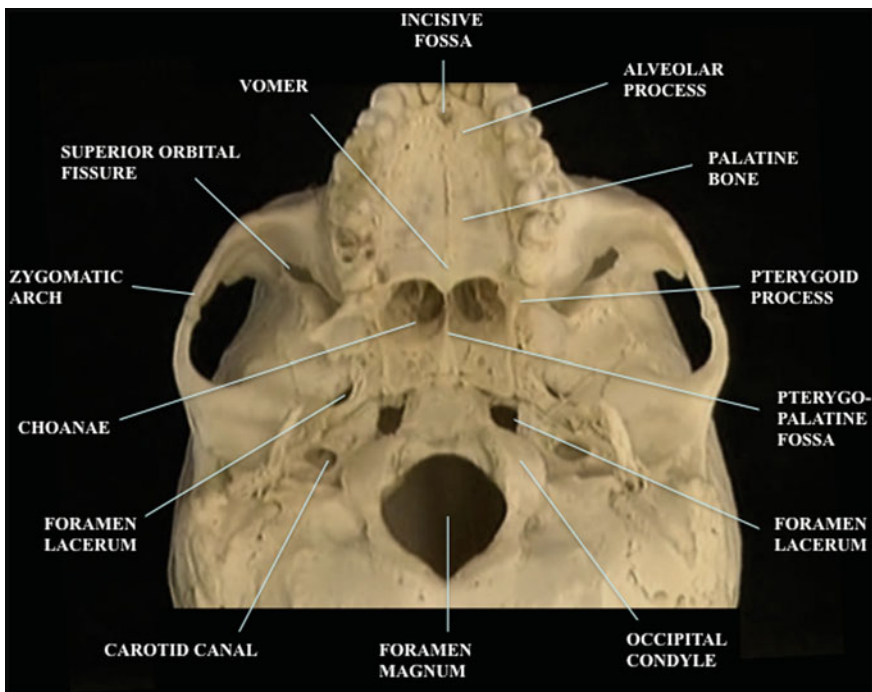
Fig. 3.3 Inferior view of the skull (mandible removed)

temporal pyramid and the greater wing of sphenoid bone. The foramen ovale and the foramen spinosum are located laterally to the sphenoid. The occipital region is constituted centrally by the great occipital foramen and laterally by the occipital condyles of the atlo-occipital joint (Fig. 3.3).

3.3 The Skull Base: Endocranial Aspect

The inner side of the neurocranium can be subdivided into three distinct fossae located onto three different transverse planes. The anterior cranial fossa is delimited on the anterior side by the squamous part of the frontal bone, which continues posteriorly, through the frontal crest and the foramen cecum, in the superior part of ethmoid bone (the roof of the nasal cavity). Laterally to the ethmoid bone, the orbital part of the frontal bone completes the anterior cranial fossa. The middle cranial fossa is constituted by the chiasmatic groove in the middle with the optic canals laterally. Right posterior to it, the hypophyseal fossa can be seen with the sella turcica, the clinoid processes, and the dorsum sellae. Adjacent to the dorsum sellae, the carotid grooves can be seen. More laterally, the greater wings of the sphenoid joining temporal pyramids can be seen. The foramen rotundum, ovale, spinosus, and superior orbital fissure (previously mentioned) are located within the greater wings of sphenoid bone. Around the pyramids the facial
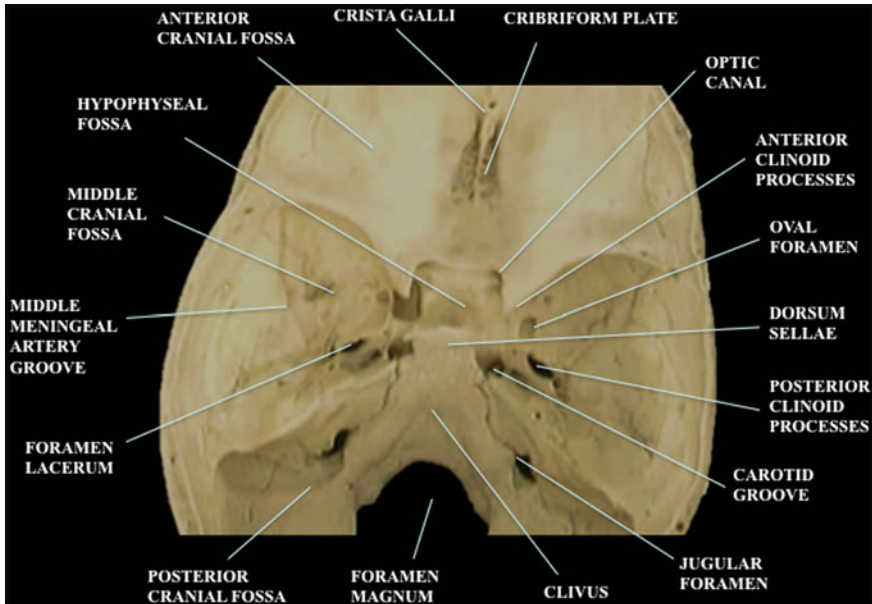
Fig. 3.4 Superior view of the skull (calvaria removed)

nerve hiatus, the internal foramen of the carotic canal, and the groove for Gasser's ganglion can be seen. The foramen lacerum results from the junction between the pyramid and the body of the sphenoid bone. Into the posterior cranial fossa, on midline, the spheno-occipital clivus can be seen, delimiting the foramen magnum on the anterior side. Laterally to the clivus, the inner foramen of the hypoglossal canal, the jugular foramen, the occipito-temporal joint, and the internal acoustic meatus can be seen within the posterior surface of sphenoidal pyramid (Fig. 3.4).

3.4   The Skull: Lateral Aspect

The lateral region of the skull (Fig. 3.5) is composed by the temporal fossa, the infratemporal fossa, and the pterygopalatine fossa. The temporal fossa is a concave area constituted by the lateral surface of the squamous part of the frontal bone, by the temporal surface of the greater wing of the sphenoid bone and by the esocranic surface of the squamous part of the temporal and parietal bones. It communicates with the infratemporal fossa through the space between the zygomatic arch and the temporal crest. The infratemporal fossa is an irregular space, open inferiorly and posteriorly, that is located among the maxilla, the zygomatic arch, the greater sphenoidal wing, the pterygoid process, and the ramus of the mandible. On its superomedial surface, the foramina ovale, spinosus, and lacerum can be seen.
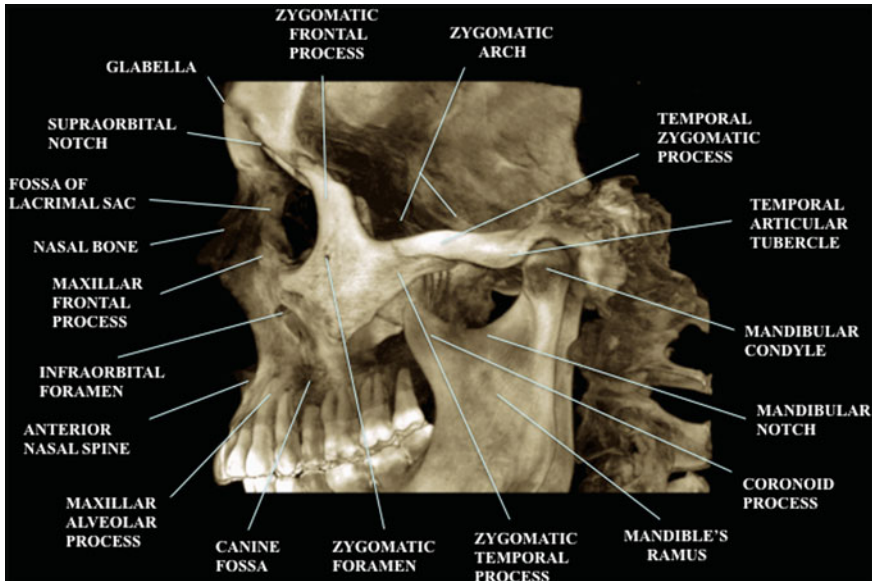
Fig. 3.5 CBCT-3D reconstruction of the facial bones: lateral view

The posterior portion of the fossa corresponds to parotid region. The pterygopalatine fossa is a bony area located below the apex of the orbit and is comprised among the maxilla, the palatine bone, and the pterygoid process. It continues into the nasal cavity through the nasopharyngeal opening and the sphenopalatine foramen, into the infratemporal fossa through the pterygomaxillary fissure.

3.5   The Skull: Anterior Aspect

The anterior aspect of the skull is composed by the maxilla, the mandible, the zygomatic, and the nasal bones. The orbital cavities are symmetrically located on the frontal side and contain the eyes and their annexes (Fig. 3.6).

The frontal bone and the lesser wing of the sphenoid bone contribute to the constitution of the orbital walls for their superior aspect. The body of the maxilla and the orbital processes of zygomatic and palatine bones form the inferior aspect of the orbits; frontal process of maxilla, ethmoidal lamina papyracea, lacrimal
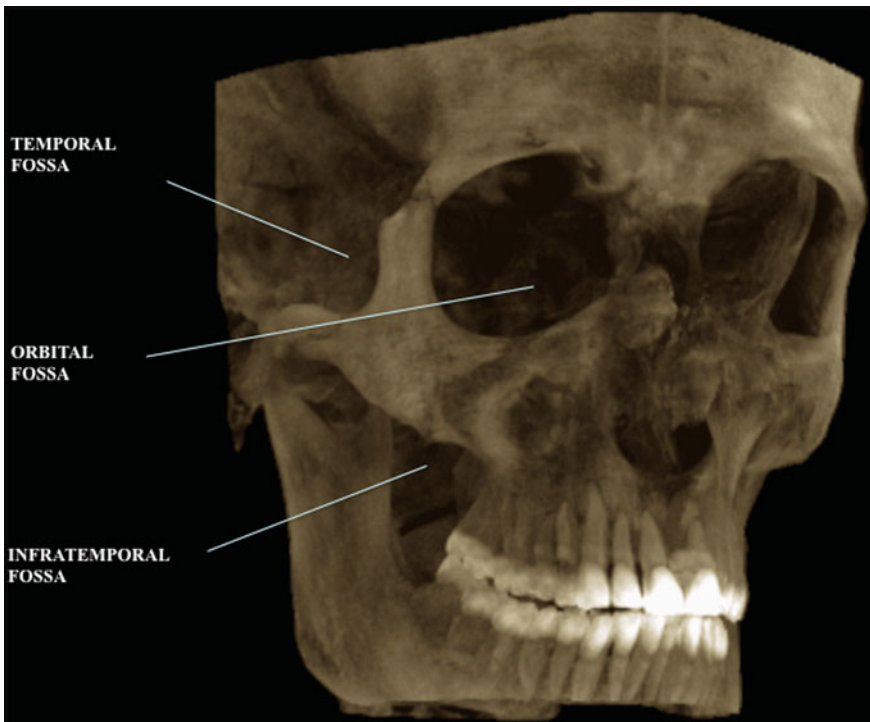
Fig. 3.6 CBCT-3D reconstruction of the skull
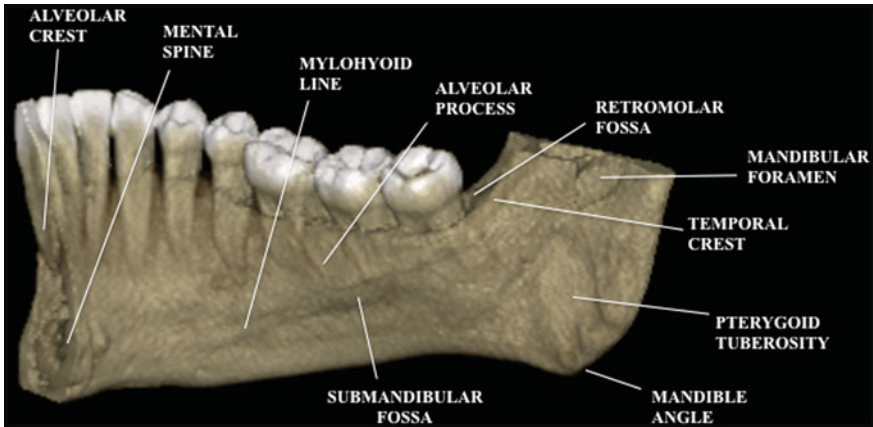
Fig. 3.7   Mandible, CBCT-3D reconstruction of right hemiarch: medial surface
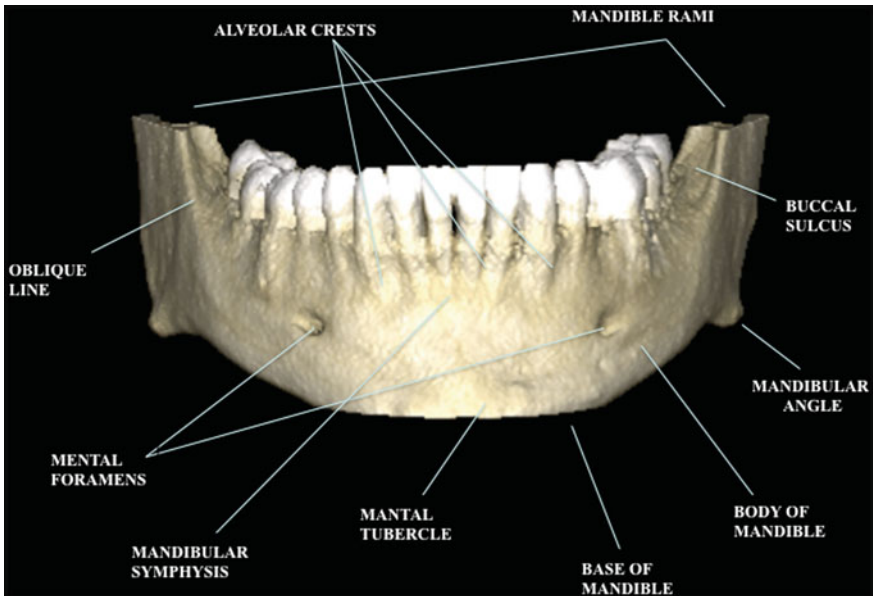
Fig. 3.8   Mandible, CBCT-3D reconstruction; outer surface, anterior view

bone and the body of sphenoid lay medially. Also, the lacrimal fossa is to be considered, which lies on the medial wall of the orbit, behind the frontal process of the maxilla (Figs. 3.7, 3.8, 3.9).
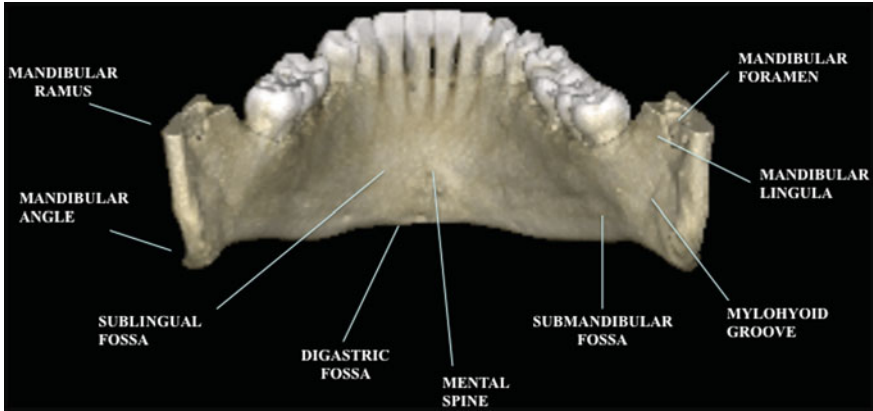
Fig. 3.9 Mandible, CBCT-3D reconstruction; inner surface, posterior view

3.6 Nasal Cavity

The nasal cavity is composed by two linear symmetrical fossae passing through the splanchnocranium and separated by a median septum (Fig. 3.10).
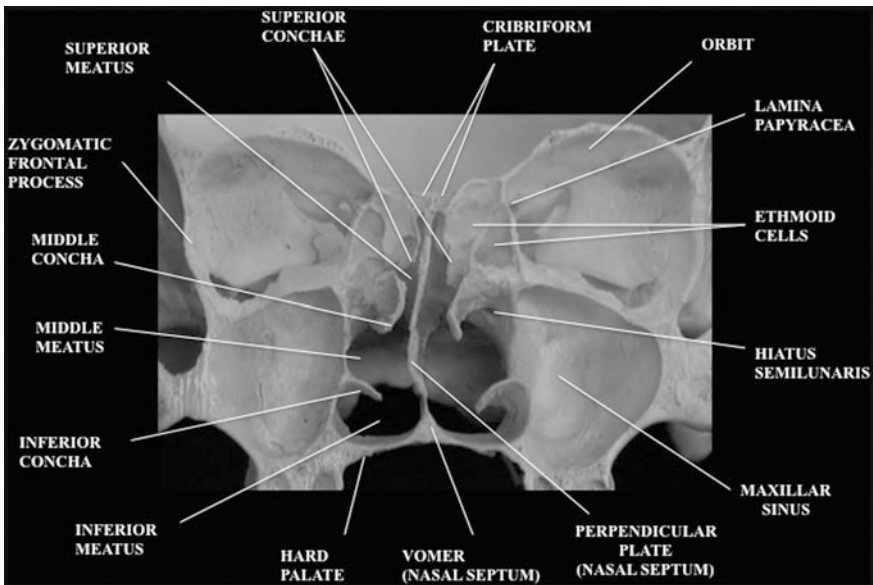
Fig. 3.10 Coronal section of the splanchnocranium passing through the crista galli; the nasal cavity, paranasal sinuses, and bones delimiting them can be seen
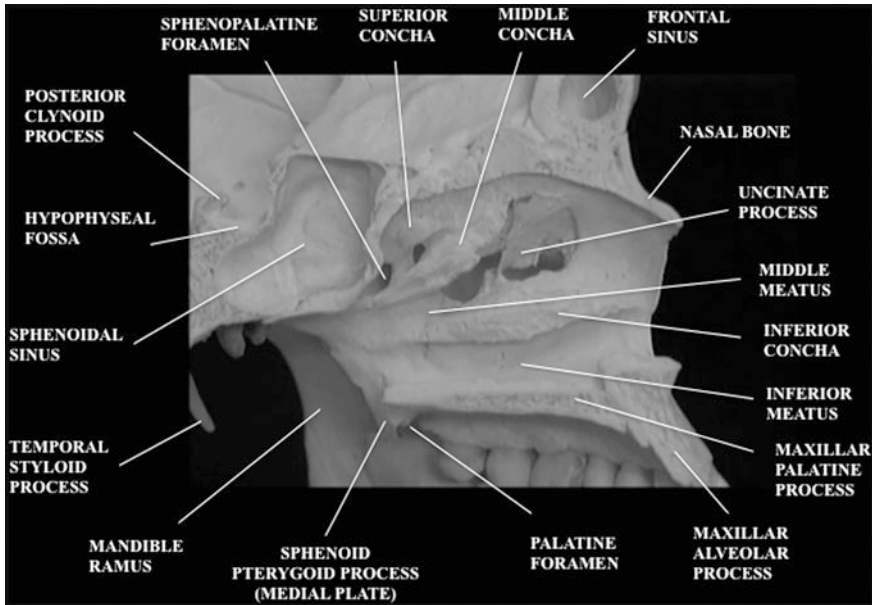
Fig. 3.11 Sagittal paramedian section of the splanchnocranium; the nasal cavity, the paranasal sinuses, and the bones delimiting them can be seen

The bony part of this septum is formed by the vomer, inferiorly, and the perpendicular plate of the ethmoid, superiorly. A thin layer of cartilage completes the septum anteriorly. The nasal cavities are open anteriorly through the common piriformis opening formed by the maxillar and the nasal bones, and posteriorly through choanae. The floor is formed by the palatine processes of the maxilla and the horizontal plates of the palatine bones. The roof is the cribriform plate of the ethmoid. The nasal bones contribute to the lateral walls of the nasal cavity: the superior and the middle conchae of ethmoid, the inferior nasal concha (which is an independent bone), a part of the maxilla, and the perpendicular plate of palatine bones. On these lateral walls, the openings of the canals and sinuses can be seen.

Each of the three conchae forms a roof over a groove-shaped air passageway called meatus: thus, there is an inferior, a middle, and a superior meatus. The nasolacrimal duct opens in the inferior meatus; the sphenoid sinuses and the posterior ethmoidal cells are connected with the superior meatus; the maxillary sinuses, frontal sinuses, and the anterior ethmoidal cells drain into the middle meatus with modalities that are better described in the next paragraph (Fig. 3.11).

3.7   Paranasal Sinuses

The paranasal sinuses are air-filled cavities contained within the frontal, the ethmoid, the sphenoid, and both maxillary bones. They cluster around the nasal cavity and are connected with it. They are:

- *Maxillary sinus* (Fig. 3.12): the widest, its air content depends on age and number of teeth. It occupies the central part of the maxillary bone and has a triangular pyramidal shape with the base facing medially. The inferior portion of its anterior wall corresponds to the fossa canina.
- *Frontal sinus*: has triangular pyramidal shape with the base facing down and it is contained within the frontal bone. Its anterior wall, whose thickness is inversely correlated with sinus dimensions, corresponds externally to the eyebrow region.
- *Sphenoid sinus*: has irregular cubic shape and is enclosed within the body of the sphenoid. Its medial wall is the posterior continuation of the nasal septum. For its deep position into the skull, it is located adjacent to important anatomical structures like the internal carotid arteries, the optic chiasm, the hypophysis, and the anterior cerebral arteries. In case of sphenoid sinuses pathology, it may cause endocranial complications.
- *Ethmoid sinus*: is composed by bony cells (often more than ten) disposed irregularly into ethmoid with a honeycomb appearance. Altogether they have a
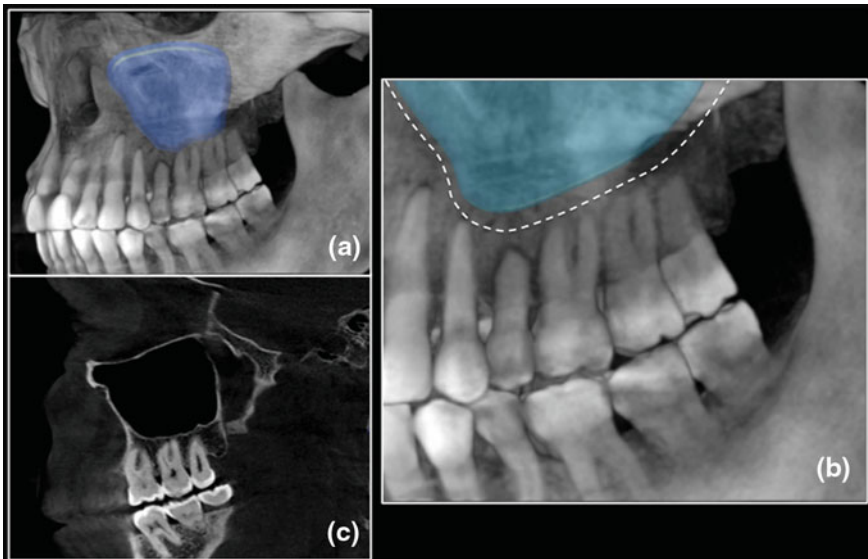
Fig. 3.12 *Left* maxillary sinus. **a** sinus representation on a CBCT-3D reconstruction of the skull; **b** anatomical detail of the relationship between the inferior sinus wall and the superior dental roots; **c** corresponding CBCT-2D sagittal image passing through the left maxillary sinus

Fig. 3.13 Graphical raffiguration of paranasal sinuses on a sagittal paramedian section of the skull: medial view. *SS* sphenoid sinus, *EC* ethmoidal cells, *FS* frontal sinus
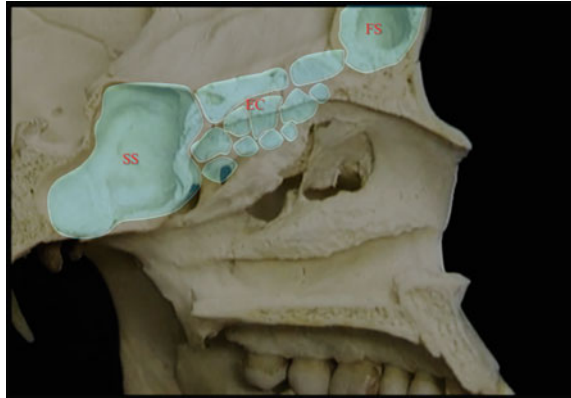
Fig. 3.14 Graphical raffiguration of paranasal sinuses on a CBCT-3D reconstruction of the splanchnocranium: frontal view. *MS* maxillary sinuses, *EC* ethmoidal cells, *NC* nasal cavity, *FS* frontal sinuses
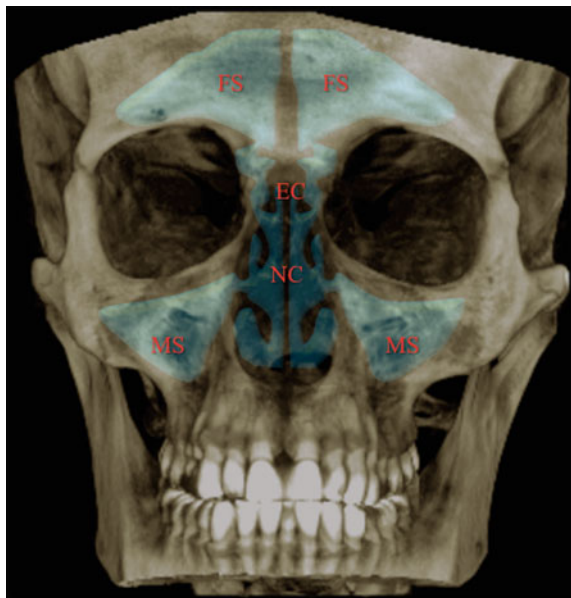
parallelepipedon shape and are subdivided into an anterior and a posterior group, having different drainage openings (Figs. 3.13 and 3.14).

The so-called *ostiomeatal complex* (OMC) is the complex anatomical framework that allows for normal ventilation of the cavities that drain into the middle meatus: the maxillary sinus, the frontal sinus, and the anterior ethmoidal cells group. Contributing to OMC are the middle meatus, the infundibulum, the ostium of the maxillary sinus, the uncinate process, and the ethmoidal bulla. The maxillary opening usually lies in the third caudal of the infundibulum, which is comprised among the uncinate process, the ethmoidal bulla and the lamina

Fig. 3.15 Sagittal paramedian section of the skull: *purple areas*: inferior, middle, and superior conchae; *red dashed line*: ostiomeatal complex; *yellow dashed line*: inferior opening of frontonasal duct; *green dashed line*: sphenopalatine foramen

papyracea. Also, the *frontonasal duct* drains into the middle meatus and its opening usually lies in the superior third of the infundibulum. It connects the frontal sinus with the nasal cavity. The *sphenoethmoidal recess* is located on the posterosuperior surface of the superior meatus, which allows for an adequate ventilation of the sphenoidal sinus and the posterior ethmoidal cells (Fig. 3.15).

3.8   Teeth

Two dentitions occur in our lifetime:

Primary dentition: it is formed by deciduous teeth (milk teeth), the first tooth erupts at about 6 months, the last one at approximately two and a half years, in the end each dental arch is formed by 10 teeth (20 in total).

Permanent dentition (Fig. 3.16): it is formed by permanent teeth, the first tooth erupts at about 6 years, the last one approximately between 18 and 25 years; in the end there are 32 teeth in total, 16 for each dental arch.
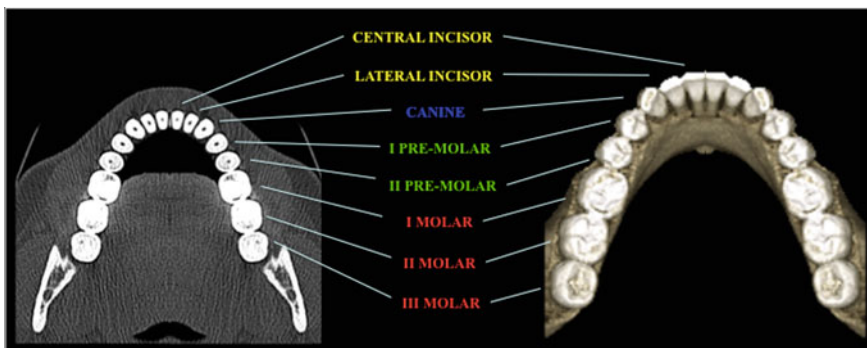
Fig. 3.16 Permanent teeth. *Left* axial CBCT scan indicating every single dental units; *Right* corresponding 3D-CBCT reconstruction
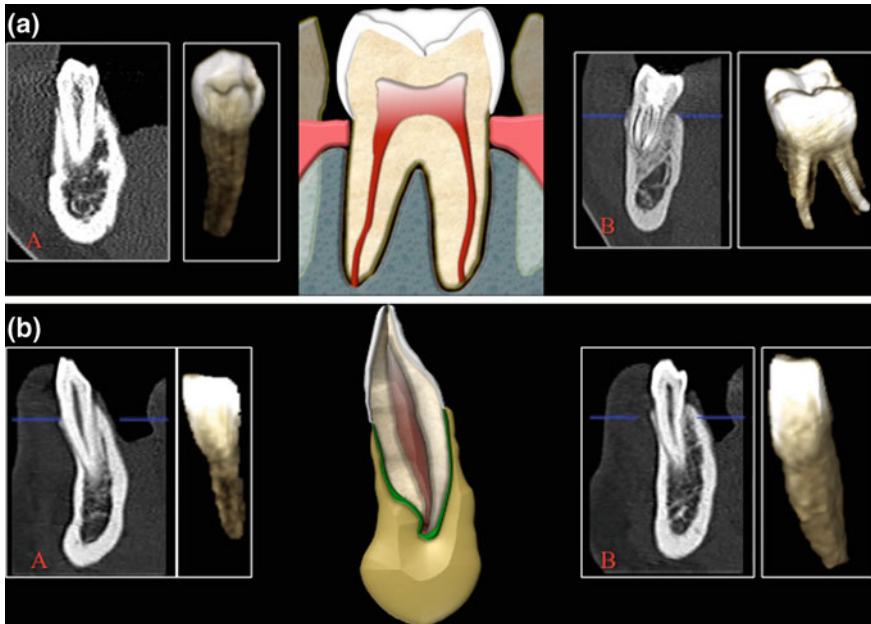
Fig. 3.17 a, **b** Teeth: bidimensional scan, corresponding 3D-CBCT reconstruction and anatomical illustration. *Below* central incisor (**A**), canine (**B**). *Above* first premolar (**A**), first molar (**B**)

Until 6 years of age, we have only deciduous teeth; from 6 to 12 years, they are progressively substituted (with a very defined sequence: maxillary first molars—mandibular central incisors—inferior first molars and superior central incisors—upper lateral incisors—lower lateral incisors—canines and premolars—second molars—third molars) by permanent teeth till the complete replacement at about 12-year old. During the following years, the definitive dental set is reached. In case that a tooth has not erupted when expected, it is called 'impacted' tooth. So it is possible to define three different sets of teeth during our lifetime:

- *Deciduous*: from 6 months to 6 years, formed by incisors, canines, and molars (dental formula: 2-1-2).
- *Mixed:* from 6 to 12 years.
- *Permanent:* from 12 years, constituted by incisors, canines, premolars, and molars (dental formula: 2-1-2-3) (Fig. 3.17a, b).

Dental formula defines the number of teeth, ordered by class, belonging to a hemiarch; in the permanent set of teeth, proceeding from midline we can see progressively: central incisor, lateral incisor, canine, first premolar, second premolar, first, second, and third molars.

Fig. 3.18 Two-digit numbering system. *Upper* and *lower* arch are divided in two quadrants and teeth are numbered from 1 to 8 in a mesial-to-distal way
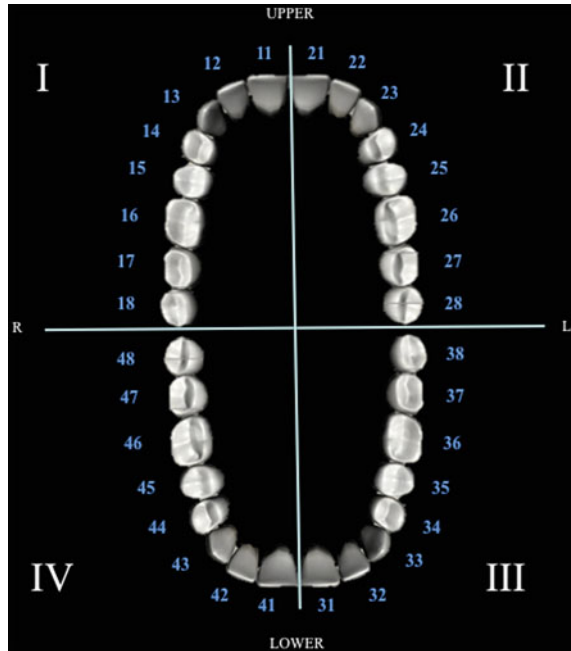
The most common notation system to define a tooth is the two-digit numbering system (Fig. 3.18) in which, for permanent teeth, the first number represents the quadrant (numbered 1–4 starting from the upper right quadrant and proceeding clockwise) and the second number represents the number of the tooth from the midline of the face (numbered 1–8 from central incisor to third molar). In deciduous teeth, quadrants are numbered clockwise from 5 to 8 and the number of dental units for each hemiarch is five.

3.9   Dental Anatomy

Crown: portion of the tooth covered by enamel.

Root: portion of the tooth covered by cementum; the roots of teeth may be single or multiple.

Root apex: the terminal end of the root.

Neck: connection area between crown and root.

Cervical line: correspond to the *cementoenamel* junction.

Cusp: is an elevation on an occlusal surface of posterior teeth and canines. It contributes to a significant portion of the tooth's surface; canines have one cusp, mandibular molars may have 4 or 5 cusps.
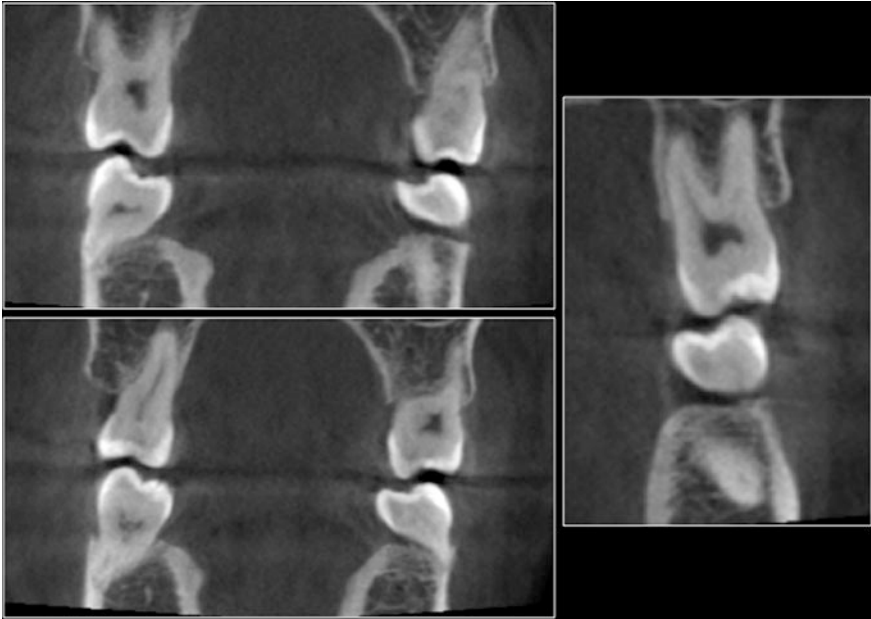
Fig. 3.19 Occlusal plane viewed from different coronal 2D-scans; opposite occlusal surfaces' relationship is visible in detail

Incisal margin: the cutting edges of the anterior teeth, the incisors and canines, which come into contact with those of the opposite teeth during occlusion.

Fissures: grooves on the occlusal surface of the teeth.

Occlusal surface: the surface of molars and premolars that comes in contact with those of the opposite side during occlusion, also called masticatory surface.

Vestibular surface: or facial surface, is the surface of a tooth that is directed outward toward the vestibule of the mouth, including the buccal and labial surfaces.

Lingual surface: or oral surface, is the surface of a tooth facing inward toward the tongue; opposite to the vestibular surface.

Mesial surface: the surface of a tooth that is closest to the midline of the dental arch.

Distal surface: the surface of a tooth that is farthest from the midline of the dental arch; opposite to the mesial surface.

Interproximal spaces: triangular spaces between the proximal surfaces of adjoining teeth (Figs. 3.19, 3.20 and 3.21).
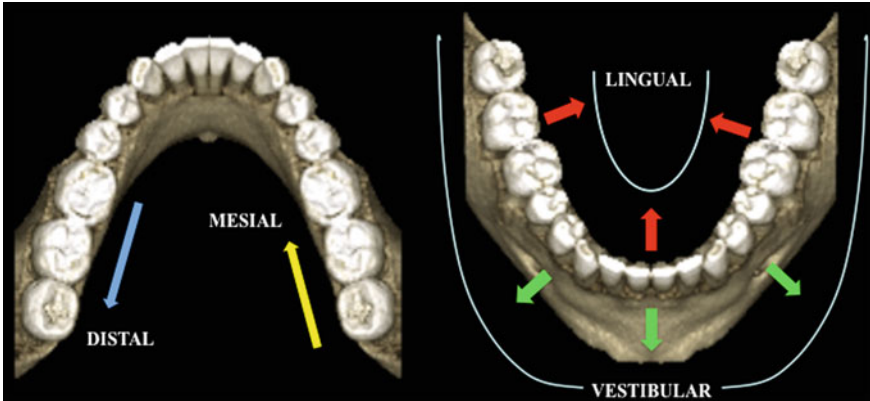
Fig. 3.20 Dental surfaces' terminology

Fig. 3.21 Teeth. *Upper row* CBCT bidimensional anterior-to-posterior sagittal scans; *lower row* 3D-reconstructions of mandibular dental arch

3.10 Dental Tissues

Three kinds of tissue (enamel, dentin, and pulp) constitute the internal dental framework and four other kinds of tissue (cementum, periodontal ligament, alveolar bone, and gingiva) form the periodontium that supports teeth.

Enamel: is an epithelial origined tissue, very hard and mineralized, without nerves, vessels, and cells. It covers the anatomic crown till the cervical line; it provides teeth with their whitish color, and is 1–2 mm thick.

Pulp-dentin complex: dentin is the main mass of the tooth and is located deep to the enamel and to the cementum. It is a mesenchymal tissue, hard, avascular but able to regenerate itself from underlying pulpar cells. Pulp is the only soft tissue of the tooth and fills the central dental cavity which develops from crown (pulp cavity) to the root apex (root canal). Dentin-producing odontoblasts are located into pulp. Dentin and pulp are usually considered as a single entity for their histoembryological and functional properties and constitute endodontium.

Cementum: is a bone-like tissue with no vessels. It provides an attachment surface for the periodontal ligament.

Periodontal ligament: is formed by collagenous fibers connecting the alveolar bone to the cementum.

Alveolar bone: is a very plastic bony tissue, it constitutes and covers the dental alveoli, in which dental roots are located. Its characteristics are the same of the tissue forming bones in other parts of human body. Its inner wall (hard plate) covers the alveolus and represents the attachment site for periodontal ligament's fibers.

Gum: is the buccal mucosae that covers the alveolar processes and surrounds teeth's neck, to which is attached through a junctional epithelium. This epithelial junction has an important role in periodontitis because it is the only anatomical barrier located between the oral cavity and dental structures.

Furthermore, it is important to mention the root's *epithelial rests of Malassez*. They are discrete clusters of residual cells from Hertwig's epithelial root sheath and, for their proliferative ability, are responsible for the formation of periapical and periodontal cysts following to inflammatory processes (Figs. 3.22, 3.23).

Fig. 3.22 Anterior tooth anatomical illustration
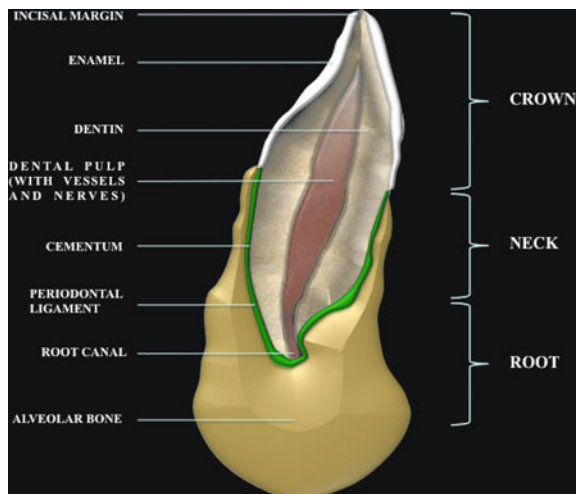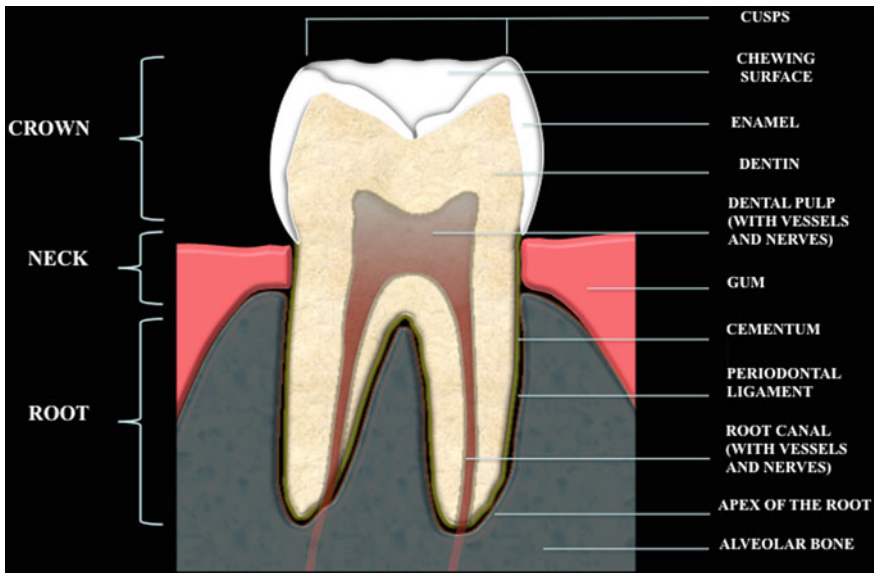
Fig. 3.23 Anatomical illustration of dental tissues (enamel and endodontium) and surrounding tissues (periodontium)

3.11 Odontostomatological Trigeminal Nerves

Trigeminal nerve, the fifth pair of cranial nerves, is composed for the most part by somatic sensory fibers and for the remaining part by somatic motor fibers. The sensory component origins from the semilunar ganglion located in the Meckel's cave; pseudounipolar cells of the ganglion give rise to all the fibers directed to the face. They divide into three main branches: opthalmic nerve (V1), maxillary nerve (V2), and mandibular nerve (V3) (Fig. 3.24).

3.11.1 V2: Peripheral Branches

- *Greater palatine nerve*: passes through the palatine canal, emerges from the omonimous foramen and runs ahead to innervate the dorsal palatal side of the gums and hard palate's mucosae. Greater palatine foramen could be identified into the oral cavity in correspondence of the last molar.
- *Nasopalatine nerve*: runs along nasal septum and through the incisive canal, enters in the oral cavity and supplies the anterior part of the gums and hard palate's mucosae.
- *Superior alveolar nerves*: the posterior nerve runs downward along the maxillary tubercle, then it divides in a few terminal branches for molars and the surrounding periodontium. The middle superior alveolar nerve runs along the
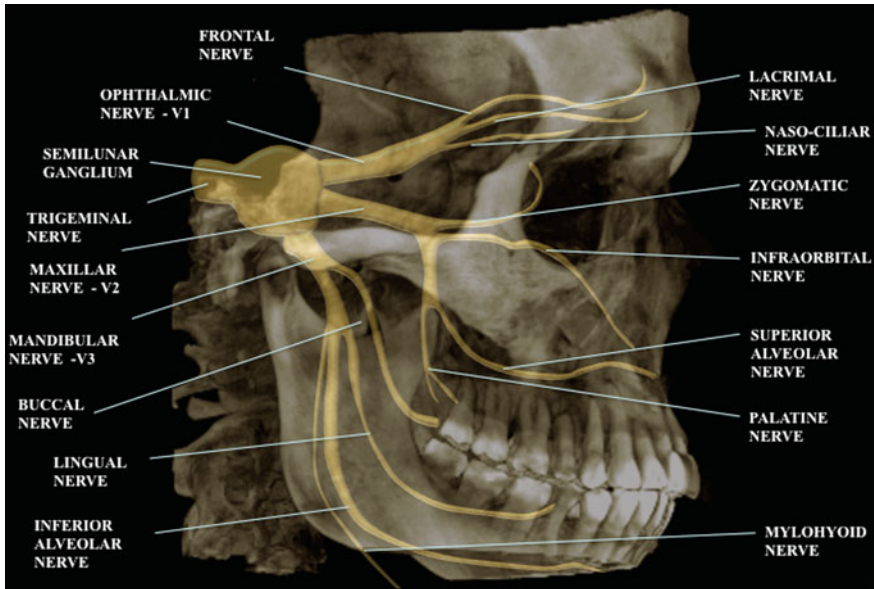
Fig. 3.24 Anatomical illustration of the trigeminal nerve's course and its main branches

lateral side of maxillary sinus to supply premolars. The anterior nerve runs along the anterior wall, then forms an anastomotical plexus with contralateral nerves which innerves anterior teeth.

3.11.2 V3: Peripheral Branches

- *Lingual nerve*: goes downward toward the mandible and, in correspondence of the mylohyoid line, turns horizontally away from the alveolar nerve. It enters the oral cavity close to the mylohyoid muscle and, at the level of third molars, runs very superficially; it innervates the lingual mucosae, the inferior palatine mucosae and the lingual side of gums.
- *Inferior alveolar nerve*: runs downward toward the mandible and, around the mandibular foramen, it passes through the sphenomandibular ligament and the mandible's ramus to enter into the mandibular canal. In the mandibular canal, it runs close to the omonimous artery and vein located anteroposteriorly and releases branches for molars and second premolars of the corresponding hemiarch and surrounding periodontium. Anteriorly, the nerve gives off the mental nerve (at about the level of the mandibular second premolars), which exits the mandible via the mental foramen (supplying sensory branches to the chin and lower lip). The inferior alveolar nerve continues anteriorly as the mandibular incisive nerve to innervate the mandibular canines and incisors. Its
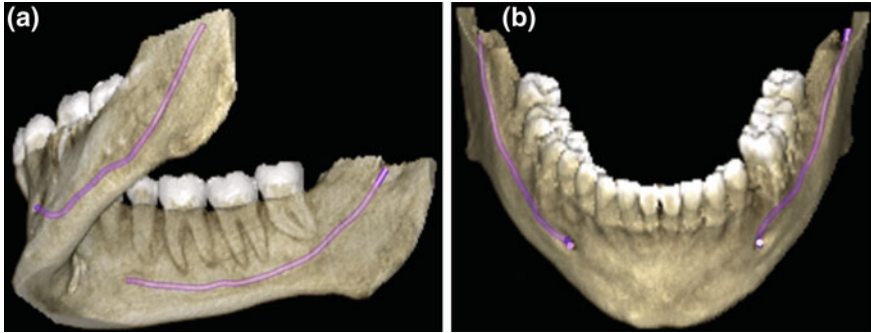
Fig. 3.25 **a**, **b** Inferior alveolar nerve's course in the mandibular canal: 3D-CBCT reconstruction. Its relationship with dental roots could easily be seen

contiguity to dental roots (in particular third molars) may create some complications during odontoiatric maneuvers (Fig. 3.25a, b).

3.12 Temporomandibular Joint

Temporomandibular joint represents the only moveable joint in the cranium; it is a double condyloid diarthrosis between the mandibular condyle and the mandibular fossa of temporal bone (Fig. 3.26).
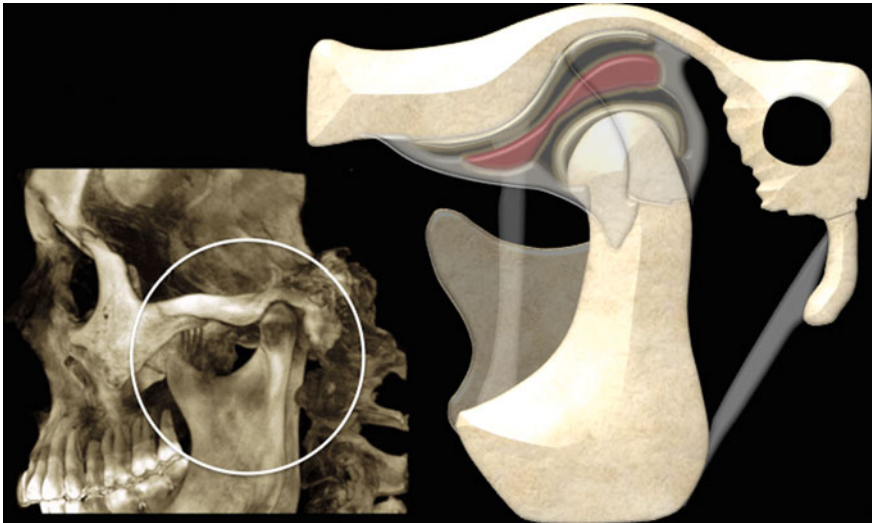
Fig. 3.26 Anatomical illustration of temporomandibular joint complex: lateral view

Its 'double' definition comes from the presence of an articular meniscus that divides the joint capsule into two intra articular, non-communicating, synovial cavities: a superior one (temporo-meniscal) and an inferior one (condylo-meniscal). Two types of movements occur in the temporomandibular joint: in the superior synovial cavity, gliding movements occur between the articular disc and the articular tubercle (protrusion and retrusion); in the inferior synovial cavity, hinge movements occur between the head of the mandible and the articular disc. Articular surfaces are constituted by the condyle covered by articular cartilage anteriorly and fibrous tissue posteriorly on the mandibular side; by the mandibular tubercle of zygomatic process and by the anterior part of mandibular fossa, both covered by hyaline cartilage, on the temporal side. The articular disc warrants the right correspondence among such anatomical structures. Joint capsule is reinforced on its lateral side by the temporomandibular ligament and is supported by two other extrinsic ligaments: the sphenomandibular and the stylomandibular. The first one runs from the angular spine of sphenoid to the ramus of mandible in correspondence of the mandibular foramen; the second extends from the styloid process to the posterior edge of mandible, up to its angle (Figs. 3.27, 3.28, and 3.29).
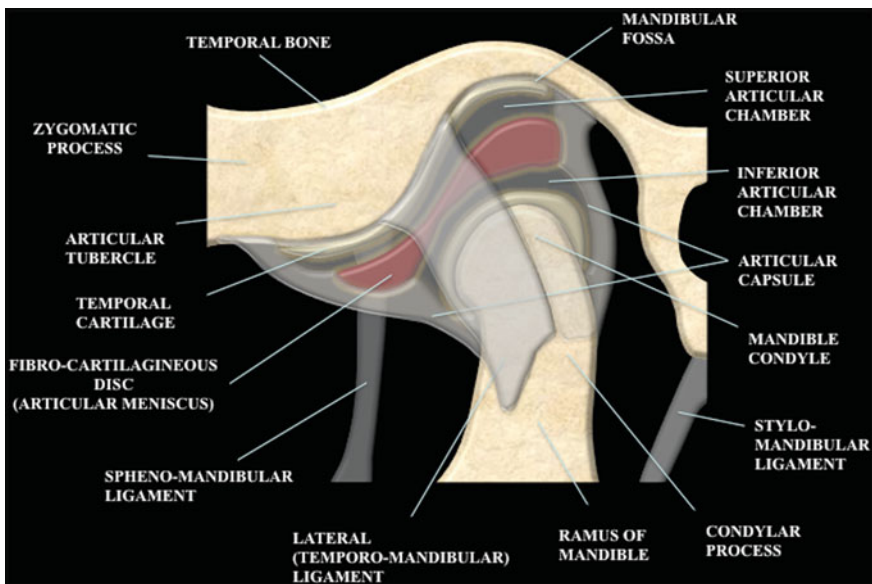
Fig. 3.27 Temporomandibular joint illustration: lateral view
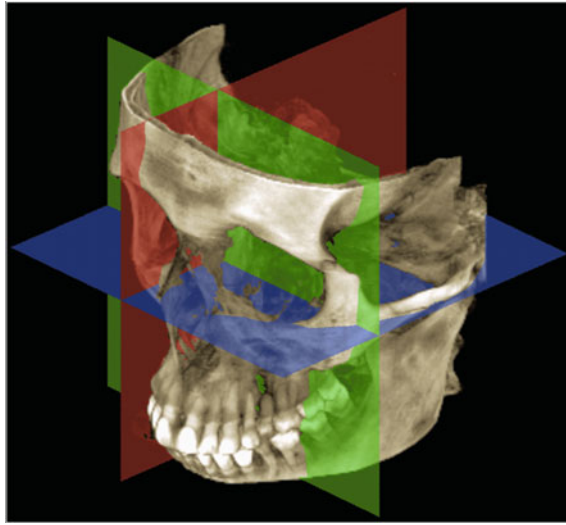
Fig. 3.28 Multiplanar visualization of CBCT images; *green* coronal; *blue* axial; *red* sagittal
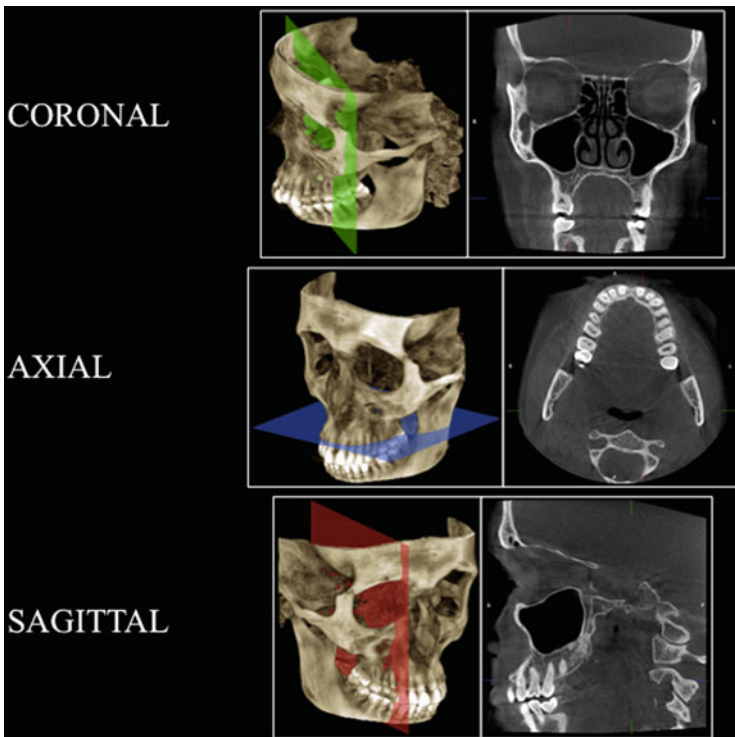
Fig. 3.29 The three scan planes (on the *left*), and corresponding CBCT bidimensional scans (on the *right*)

3.13 Lateral Sagittal Scans
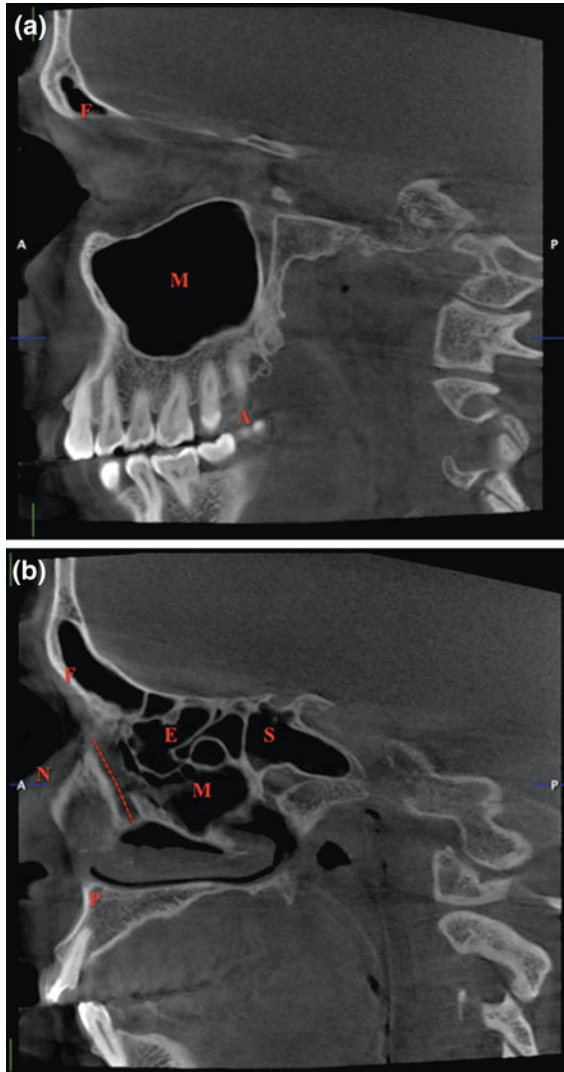
Fig. 3.30 **a**, **b** *Above* more lateral sagittal scan; *below* more medial sagittal scan *F* frontal sinus, *M* maxillary sinus, *A* dental arches, *N* nasal bone, *E* ethmoid cells, *P* alveolar process, *S* sphenoid process, *Red dashed line* nasolacrimal duct

3.14 Medial Sagittal Scans
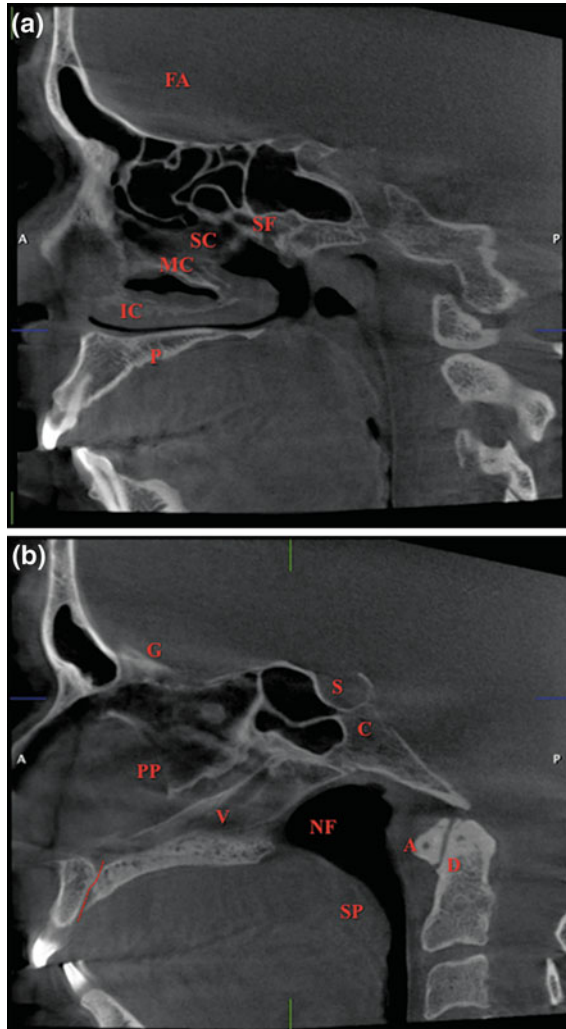
Fig. 3.31 a, **b** *Above* more lateral sagittal scan; *below* more medial sagittal scan. *NF* nasopharynge, *G* Crista galli, *S* sella turcica, *C* Clivus, *D* axis dens, *A* anterior atlas arch, *SP* soft palate, *P* palatine bone, *V* Vomer (nasal septum), *PP* perpendicular plate (nasal septum), *IC* inferior concha, *MC* middle concha, *SC* superior concha, *Red dashed line* incisive canal, *AF* anterior cranial fossa, *SF* sphenopalatine foramen

3.15   Inferior Axial Scans
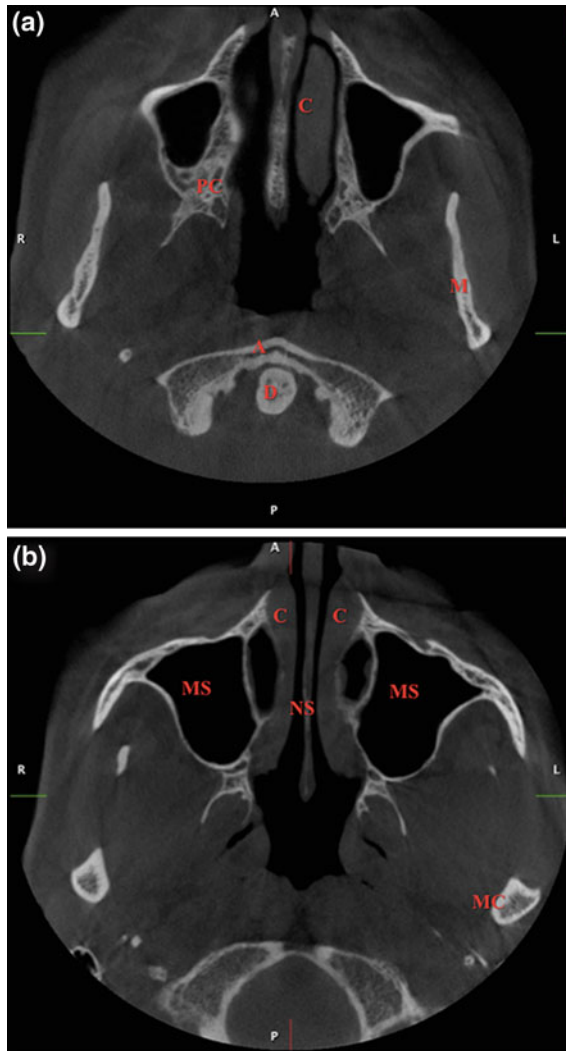
Fig. 3.32   a, **b** *Above* lower axial scan; *below* upper axial scan. *C* inferior conchae, *MS* maxillary sinus, *NS* nasal septum, *MC* mandibular condyle, *M* mandibular body, *PC* palatine canals, *A* anterior atlas arch, *D* axis dens

3.16 Middle Axial Scans
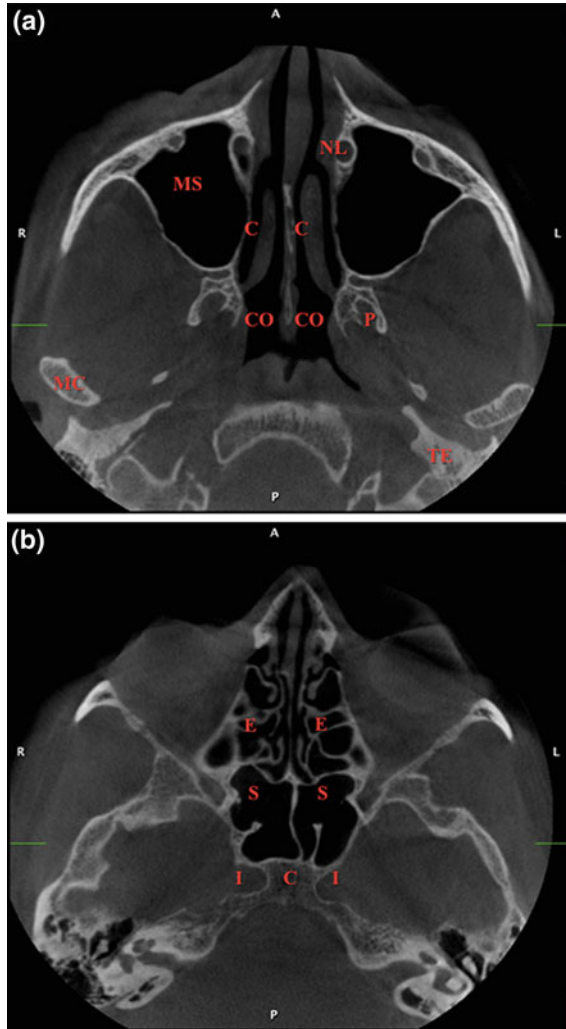
Fig. 3.33 a, **b** *Above* lower axial scan; *below* upper axial scan. *NL* nasolacrimal duct, *MS* maxillary sinuses, *C* middle conchae, *CO* Choanae, *TE* temporal bone, *MC* mandibular condyle, *P* pterygoid process, *E* ethmoid cells, *S* sphenoid sinuses, *I* internal carotid grooves, *C* Clivus

3.17   Superior Axial Scans
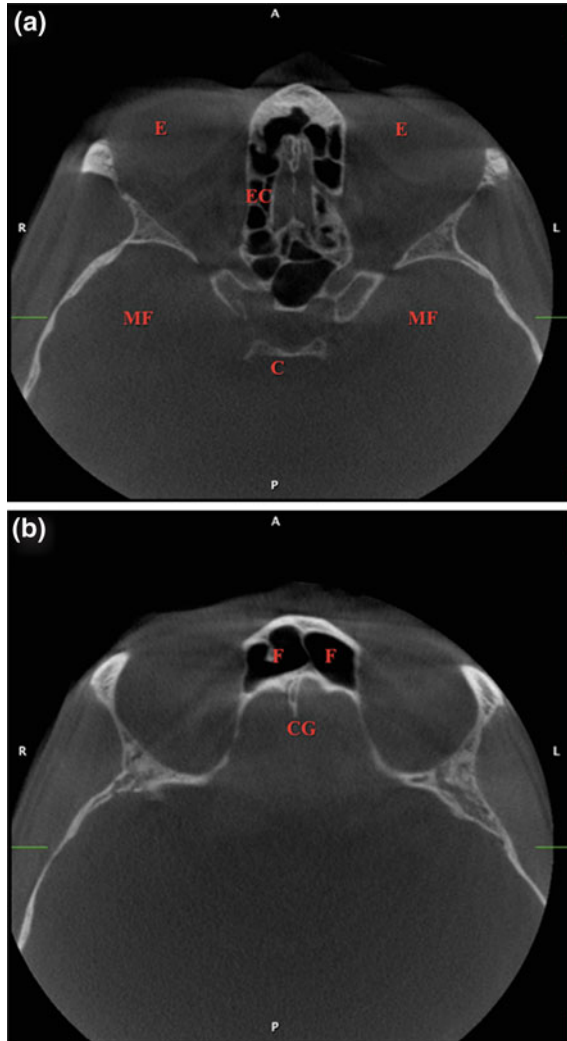
Fig. 3.34 a, **b** *Above* lower axial scan; *below* upper axial scan. *E* ocular globes, *F* frontal sinuses, *CG* crista galli, *C* posterior clynoid processes, *EC* ethmoid cells, *MF* middle cranial fossa

3.18 Posterior Coronal Scans
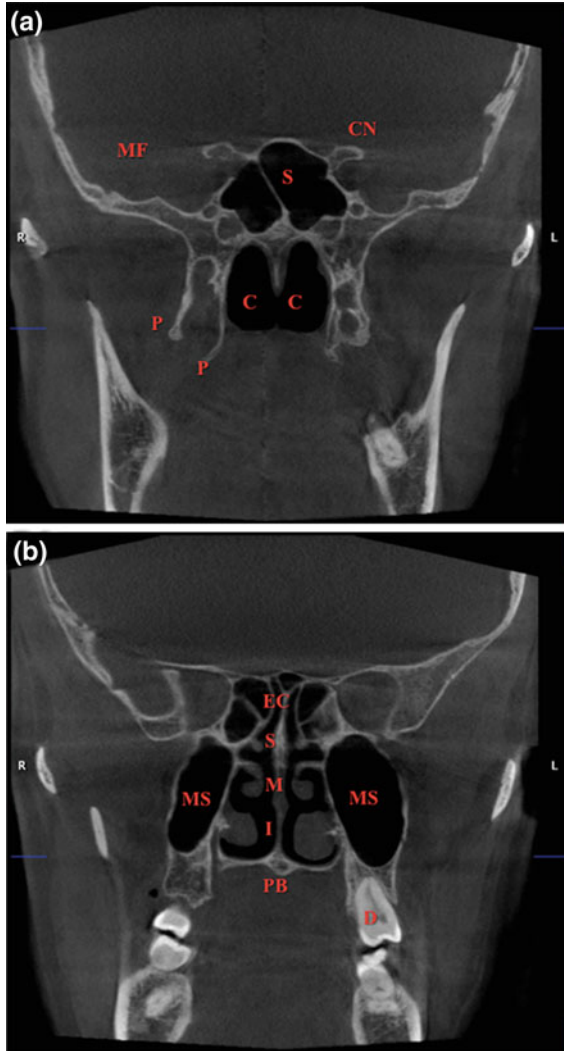
Fig. 3.35 **a**, **b** *Above* more dorsal coronal scan; *below* more frontal coronal scan. *CN* anterior clynoid processes, *S* sphenoid sinuses, *C* Choanae, *P* pterygoid processes and omonimous fossa, *S* superior conchae, *M* middle conchae, *I* inferior conchae, *D* third molar, *MF* middle cranial fossa, *PB* palatine bone, *EC* ethmoid cells

3.19   Middle Coronal Scans
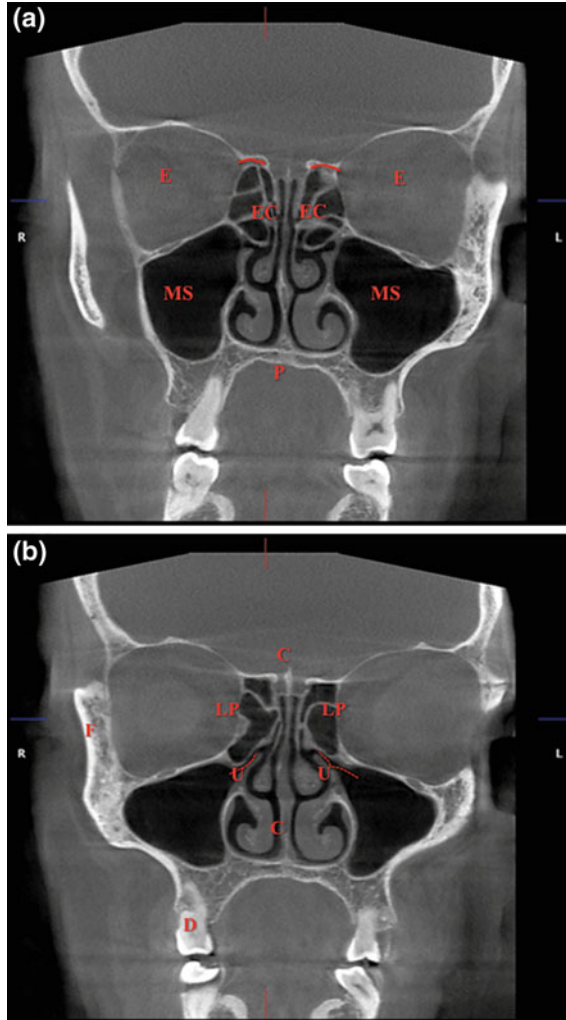
Fig. 3.36 a, **b** *Above* more dorsal coronal scan; *below* more frontal coronal scan. *C* cribriform plate, *MS* maxillary sinuses, *EC* ethmoid cells, *E* ocular globes, *P* hard palate, *F* zygomatic frontal process, *U* uncinate process, *C* inferior conchae, *D* first molar, *LP* Lamina papyracea, *Red continuos lines* anterior ethmoid arteries, *Red dashed lines* maxillary sinus ostium

3.20 Anterior Coronal Scans
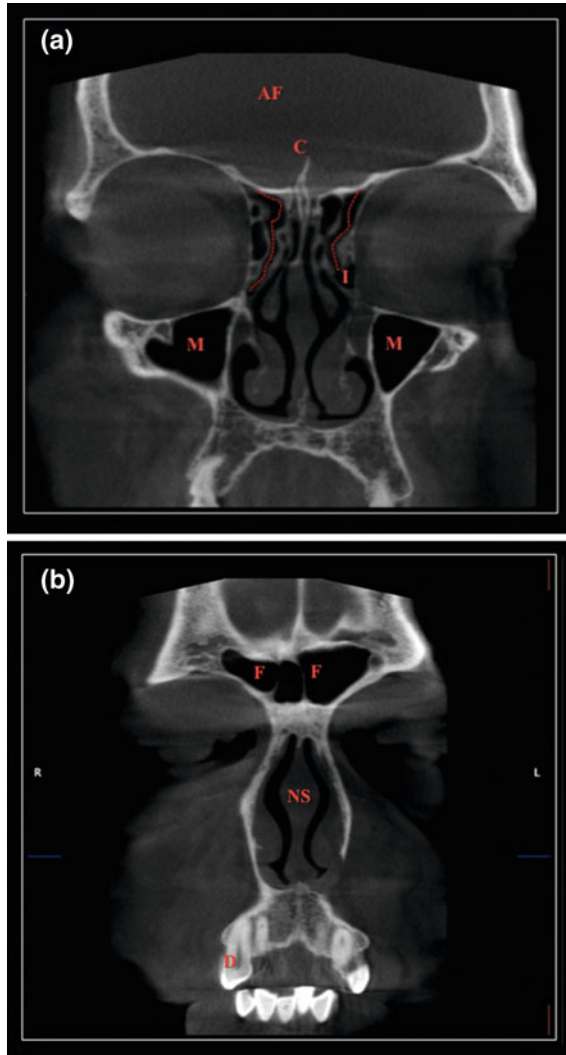
Fig. 3.37 **a**, **b** *Above* more dorsal coronal scan; *below* more frontal coronal scan. *C* Crista galli, *I* Infundibulum (drainage of frontal and maxillary sinuses), *F* frontal sinuses, *D* canine, *NS* nasal septum, *Red dashed lines* frontonasal ducts, *AF* anterior cranial fossa, *M* maxillary sinuses

3.21   Temporomandibular Joint
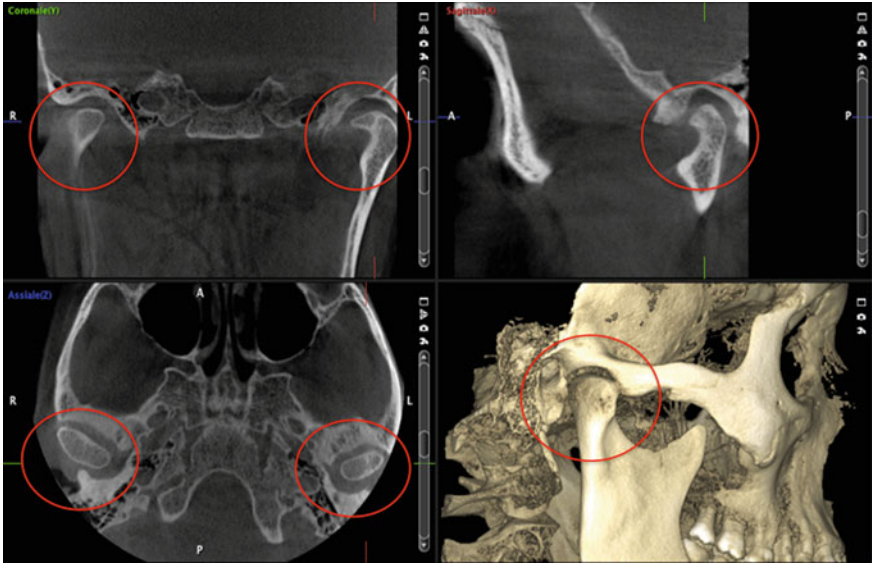
Fig. 3.38 Temporomandibular joint: screenshot of the CBCT software window; it is easy to visualize joint components in the coronal, axial, sagittal planes, and the 3D-reconstruction

Suggested Readings

Baker EW, Schünke M, Schulte E, Schumacher U (2010) Head and neck anatomy for dental medicine. Thieme Medical Publishers, New York

Ellis H, Logan BM, Dixon AK (2007) Human sectional anatomy atlas of body sections, CT and MRI images. Hodder Arnold, London

Marieb EN, Wilhelm PB, Mallatt J (2012) Human anatomy, 6th edn (media update). Benjamin Cummings, San Francisco

Netter FH (2001) Atlas of human anatomy. Masson, Barcelona

Norton NS (2011) Netter's head and neck anatomy for dentistry. Elsevier, Philadelphia

Olson TR (2008) Adam student atlas of anatomy. Cambridge Medicine, New York

Tank PW (2010) The head and neck. In: Grant's dissector (13th edn). Lippincott Williams & Wilkins, Philadelphia, pp 150–210

Exam Technique

4

Francesca Nosenzo, Tito Luminati and Enzo Silvestri

4.1 Exam Setting

Step 1
Before Starting the Examination
- Look carefully to the dentist's request.
- Collect patient's history that will help to perform the examination correctly and to orient subsequent reporting.
- In case of women of childbearing age, always ask about a possible pregnancy. A declaration of nonpregnancy should always be signed.

Step 2
Patient Preparation
- Patient must remove all metal objects such as earrings, necklaces, hairpins, and dentures (Fig. 4.1).
- Patient must wear radiation protective equipment (Fig. 4.2).

F. Nosenzo (✉)
Post Graduate School of Radiodiagnostic—University of Genoa, Via Alberti,
16100 Genoa, Italy
e-mail: francesca.nosenzo@gmail.com

T. Luminati · E. Silvestri
Ospedale Evangelico Internazionale—Unit of Radiology, Corso Solferino 1,
16100 Genoa, Italy
e-mail: tluminati@oeige.org

E. Silvestri
e-mail: silvi.enzo@gmail.com
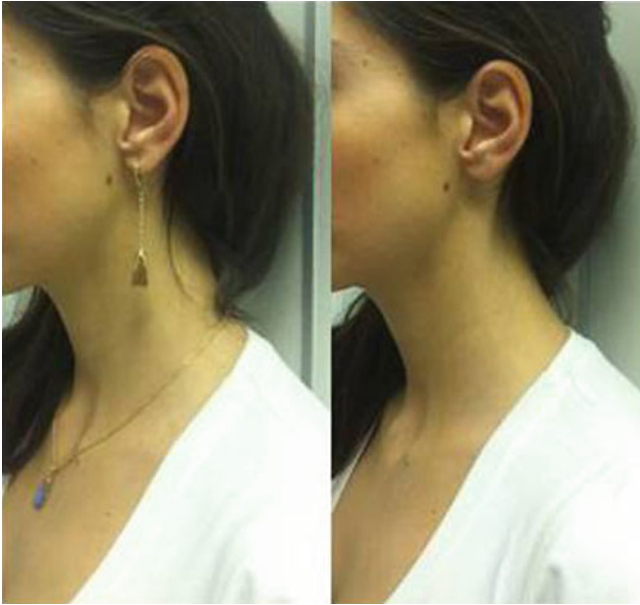
Fig. 4.1 Removal of metal objects
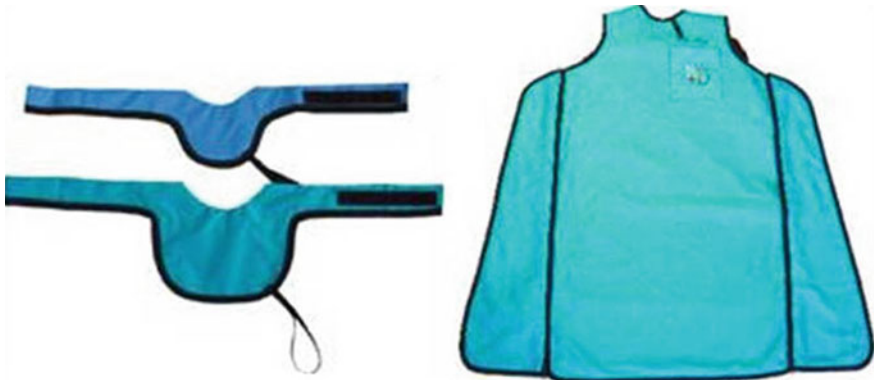
Fig. 4.2 Personal protective equipment

Fig. 4.3 Surgical template for dental implant

The patient should also wear surgical template that is prescribed by the dentist. They are acrylic radiotransparent masks that fit perfectly to the teeth and residual alveolar processes.

Radio-opaque markers are applied in specific places of the masks to facilitate information transfer from the images to the patient, in respect to implant orientation (Fig. 4.3).

For some procedures, scanning of the surgical template alone should be performed. This allows for digitally subtracting the images of the implant from the whole examination of the patient at later stages.

Step 3
Patient Positioning
Patient positioning is crucial to obtain adequate images. As acquisition time may be long, the patient should be positioned in a comfortable position, to avoid motion artifacts.

Patient has to:
- Maintain the position according to the relevant imaging system in use (Fig. 4.4);
- Grip both handles;
- Relax shoulders to allow for a complete movement of the swivel arm;
- Place the chin on the support, according to the relevant imaging system in use (Fig. 4.5).

Fig. 4.4 Correct position of the patient

Fig. 4.5 Position of the face

The same operation can also be done with the patient sitting on a chair/wheelchair, placing feet slightly forward (Fig. 4.6) to reduce motion artifacts.

Check the correct position of the patient using laser markers (Fig. 4.7).

Fig. 4.6 Correct position of the patient sitting on a chair/wheelchair

Fig. 4.7 Detail on the centering laser

Children undergoing this type of examination deserve a particular attention in terms of radioprotection. It has been estimated that radiation exposure during the first 10 years of life produce an overall risk of health detriment two to three times higher than that incurred between 30 and 40 years, and five to seven times higher than that incurred over 50. Thus, it is important to protect not only the gonads but also other radiosensitive tissues, such as bone marrow, breast, and thyroid. Approximately 35 % of red marrow is found in long bones and 40 % in the skull.

To reduce the dose, particular attention should be paid to acquisition data. Also, all cares should be taken to obtain a good scan at first attempt. As far as possible, cooperation of the young patient is crucial. The operators should speak to the child and to parents, explaining the procedure. The waiting room may be equipped with color furniture and toys suitable for different ages. Also, drawings and cartoons on the walls of the examination room may reduce fear and make the process easier. The examination should be performed as quick as possible. Also, remember how useful the so-called "positive reinforcement" is, i.e., continuous encouragement and confirmation that he is doing well during the examination. In some cases, presence of parents during examination may help.

4.2   Scanning Parameters

Examination duration, image quality, and radiation dose depend on the parameters of the scan. Thus, it is extremely important to take advantage of the features and benefits they bring in terms of quality and radiation protection.

Scanning parameters include:
1. *exposure parameters*
2. *geometric parameters*

The *exposure parameters* modulate the emission of radiations by the X-ray tube acting on different variables, such as:
- kilovolts (kV), measurement of the difference of potential between the anode and cathode;
- milliamperes (mA), a measure of the current intensity;
- scan time, expressed in seconds (s).

The X-ray beam has different characteristics depending on the value of these parameters. For example, higher values of kV produce beams with higher penetration potential, also increasing the radiation energy.

CBCT usually uses X-ray beams at high kilovoltage (around 100 kV), thus allowing for obtaining high-quality images. The operator can modify effectively the milliampere value and the acquisition time, that are interrelated in a parameter called milliamperes per second (mAs).

The use of appropriate exposure parameters is aimed at reducing the radiation dose delivered to the patient. On the other hand, increasing X-ray beam intensity and exposure time, image quality improves. Thus, a careful work must be done to optimize scan parameters to obtain the highest quality with the lowest radiation dose.

Each equipment has different software and settings. However, most systems can be customized to obtain excellent results. When setting up a new examination on the CBCT system, the "type of patient" in terms of body build (baby, boy, woman, man, robust man) should be chosen. While kV remain constant (usually around 96 kV), the system provides different values of amperage and exposure times for each type of patient. Another option for adjusting exposure settings (amperage and exposure times) can be done modifying the 'Resolution' parameter, that can be switched from "normal dose" to "low dose".

For example, in case of a child, a "low dose" scan decreases the acquisition time and this can help to reduce motion artifacts, whereas amperage and scan time reduction may be indicated in cases of female patients of childbearing age. Conversely, increase of milliamperes per second (mAs), switching the "normal dose" scan, can be used in case of robust men to obtain good image quality.

The *geometric parameters* allow for adjusting the volume of the body area to be examined according to clinical indication. In particular, it is important to set the correct width of scan volume, defined as "Field Of View" (FOV), which must contain the entire anatomical structure to be investigated and must be as small as possible in order to reduce the radiation dose. From a practical point of view, the choice of the appropriate geometrical parameters allows for focusing the examination not only on both dental arches or on one of them, but also on a single group of teeth or on temporomandibular joint.

With most equipments, the FOV can be adjusted with various settings:

Arches Dental study—setting of the "Diameter volume" (100 mm) and the "Height volume" (90 mm), suitable to fully include both dental arches. With the command "Arch Size" you can optimize the scan according to the type of the dental arch of the patient. The "Height volume" can assume values of 55 mm for the single arch (upper or lower) and 90 mm for the study of both arches.

Specific Anatomic Region study (incisor)—Choosing "Diameter volume" smaller, it is possible to focus the acquisition on the region of interest, based on the diagnostic question.

Temporomandibular joints study—for the examination of the temporomandibular joints (TMJ) the specific command ("side"), allows for choosing the side of interest, right or left.

Paranasal sinuses study—A wide FOV (230 mm) should be used to evaluate the paranasal sinuses. With the right devices for positioning, the volume of the sinuses can be acquired in a single scan. To acquire an entire skull volume, from the mandibular angle to the vertex, two different scans should be performed. Then, a specific software is able to merge the two scans using the "stitching" tool.

Prior to volume acquisition, a scout scan is performed. This allows for checking the correct positioning of the patient and to set up a correct scan protocol. During the scan, the operator should verify that the patient do not move from the assigned position nor he moves during the examination, as this may lead to artifact that may affect the final quality of the image (Table 4.1).

Table 4.1 Exposure (kV/mA/mAs/s) and geometrical parameters (volume scan) related to the radiation dose. Note that as the parameters are optimized, a remarkable dose reduction can be achieved

Low dose	FOV × Height	kV/mA/mAs/s	Dose (μSv)
Adult teeth	50 × 55 mm	96/6/29.0/4.8	55
Adult teeth	100 × 90 mm	96/6/34.2/5.7	159
Child teeth	42 × 50 mm	96/4/19.3/4.8	29
Child teeth	85 × 75 mm	96/4/22.8/5.7	86
Skull—lower	230 × 160 mm	96/6/54.2/9	156
Skull—whole	230 × 260 mm	96/6/108/18	196
Normal/high resolution	FOV × Height	kV/mA/mAs/s	Dose (μSv)
Adult teeth	50 × 55 mm	96/10/121/12	192
Adult teeth	100 × 90 mm	96/10/121/12	490
Child teeth	42 × 50 mm	96/8/96.6/12	122
Child teeth	85 × 75 mm	96/8/96.6/12	330
Skull—lower	230 × 160 mm	96/10/90.4/9	260
Skull—whole	230 × 260 mm	96/10/181/18	324

Suggested Readings

Baba R, Ueda K, Kawai H, Kuba A, Takagi H (1999a) Development of three- dimensional imaging method with cone-beam X-ray. MEDIX 31:42–47

Baba R, Ueda K, Kuba A, Kohda E, Shiraga N, Sanmiya T (2001) Development of a subject-standing-type cone-beam computed tomography for chest and orthopedic imaging. Front Med Biol Eng 11:177–189

Baba R, Ueda K, Kadomura T (2002) High-resolution FPD cone-beam CT for dental and orthopedic surgery. Radiology 225(P):194 (Abstr)

Baba R, Ueda K, Okabe M (2004) Using a flat-panel detector in high resolution cone beam CT for dental imaging. Dentomaxillofacial Radiol 33:285–290

Baba R, Ueda K, Ueki H, Umetani K (1999b) Ellipsoid scan: chest cone-beam CT with a large ellipsoidal view field using a 16-inch X-ray image intensifier. Proc SPIE 3032:349–357

Colbeth RE, Allen MJ, Day DJ, Gilblom DL, Harris R, Job ID et al (1998) Flat panel imaging system for fluoroscopy applications. Proc SPIE 3336:376–387

Granfors PR, Aufrichtig R (2000) Performance of a 41 £ 41-cm^2 amorphous silicon flat panel X-ray detector for radiographic imaging applications. Med Phys 27:1324–1331

Maki K, Usui T, Kubot M, Nakano H, Shibasaki Y, Araki K, et al (2002) Application of cone-beam X-ray CT in dento-maxillofacial region. Proc CARS 2002:1–5

Seo K, Yamamoto K, Ueno K, Tanaka K, Matsuoka M, Okabe K et al (2002) Development of dentomaxillofocial conebeam X-ray CT system model CB MercuRay. MEDIX 37:40–45

Sukovic P (2002) Cone beam computed tomography in craniofacial imaging. COAST 9 (Abstr)

Sukovic P, Brooks S, Perez L, Clinthorne NH (2001) DentoCATe—a novel design of a cone beam CT scanner for dentomaxillofacial imaging: introduction and preliminary results. Proc CARS 2001:659–664

Yamada S, Umazaki H, Takahashi A, Honda M, Shiraishi K, Rudin S et al (2000) Image quality evaluation of a selenium-based flat-panel digital X-ray detector system based on animal studies. Proc SPIE 3977:429–436

Post-Processing, 2D/3D Reformat, and Dedicated Software for Implantology

5

Riccardo Sartoris and Pietro Caruso

Modern odontomaxillofacial imaging techniques are mainly represented by the digital evolution of conventional 2D modalities and by the multidimensional representation achieved through multiplanar reformats of CT scan.

The configuration of the dental arches is characterized by a 180° curvature. The particular arrangement of dental elements can be represented without overlap on a single plane using orthopantomography.

The development of software to create 2D/3D reformatted multiplanar images from CBCT data has allowed for representing correctly also the maxillary bone.

CBCT has revolutionized dental and maxillofacial radiology, making 3D reconstruction of anatomical structures possible. Such method finds indications, as well as in the field of implantology and maxillofacial surgery, in the orthodontic field, in the study of held, ectopic, or supernumerary teeth and it is able to show the quantity and the quality of the available bone in perspective of an orthodontic mobilization.

CBCT scanners generate a huge amount of isotropic data that are stored in a particular format (DICOM); these data can be used to obtain 3D anatomical images on different planes (multiplanar reconstruction—MPR).

With further processing, automatically performed by the software, it is possible to create anatomical 3D images and multiplanar reconstructions.

In addition, using simple tools, it is possible to:
- Create panoramic images of the upper and lower dental arch
- Locate and depict the course of the mandibular nerve

R. Sartoris (✉)
University of Genoa, Via L.B. Alberti 4, 16100, Genoa, Italy
e-mail: riccardo.sartoris@hotmail.it

P. Caruso
Ospedale Evangelico Internazionale—Unit of Radiology, Salita Superiore San Rocchino 31A, 16100 Genoa, Italy
e-mail: pietro.caruso@oeige.org

- Accurately display every single dental element separately
- Effectively support implant surgery

These softwares are provided by diagnostic imaging companies or they are free downloadable from the web. Each software has its graphical interface but commands and applications are very similar one to the other. Thus, the indications provided in the next pages can be easily adapted to any software.

The graphical interface of these software is constituted by a set of windows which allows the operator for analyzing the images and provide 2D and 3D reconstructions. An example of the windows is as follows:

- Volumes: examination preview of the chosen patient
- Explorer: shows 2D images and 3D reconstruction
- Overview: allows for creating panoramic images
- Transverse sections: shows the individual transverse images and allows for creating the path of the mandibular nerve

5.1   Planar Images and 3D Rendering

The study begins with examination choice through the selection of patient demographics, time, and date of the examination.

The first analysis takes place through a screen containing three windows with planar images (Coronal, Sagittal, Axial) and a window with 3D reconstruction. (Fig. 5.1).

Operations that can be done at this level allow for improving the quality of 2D and 3D images in order to optimize their use.

Scroll bars can be used to browse through images, each linked to a type of section. The visual reference is shown by lines on complementary planes.

Focus On

Coronal section: vertical plane that extends from left side to right side (or vice versa) and that divides the skull in front and rear portions.

Axial section: sections of the axial plane. These sections correspond to horizontal cut of the reconstructed volume.

Sagittal section: vertical plane which extends from the front part to the rear one (or vice versa) and that divides the skull in right and left portions Fig. 5.2.

The operator can move and rotate the image plane clockwise/counterclockwise; the software records these shifts and changes the images of the other two planes in order to have a proper centering in space. The operator can also scroll through each single image that compose the exam.
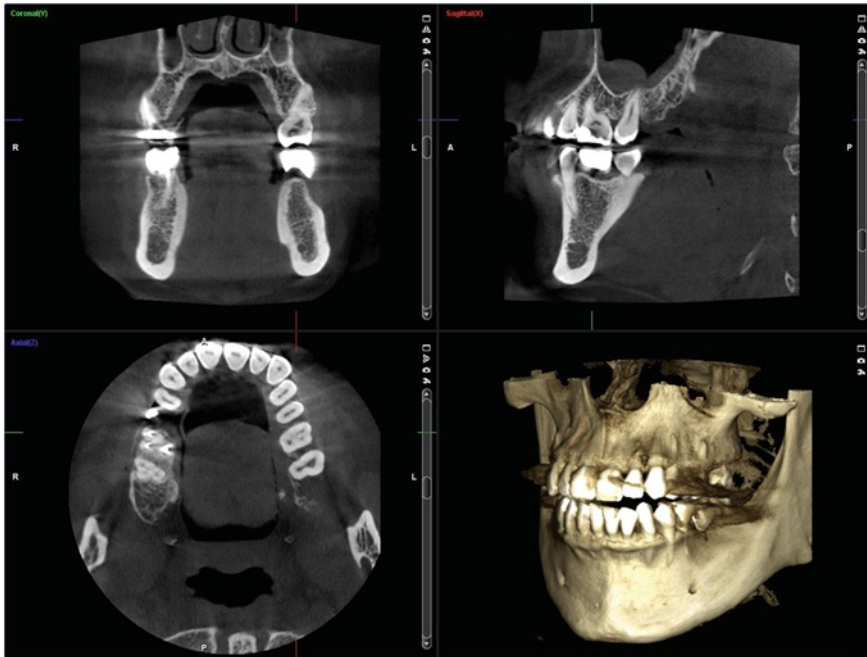
Fig. 5.1 Explorer window
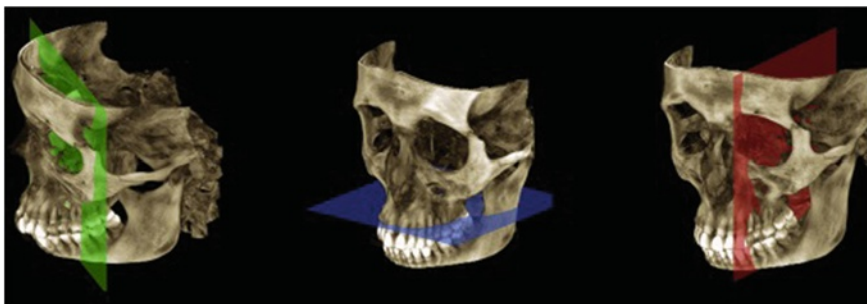
Fig. 5.2 Anatomical planes

The operator can adjust the properties of planar images by modifying saturation, contrast, and, brightness; it is also possible to change slice thickness and crop images to highlight a specific area.

The volume cutout applied to 3D rendering is applied on planar images but affects only the three-dimensional reconstruction; the result is a 3D volume that recreates the area of interest of the patient, thus promoting its clinical focus.
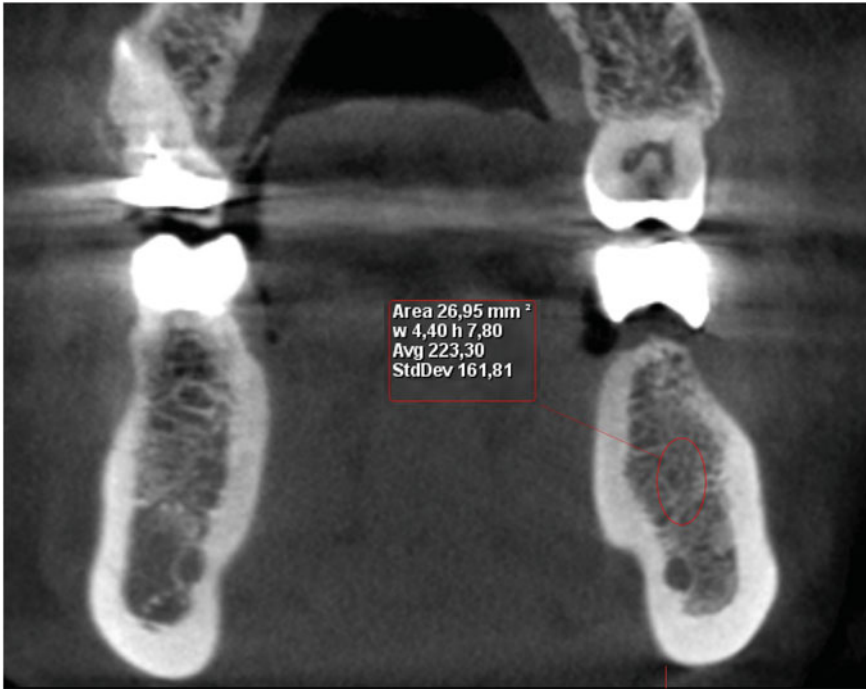
Fig. 5.3 Bone density measurement

Bone density can be measured in a circumscribed area using a circular tool that creates a region of interest (ROI), that can be placed on any projection.

The measurement is given in Hounsfield Units. However, due to the intrinsic property of CBCT, the densitometric result may not be as precise as what would be obtained by CT (Fig. 5.3).

Focus On
Different systems of analysis of the densitometric data have been proposed in order to choose the best screws for implants: weak bone requires thin but long screw, while a bone in good condition can be implanted with shorter screws.

The most widely used classification is by Misch, which includes four density classes (D1–D4) that indicate a decreasing bone demineralization:
D1: thick cortical and dense cancellous bone
D2: thick cortical and fenestrated cancellous bone
D3: thin cortical and dense cancellous bone
D4: thin cortical and fenestrated cancellous bone

Currently, the Misch classification is highly debated. Some authors proposed a correspondence with the values of Hounsfield Units, while others have questioned the validity of the classification.

The 3D reconstruction can be navigated separately from the planar representations, in order to permit a full exploration of the three-dimensional model without changing the axial images. The exploration of the rendering happens through rotations and enlargements.

A number of 3D image adjustments are possible, which allow for creating high-quality models in a few steps. Adjustments can be made in respect to image parameters (contrast, brightness) and to series of advanced tools, such as the choice of lighting source (to eliminate shadows in areas of interest), the transformation from isometric model to model in perspective, or anti-aliasing to smooth the edges (Fig. 5.4).

Finally, it is possible to highlight on the model the axial planes (Fig. 5.5).

Fig. 5.4 Advanced graphics settings
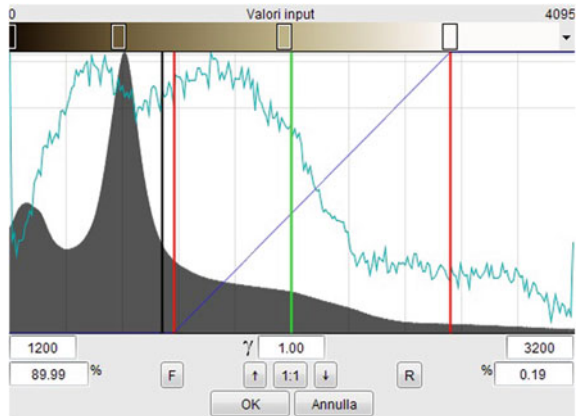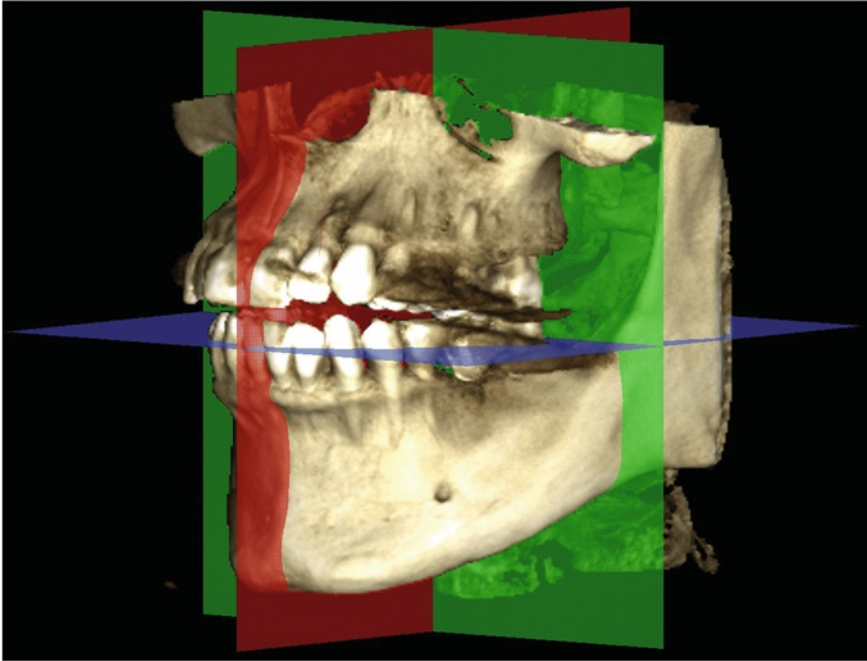
Fig. 5.5 Anatomical planes on the 3D model

5.2   Dental Arch and Panoramic Images

The second phase of the study is concerned with the analysis of panoramic images.

Panoramic images are sections perpendicular to the axial plane, typically designed to represent the entire dental arch (preferably to include the temporo-mandibular joints).

The panoramic reconstruction is most familiar for dentists, as it resembles orthopantomography.

The importance of panoramic view, besides giving the spatial reference on the frontal plane of the paraxial extracted, is to allow for the visualization of the teeth completely, in the position they occupy in the dental arches, and in the bone structure of the jaw, seen as a "classic" orthopantomography.

Normally is displayed a screen containing three windows: (Fig. 5.6).

- Sagittal window, where can be displayed images in sagittal sections
- Axial window, where images can be viewed in axial slices
- Panoramic window, where you can view the generated "panoramic" image (Figs. 5.7, 5.8, 5.9).
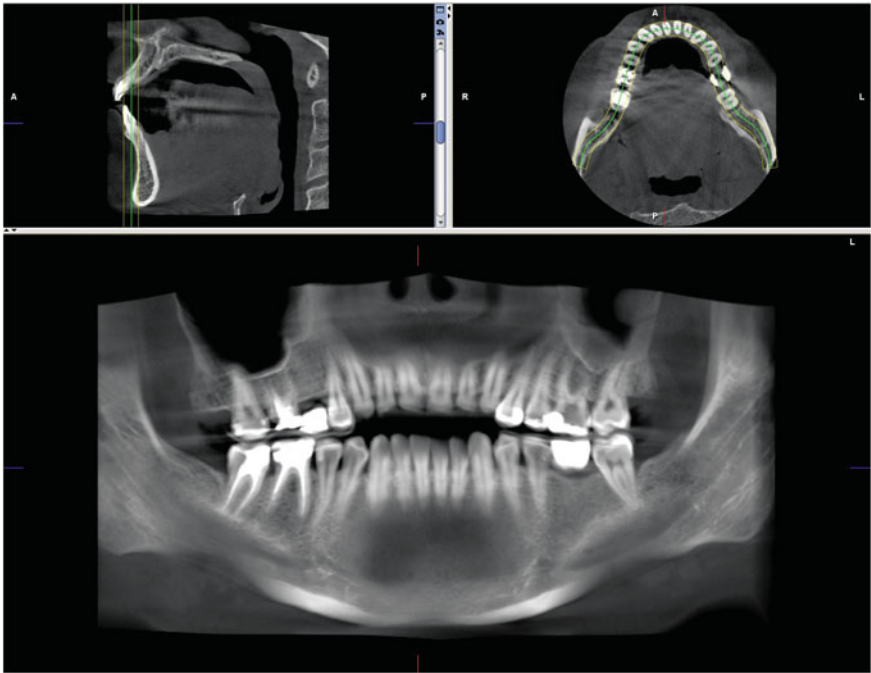
Fig. 5.6 Panorex window

Fig. 5.7 The operator clicks
with the mouse at the starting
point of the curve, drag and
click with the *left* button at
the points where it is
necessary to deviate and to
curve the track. *Note* the
curve should start at the
ascending branch of the
mandible. (step 1)
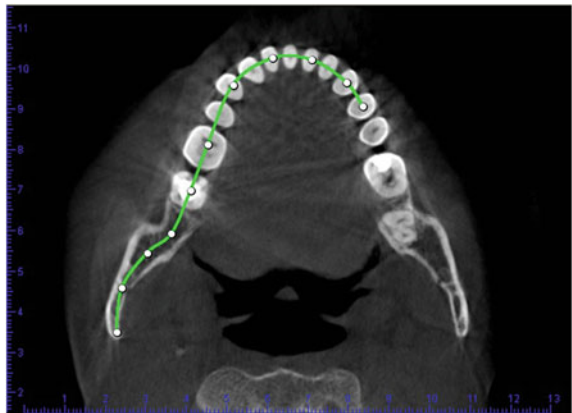
Fig. 5.8 Set the final point of the curve, it will be automatically saved and the operator can determine the slice thickness to find an adequate reconstruction overview. (step 2)
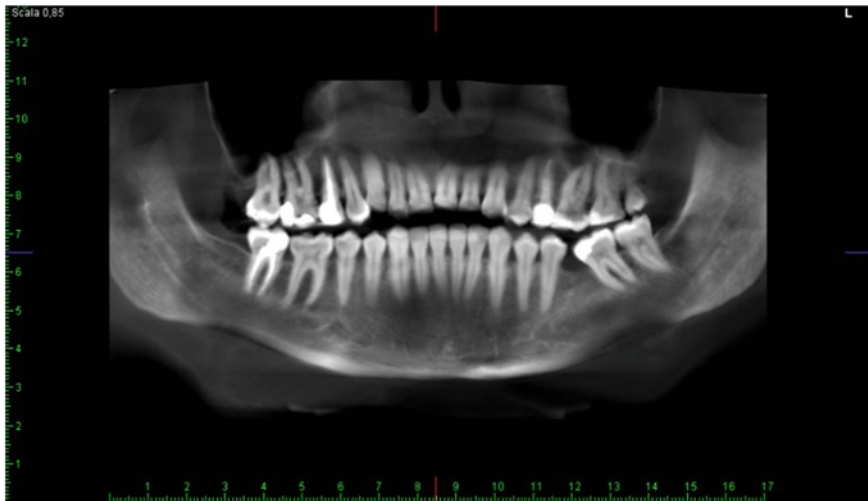
Fig. 5.9 Finally, the "panoramic" picture is completed. (step 3)

5.3   Cross-Sections and Mandibular Nerve Evaluation

The cross-section, also called para-axial image, is an image perpendicular to the plane reconstructed along the dental arch.

The image height is the height of the acquired volume.

The para-axial image represents the real innovation in CT dental examination; this provides also the depth of the image, thus allowing for studying the dental arch on a third dimension. These images are 0.5–1 mm thick slices of the arch, including the tooth, the mandibular nerve, and the alveolar bone (Fig. 5.10).
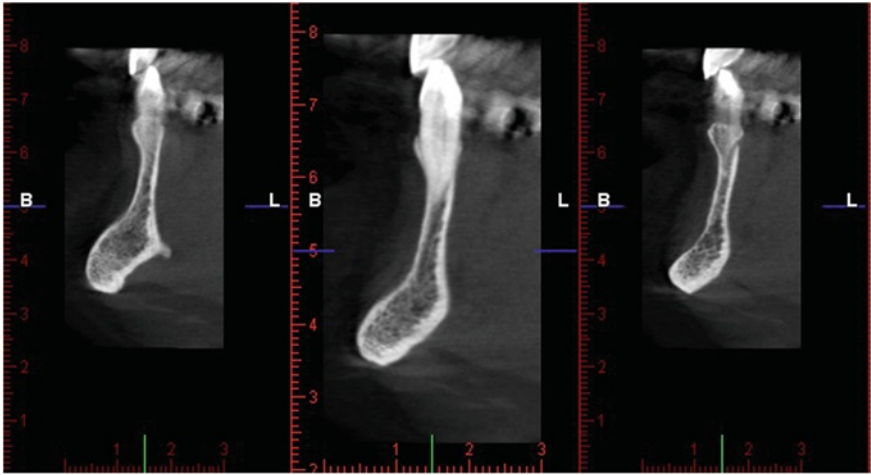
Fig. 5.10 Cross-section images
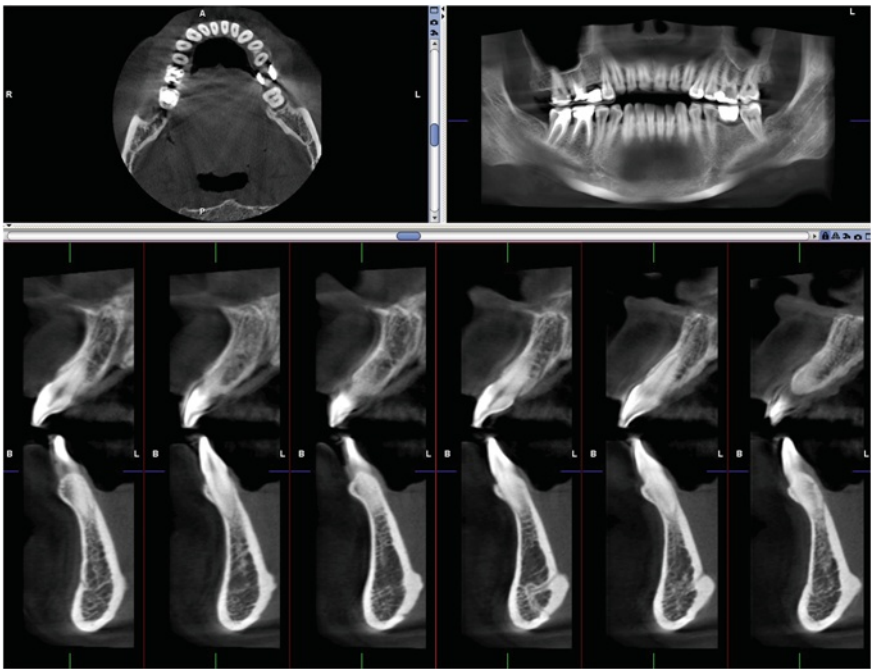
Fig. 5.11 Cross-section window
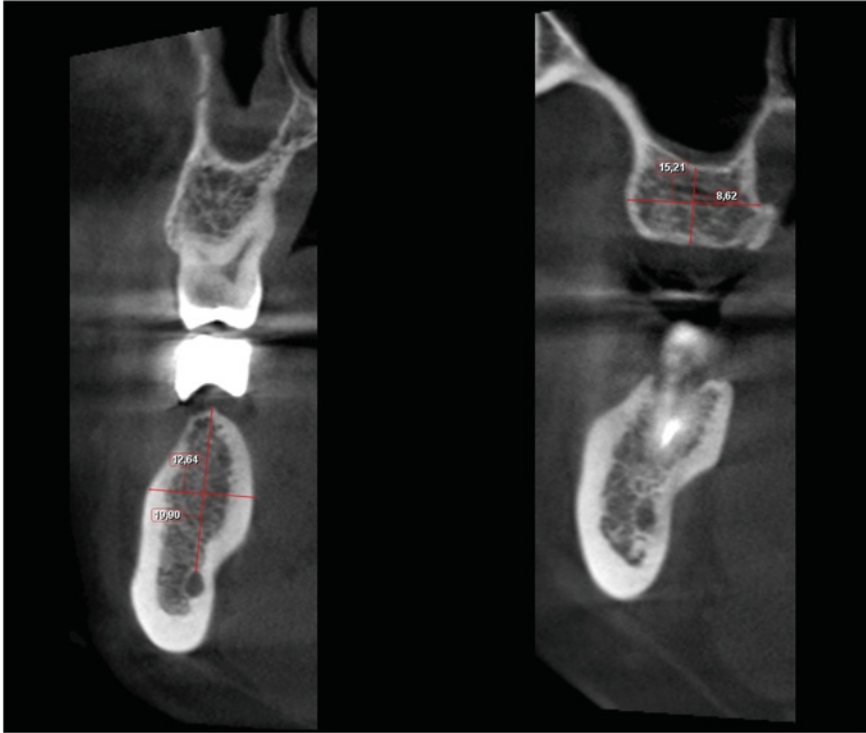
Fig. 5.12 Thickness and height measurement of the alveolar crest

Images are typically displayed on three windows: (Fig. 5.11).
- Axial window, in which images can be seen in axial slices
- Panoramic window, in which panoramic images can be seen
- Cross window, in which para-axial images can be seen

Similarly to panoramic reconstructions, the software automatically generates para-axial reconstructions from axial image. Even in this case, the operator can manually select one axial image and draw the curve on which the software will rebuild the final image.

Once the curve is finished, cross-sections to evaluate individual tooth in relation to the periodontium and the surrounding bone structures can be seen; browsing through the cross-sectional images, the exact location of these images will be displayed in the other windows.

These reconstructions are crucial, as the dentist works to make precise measurements for implantologic purposes (Fig. 5.12).
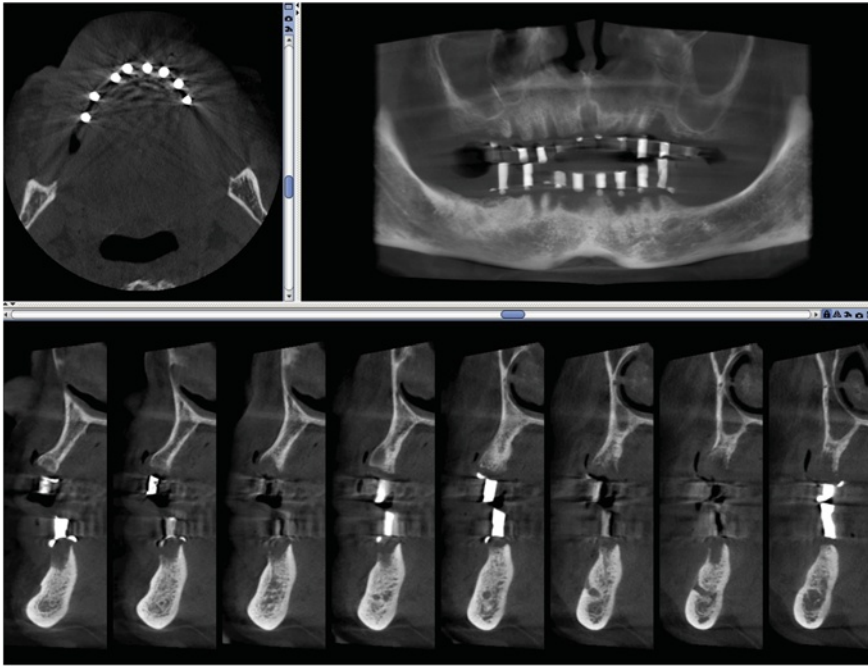
Fig. 5.13 Landmarks provided by the dentist

The operator can then measure both the thickness and the height of the alveolar crest in different points in which the implant screw should be placed; particular attention must be paid to the distance from the floor of the maxillary sinus for the upper jaw and the mandibular canal for the lower jaw.

These measurements can be made in respect of landmarks provided by the dentist (Fig. 5.13).

Some software also allows for inserting virtual images of the various types of implants to simulate the final result.

For a correct evaluation of the implant site, it is important to highlight the course of the maxillary canal, both in the axial images and in 3D reconstruction, to prevent damage to the nerve that runs in the channel.

The operation is similar to that performed to create panoramic reconstructions, i.e., draw a line passing through the mandibular canal on cross-sectional or on panoramic images (Figs. 5.14, 5.15, 5.16, 5.17, 5.18).
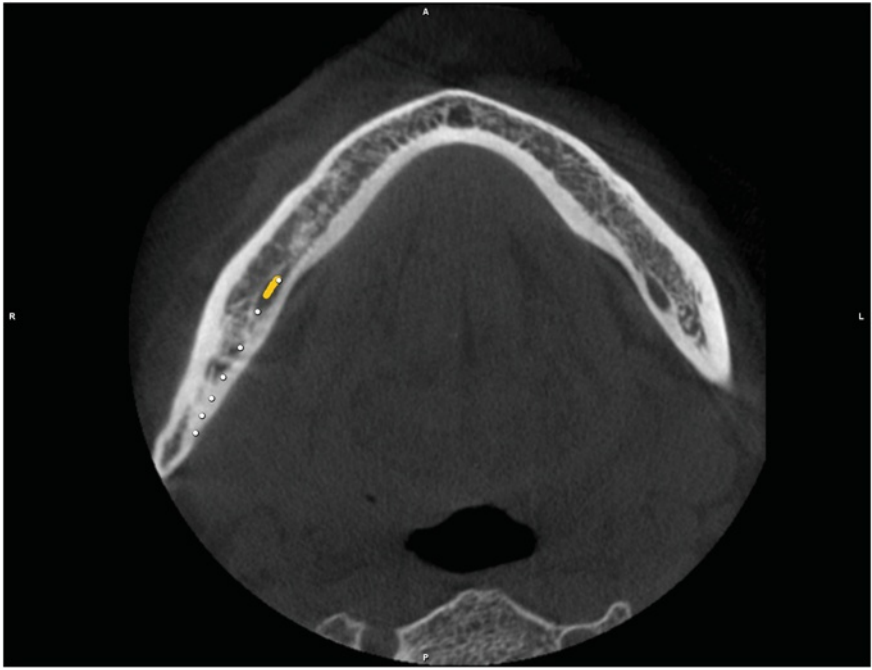
Fig. 5.14 The creation process takes place via the insertion of a sequence of points, along the course of the channel, which are automatically connected to each other by the software; these points can be taken on both the MPR (usually axial) and in the paraxial images. (step 1)
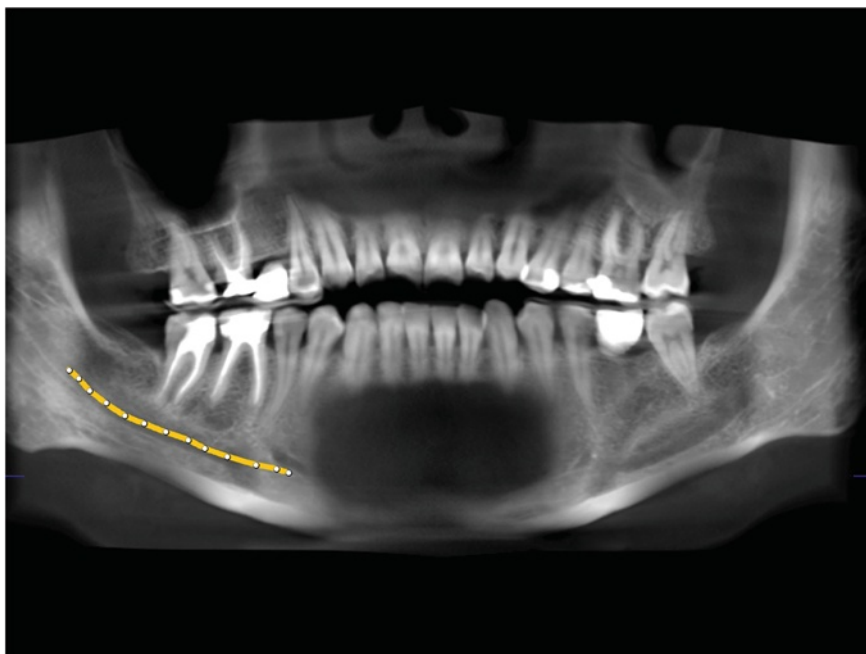
Fig. 5.15 These points are printed automatically on all projections and, simultaneously, appears on the panoramic image the nerve, on which you can apply any changes to the track. (step 2)
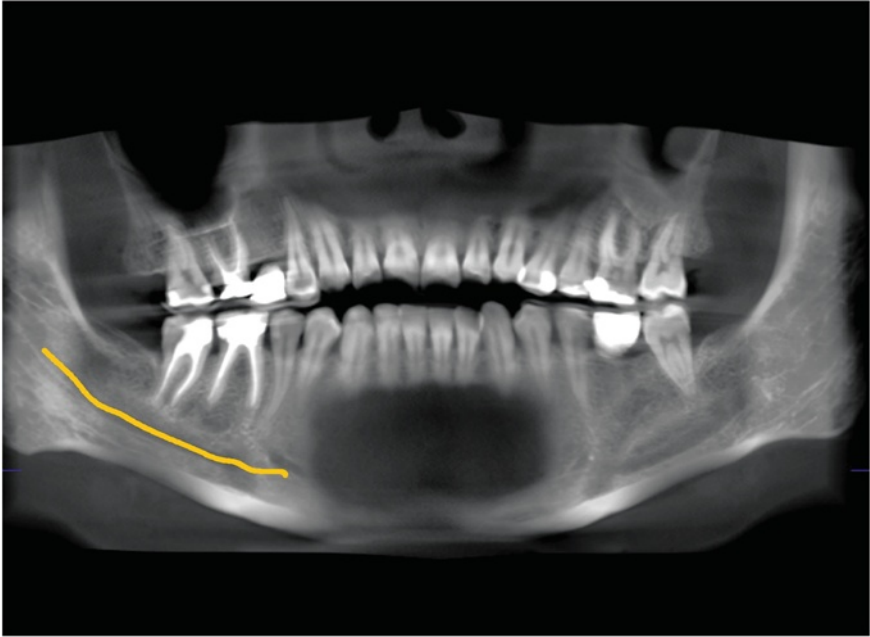
Fig. 5.16 The course of the maxillary nerve, when completed, will be displayed in all the windows, and you can bring this out whenever necessary. (step 3)
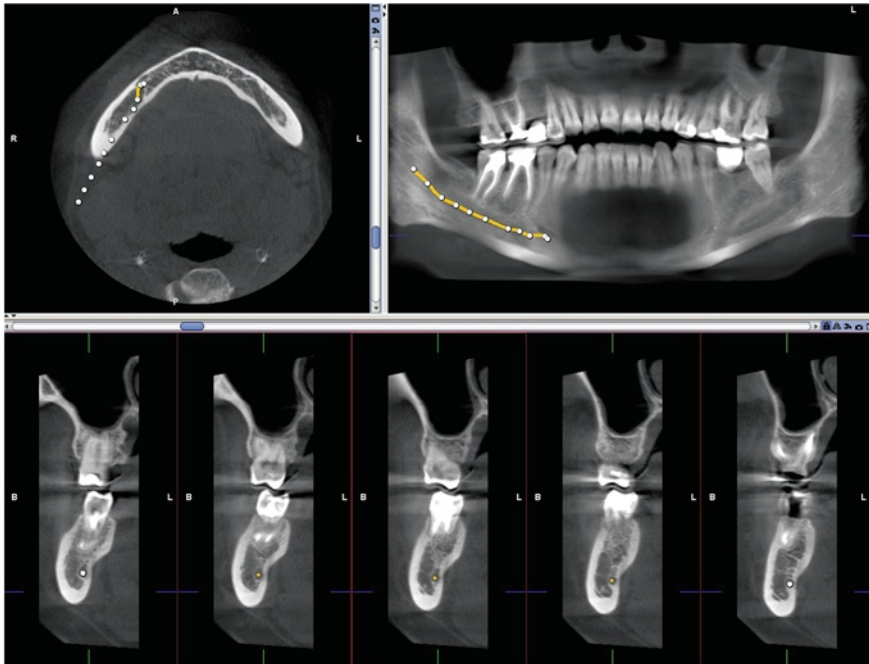
Fig. 5.17 Nerve window
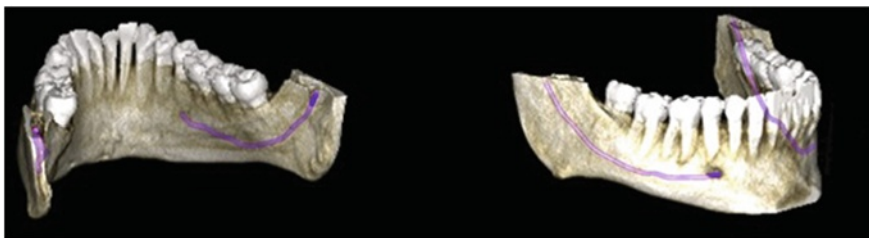
Fig. 5.18 Nerve 3D rendering

Further Readings

Chadwick JW, Lam EW (2010) The effects of slice thickness and interslice interval on reconstructed cone beam computed tomographic images. Oral Radiol Endod 110(4):e37–e42. doi:10.1016/j.tripleo.2010.05.008

Correa LR, Spin-Neto R, Stavropoulos A, Schropp L, da Silveira HE, Wenzel A (2013) Planning of dental implant size with digital panoramic radiographs, CBCT-generated panoramic images, and CBCT cross-sectional images. Clin Oral Implants Res. doi:10.1111/clr.12126

Garg AK (2007) Dental implant imaging: TeraRecon's dental 3D cone beam computed tomography system. Dent Implantol Update 18(6):41–45

Oliveira-Santos C, Capelozza AL, Dezzoti MS, Fischer CM, Poleti ML, Rubira-Bullen IR (2011) Visibility of the mandibular canal on CBCT cross-sectional images. J Appl Oral Sci 19(3):240–243

Orentlicher G, Abboud M (2011) The use of 3-dimensional imaging in dentoalveolar surgery. Compend Contin Educ Dent 32(5):78–80, 82, 85–86

Patel S, Dawood A, Ford TP, Whaites E (2007) The potential applications of cone beam computed tomography in the management of endodontic problems. Int Endod J 40(10):818–830. Epub 2007 Aug 14. Review

Periago DR, Scarfe WC, Moshiri M, Scheetz JP, Silveira AM, Farman AG (2008) Linear accuracy and reliability of cone beam CT derived 3-dimensional images constructed using an orthodontic volumetric rendering program. Angle Orthod 78(3):387–395

Santos Junior O, Pinheiro LR, Umetsubo OS, Sales MA, Cavalcanti MG (2013) Assessment of open source software for CBCT in detecting additional mental foramina. Braz Oral Res

Cases Presentation and Discussion

6

Silvia Perugin Bernardi, Chiara De Angelis
and Orlando Di Donato

6.1 Paranasal Sinuses

Case No. 1
- 51-year-old male.
- Clinical notes:
  - Difficulty in breathing during the night
  - Liquid sliding from nose to throat (Fig. 6.1).

S. Perugin Bernardi (✉)
Post Graduate School of Radiodiagnostic, University of Genoa,
Via L.B. Alberti 4, 16100, Genoa, Italy
e-mail: silvy-86-@hotmail.it

C. De Angelis
Private Practitioner, Via Piave, 20B/12, 16145, Genoa, Italy
e-mail: dott.ssachiara@libero.it

O. Di Donato
Post Graduate School of Radiodiagnostic, University of Naples,
Via Pansino 5, 80131, Naples, Italy
e-mail: orlandodd@hotmail.com

Fig. 6.1 CBCT coronal (**a**), right and left sagittal (**b**, **d**) and axial (**c**) sections showing massive osteolysis of maxillary sinus floor in the molar region (*thin arrow*). Right and left maxillary sinuses were partially opacified

Case No. 2
- 50-year-old male.
- Clinical notes:
  - Difficulty in breathing,
  - Headache,
  - Nasal congestion,
  - Frequent sinusitis (Figs. 6.2 and 6.3).
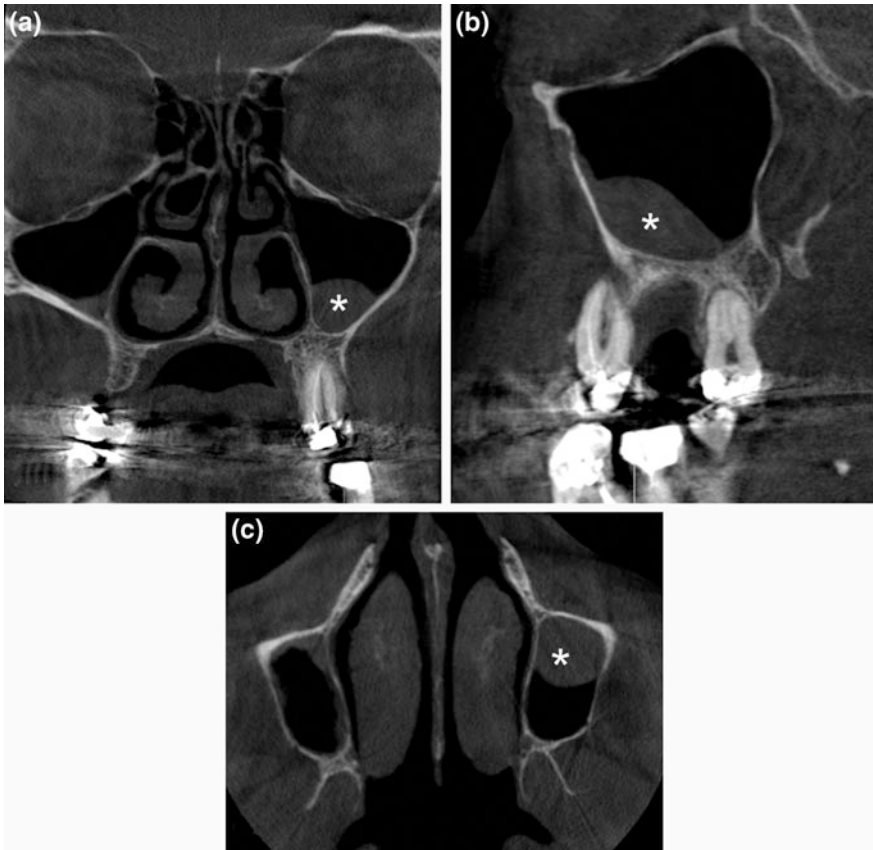
Fig. 6.2 CBCT coronal (**a**), sagittal (**b**) and axial (**c**) sections demonstrating mucosal thickening (*) specially in the right maxillary sinus. Note the right and left draining channels (ostium) are opened
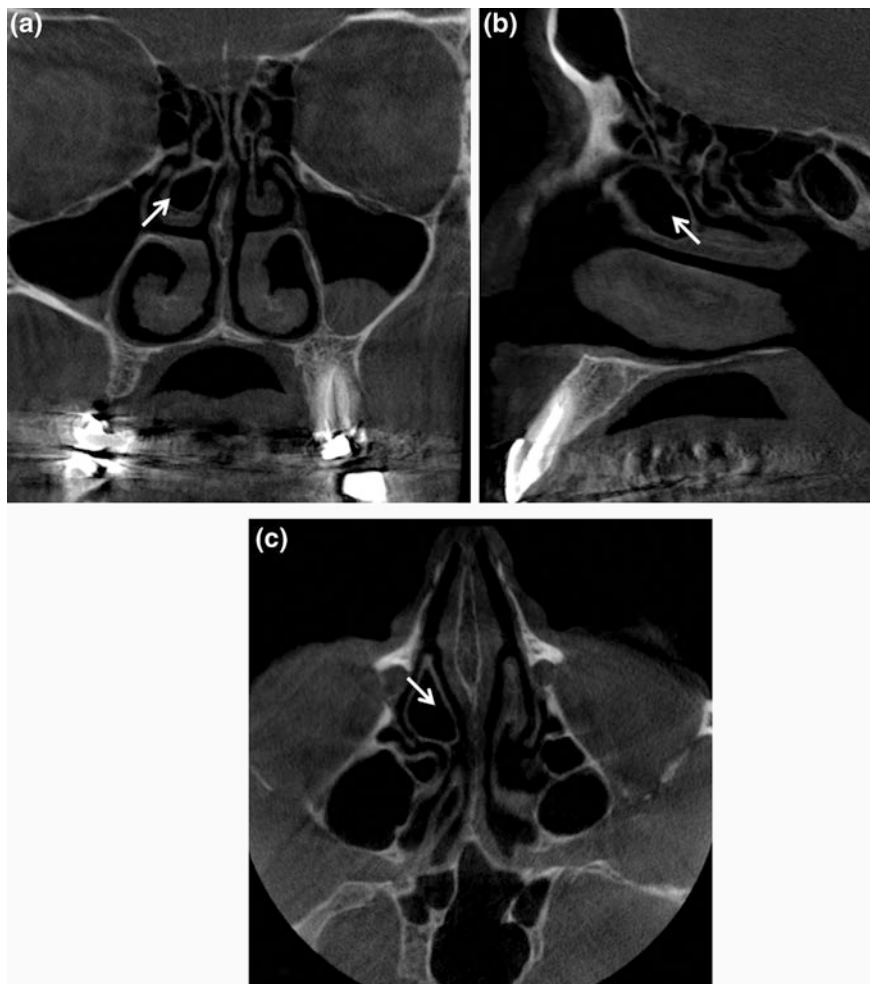
Fig. 6.3 CBCT coronal (**a**), sagittal (**b**) and axial (**c**) sections showing the pneumatisation of the right middle turbinate also known as concha bullosa (*thin arrow*) which can potentially narrow the middle meatus. Note that there is preservation of the air channel between the concha and the nasal septum. Severe deviation of the nasal septum with double curve can be seen

Case No. 3
- 66-year-old female.
- Clinical notes:
  - Headache
  - Chronic upper respiratory tract inflammation for 5 years
  - Therapy with antibiotics and mucolytics, but the problem persists (Fig. 6.4).
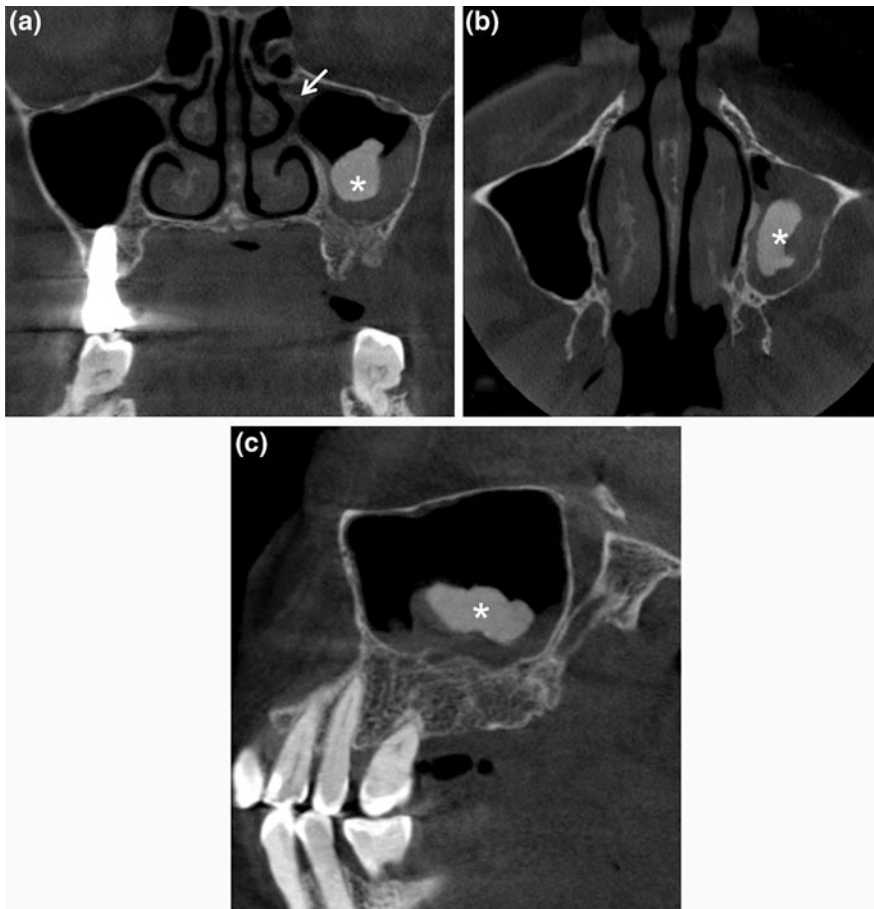
Fig. 6.4 CBCT coronal (**a**) axial (**b**) and sagittal (**c**) sections showing irregular calcification tissue (*) at the center of the opacified left maxillary sinus. Note that the omolateral draining channels (ostium) is not preserved (*thin arrow*)

> **Case No. 4**
> - 43-year-old male.
> - Clinical notes:
>   – Nasal congestion
>   – Headache
>   – Facial tenderness, pressure, and pain (Fig. 6.5).
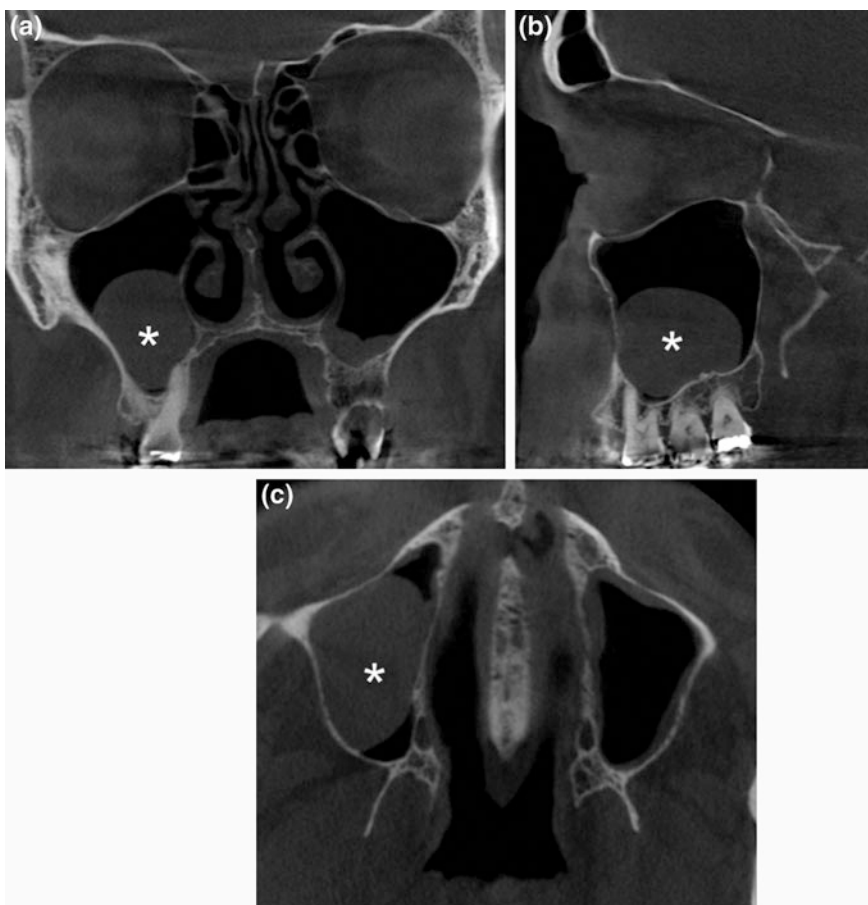
Fig. 6.5 CBCT coronal (**a**), sagittal (**b**), and axial (**c**) sections demonstrating extensive soft tissue inflammation in the right maxillary sinus that appears like an antral mucosal pseudocyst, also called mucoceles (*) and a thin mucosal thickening on the floor of left maxillary sinus. Also note that the nasal septum is deviated with convexity to the right

Case No. 5
- 32-year-old male.
- Clinical notes:
  - In anamnesis allergy and bronchial asthma
  - Headache
  - Nagging pain of the teeth in the left maxilla (Fig. 6.6).
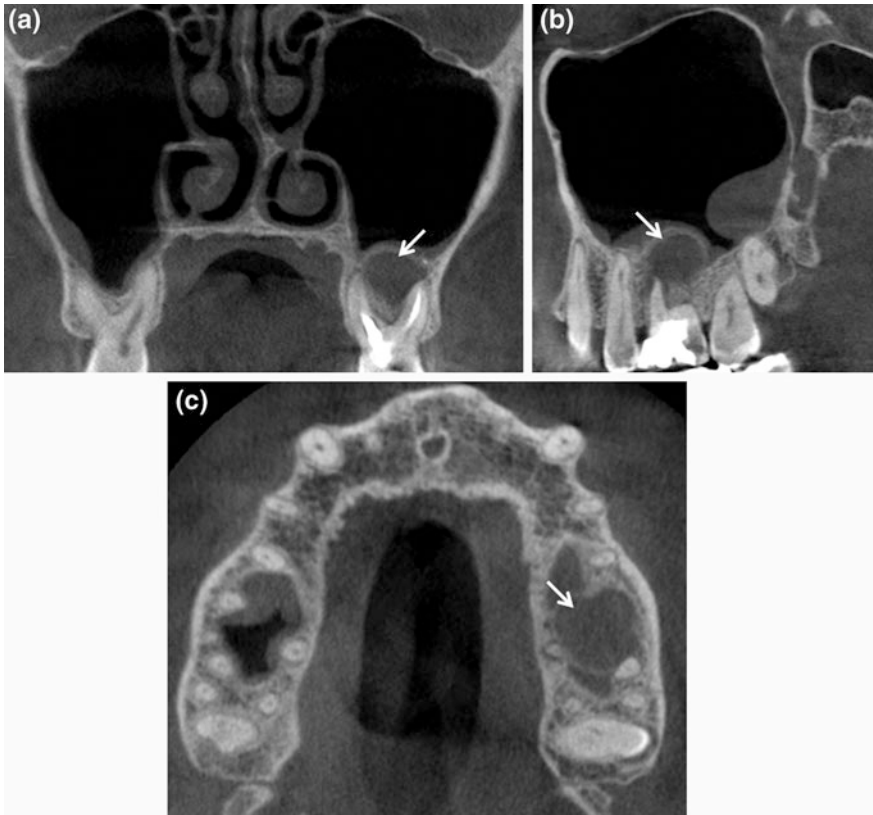
Fig. 6.6 CBCT coronal (**a**), sagittal (**b**) and axial (**c**) scans demonstrating presence of odontogenic sinusitis in left paranasal sinus (*thin arrow*). Note the reactive bone formation within the sinus and the associated mucosal thickening

6.2   Inflammatory Diseases

Case No. 6
- 34-year-old male.
- Clinical notes:
  - Asymptomatic patient
- Radiopaque lesion found during a routine orthopantomography (Figs. 6.7 and 6.8).
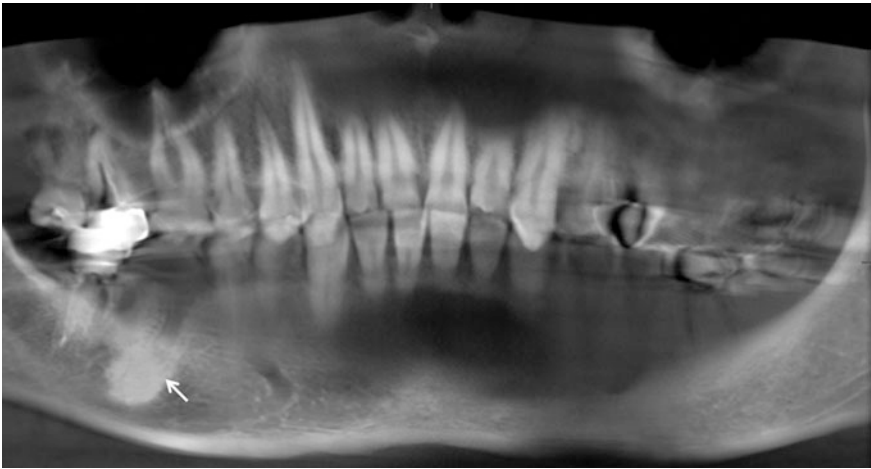
Fig. 6.7 CBCT panorex showing bone radiopacity in correspondence of 46 extracted (*thin arrow*). It seems a periapical inflammatory disease like condensant osteitis
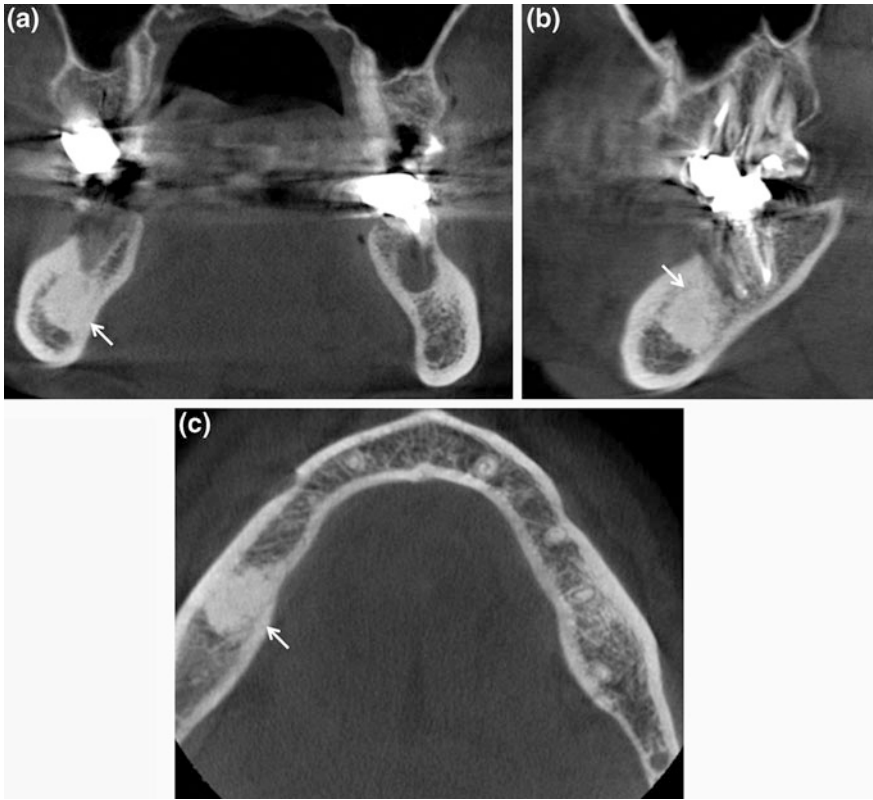
Fig. 6.8 CBCT coronal (**a**), sagittal (**b**) and axial (**c**) scans demonstrating, in the right posterior mandible, at the site of 46 extracted, a bone sclerosis that confirms the diagnosis of condensant osteitis (*thin arrow*)

Case No. 7

- 42-year-old male.
- Clinical notes:
  - Persistent pain in 16–17 area, even after root canal therapy (Figs. 6.9 and 6.10).
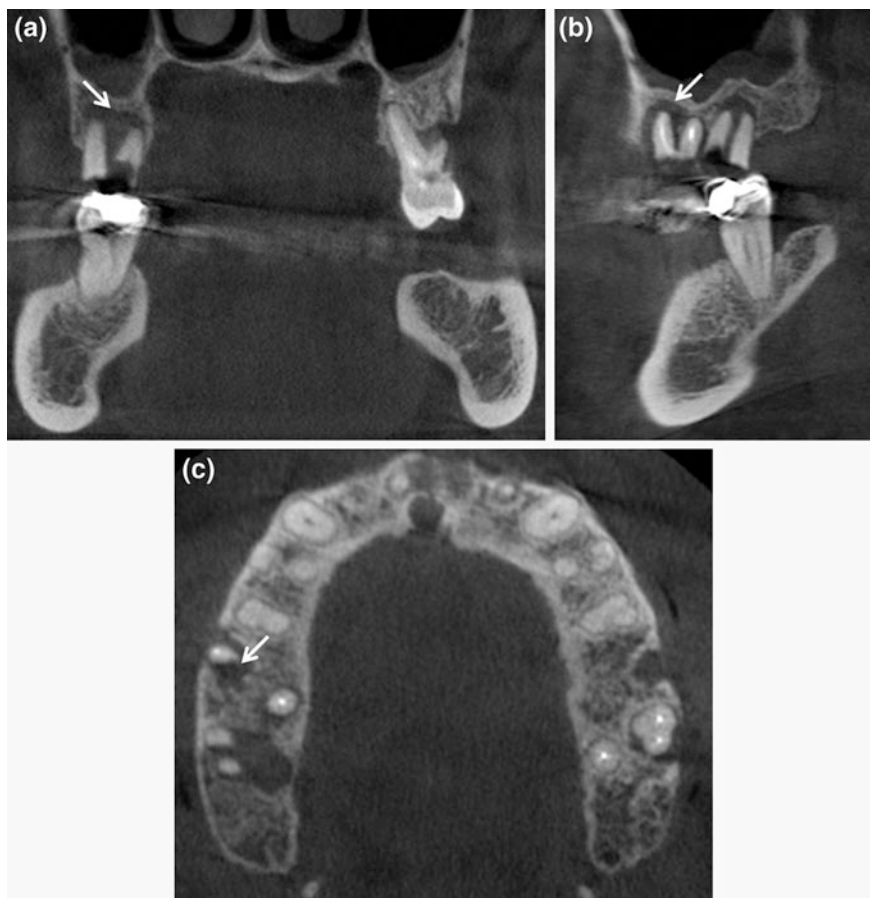
Fig. 6.9 CBCT coronal (**a**), sagittal (**b**) and axial (**c**) sections showing a wide radiolucent periradicular area dependent to the element 16 surrounding the mesial root (*thin arrow*). The radiographic signs suggest periradicular periodontitis
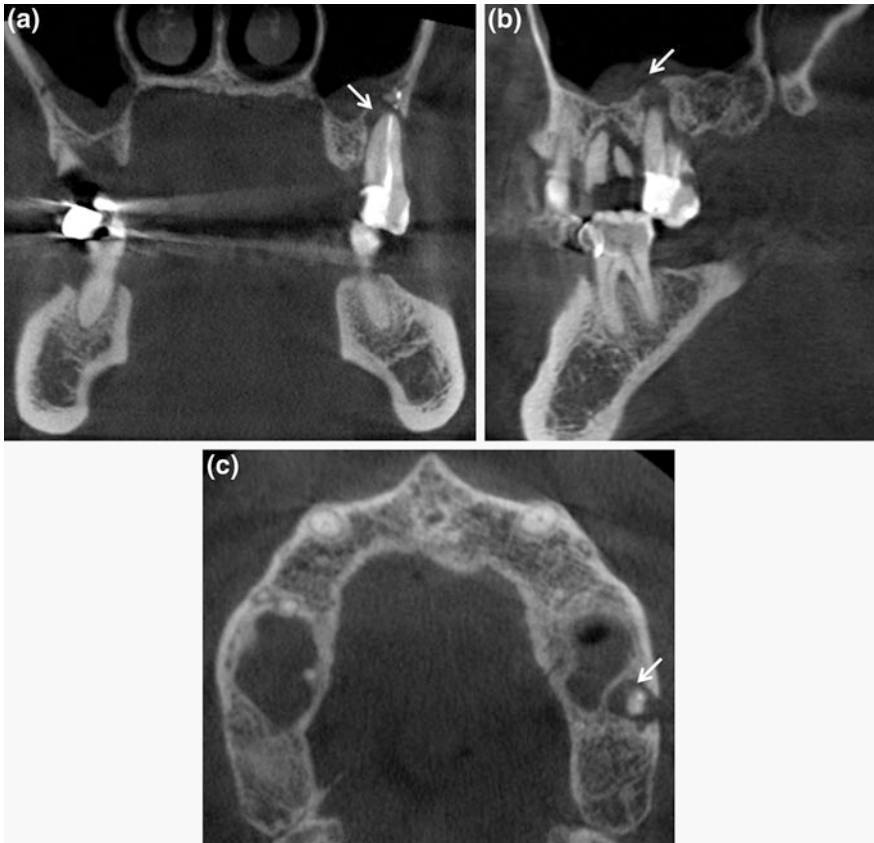
Fig. 6.10 CBCT coronal (**a**), sagittal (**b**) and axial (**c**) sections demonstrating the presence of an extensive periradicular lesion associated with tooth 27 (*thin arrow*). Note the degree of root resorption that determinate a periapical osteolysis

Case No. 8
- 58-year-old male.
- Clinical notes:
  - Pain after root canal therapy of 45
  - Large spectrum antibiotic therapy (Fig. 6.11).
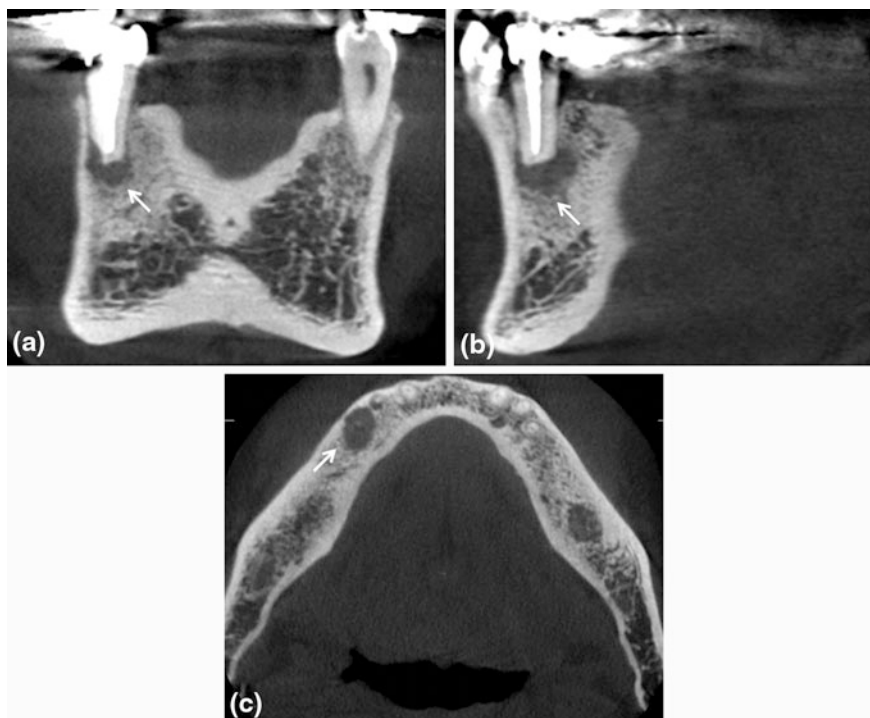
Fig. 6.11 CBCT coronal (**a**), sagittal (**b**) and axial (**c**) sections evidencing an area of low density at the apex of 45 tooth (*thin arrow*). It is a chronic periapical osteoperiostitis, or "halo lesion" determining displacement of the periosteum

Case No. 9
- 24-year-old male.
- Clinical notes:
  - Pain on the I quadrant, in 16–17 area, worsening with hot food and/or drinks and lying
  - Sometimes right eye swollen (Figs. 6.12 and 6.13).

Fig. 6.12 CBCT panorex: well-defined, corticated, wide ovoid radiopaque area extending from 16 to 17 tooth (*). Note the conservative restoration of 25, 36 and 46
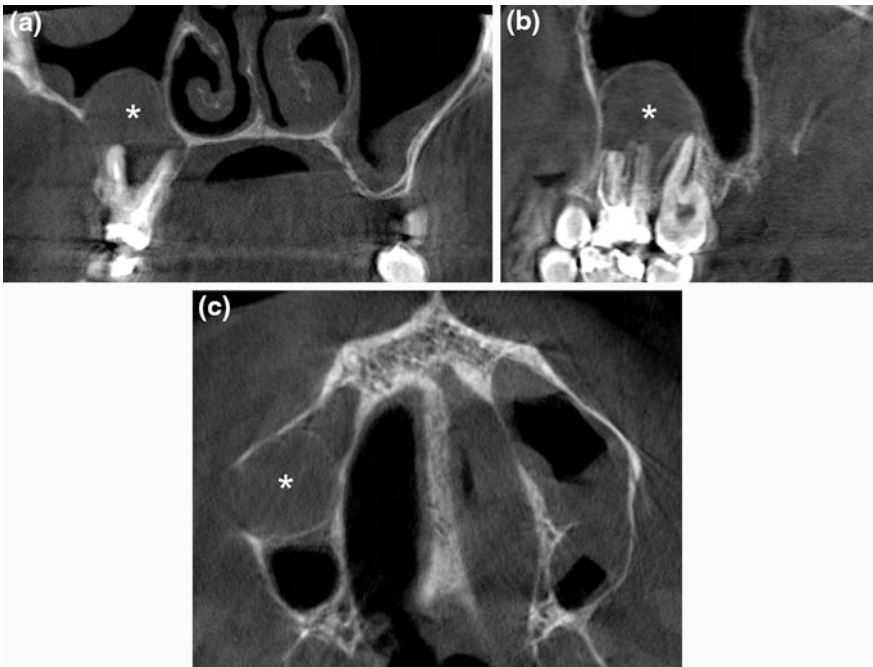
Fig. 6.13 CBCT coronal (**a**), sagittal (**b**) and axial (**c**) sections showing an oval radiopaque with well-defined peripheral borders (*). The pathology involves the apical region of tooth 16 and 17, and protrudes into the adjacent right maxillary sinus. Note the moderate bilateral maxillary sinus mucosal thickening without blockage of both osteomeatal complexes

Case No. 10
- 47-year-old female.
- Clinical notes:
  - Pain on III quadrant mostly during mastication
  - Feeling a bad taste in the mouth
  - Swallowing pus and blood
  - High bleeding index at the periodontal probing and washing her teeth (Fig. 6.14).
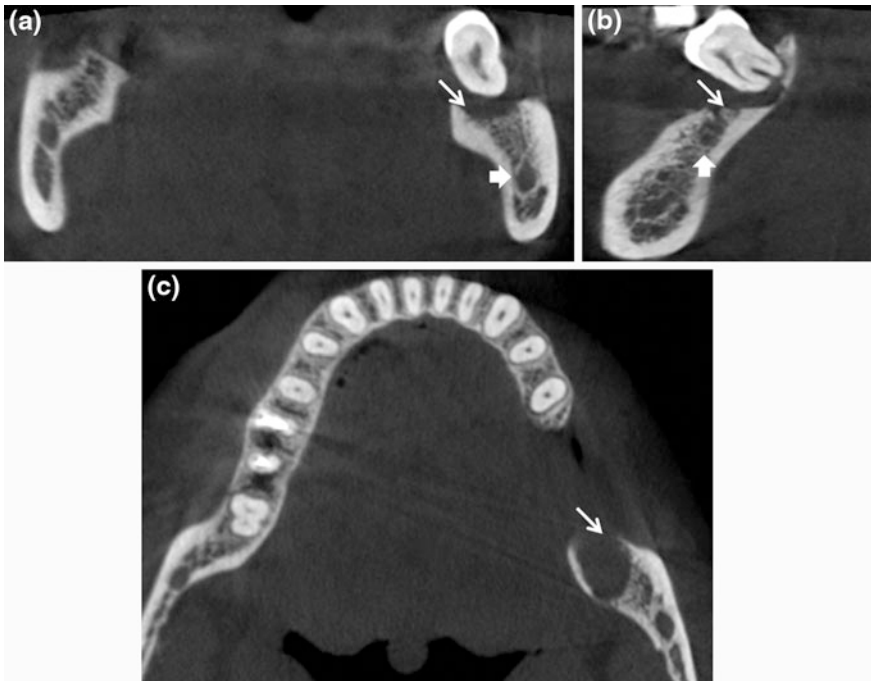
Fig. 6.14 CBCT coronal (**a**), sagittal (**b**) and axial (**c**) sections showing a radiolucent area in close proximity to teeth 38 (*thin arrow*). The mandibular canal (*arrow*) is not involved

6.3   Benign Neoplastic Lesions

Case No. 11
- 41-year-old female.
- Asymptomatic lesion found during a routine orthopantomography (Fig. 6.15).
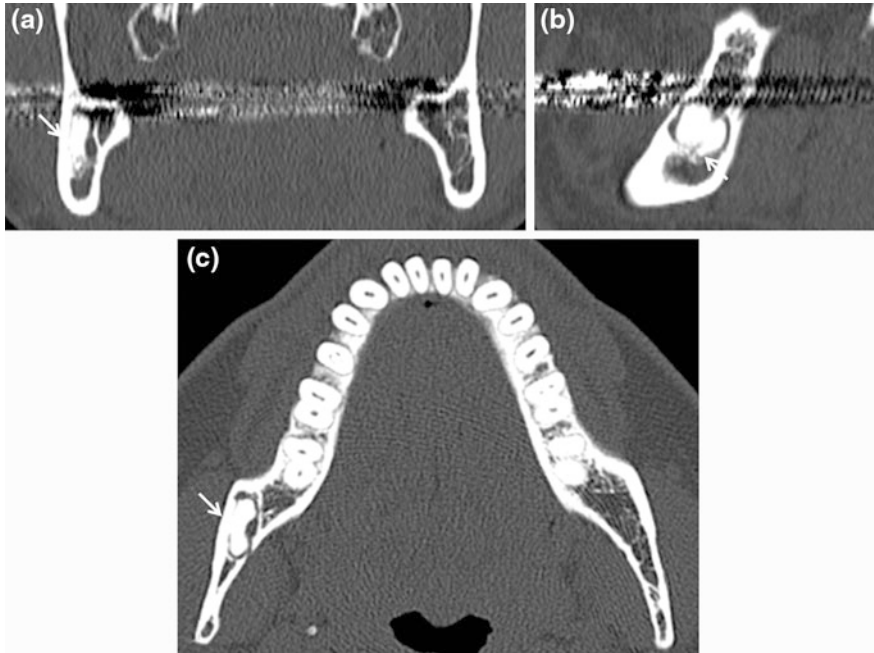
Fig. 6.15   CBCT coronal (**a**), sagittal (**b**) and axial (**c**) sections showing well-defined radiopaque lesion (*thin arrow*) in the posterior branch of the mandible. The lesion is surrounded by radiolucent band and radiopaque cortex giving it a target appearance. There are no signs of root resorption and of invasion of mandibular canal. The radiographic signs suggest a benign process and are consistent with complex odontoma

Case No. 12
- 11-year-old male.
- Asymptomatic lesion found during a routine orthopantomography to evaluate the dental growth (Fig. 6.16).
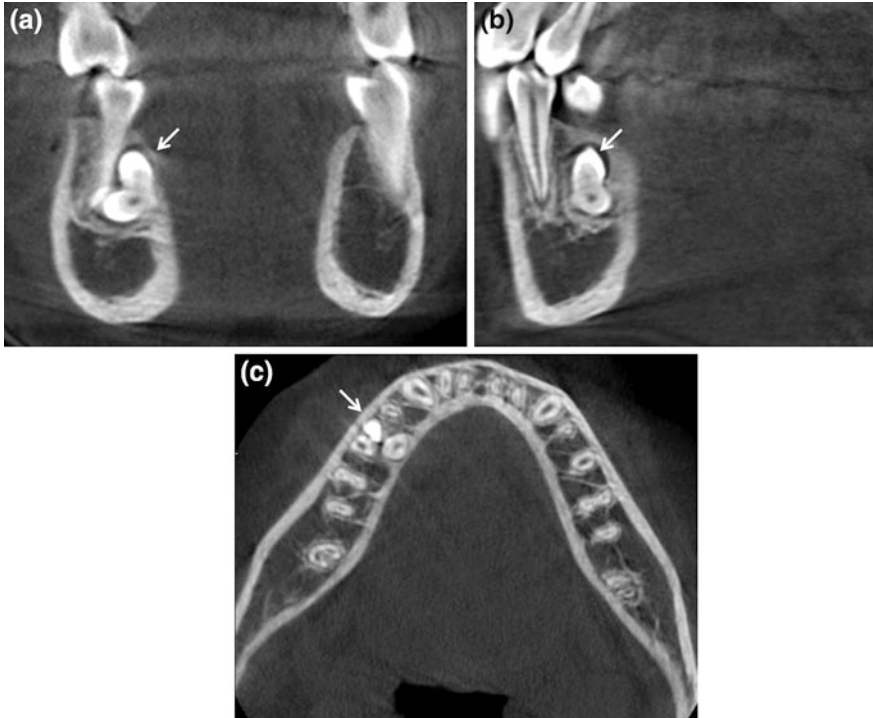
Fig. 6.16 CBCT coronal (**a**), sagittal (**b**) and axial (**c**) sections demonstrating, in correspondence of the lingual plate of the root of 45, a radiopaque masse that has tooth like appearance and density (*thin arrow*). The radiographic signs suggest a benign process and are consistent with compound odontoma

Case No. 13
- 63-year-old female.
- Clinical notes:
  - Typical pulpitis symptomatology on 44
  - The pain is gone after root canal therapy
- Asymptomatic lesion identified during the root canal therapy (Fig. 6.17).
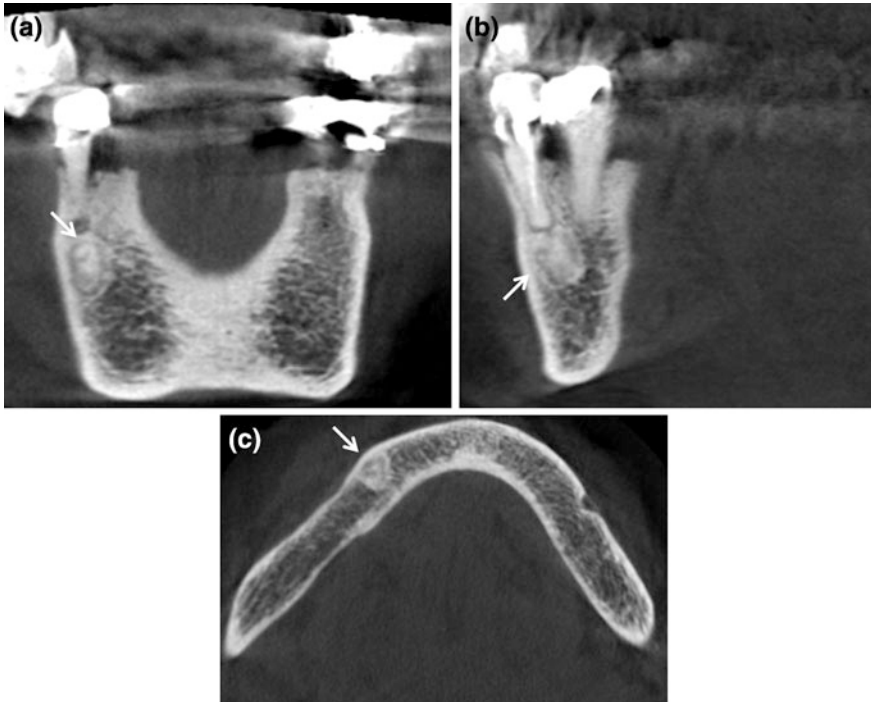
Fig. 6.17 CBCT coronal (**a**), sagittal (**b**) and axial (**c**) sections showing central high-density mass attached to the apex of 44 surrounded by a well-defined low-density area (*thin arrow*). The radiographic signs suggest a benign tumor like a benign cementoblastoma

Case No. 14
- 56-year-old male.
- Asymptomatic lesion found during an ordinary orthopantomography to evaluate the extraction of element 48 (Fig. 6.18).
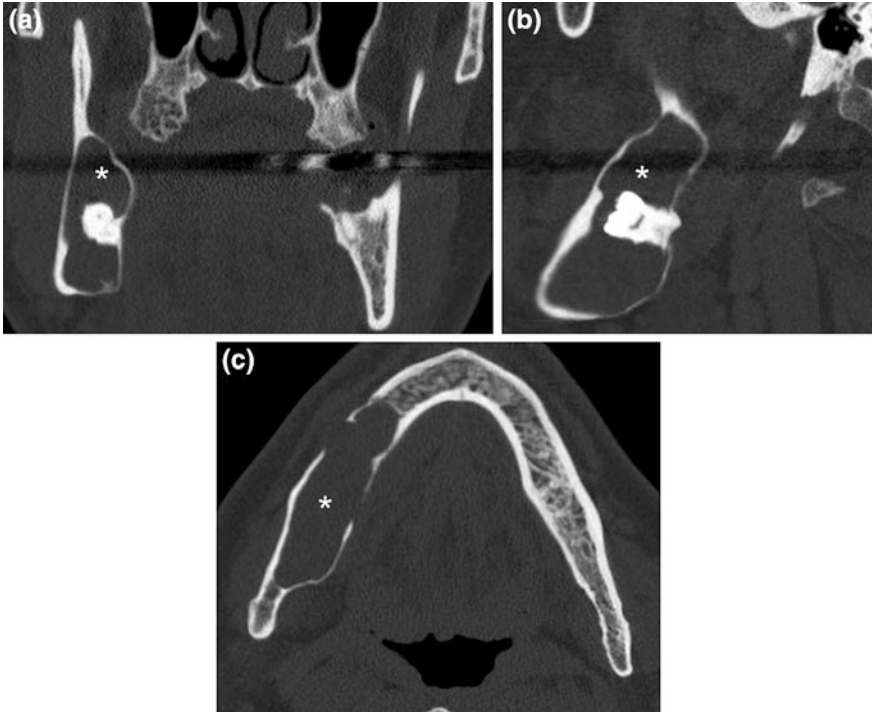
Fig. 6.18 CBCT axial (**a**), sagittal (**b**) and coronal (**c**) sections showing an expansive osteolytic lesion located on the right mandibular body: well-circumscribed multi-loculated radiolucency bounded by a thin rim of cortical bone with smooth or scalloped margins (*). This lesion tends to expand the marked buccal-lingual and vestibular cortical bone. Note the dysodontiasis of 48. The radiographic signs suggest an ameloblastoma

Case No. 15
- 48-year-old female.
- Multiple asymptomatic lesions found during an ordinary orthopanto-mography (Figs. 6.19 and 6.20).

Fig. 6.19 CBCT coronal (**a**), sagittal (**b**) and axial (**c**) sections demonstrating periradicular to 41 a small high density mass surrounded by a low density layer (*thin arrow*). The radiological signs directs to a florid cemento-osseous dysplasia
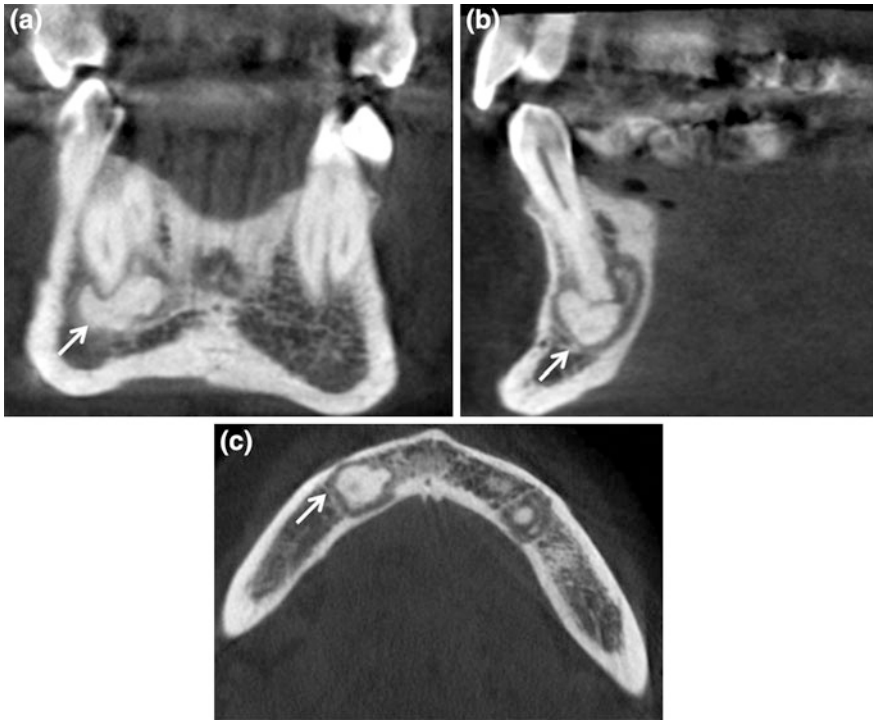
Fig. 6.20 CBCT coronal (**a**), sagittal (**b**) and axial (**c**) sections showing a dense, lobulated radiopaque shadow extending into the mandible near the apex of 44 (*thin arrow*). This high density masse surrounded by a low density layer appears connected with the buccal–lingual and vestibular cortical plates and confirms the diagnosis of multiple cementoma

6.4 Dysodontiasis

Case No. 16
- 12-year-old male.
- Clinical notes:
  – Asymptomatic patient
- CBCT required for the orthodontic study (Figs. 6.21, 6.22, and 6.23).

Fig. 6.21 CBCT panorex: impacted canine 23 in the right upper jaw (*thin arrow*)
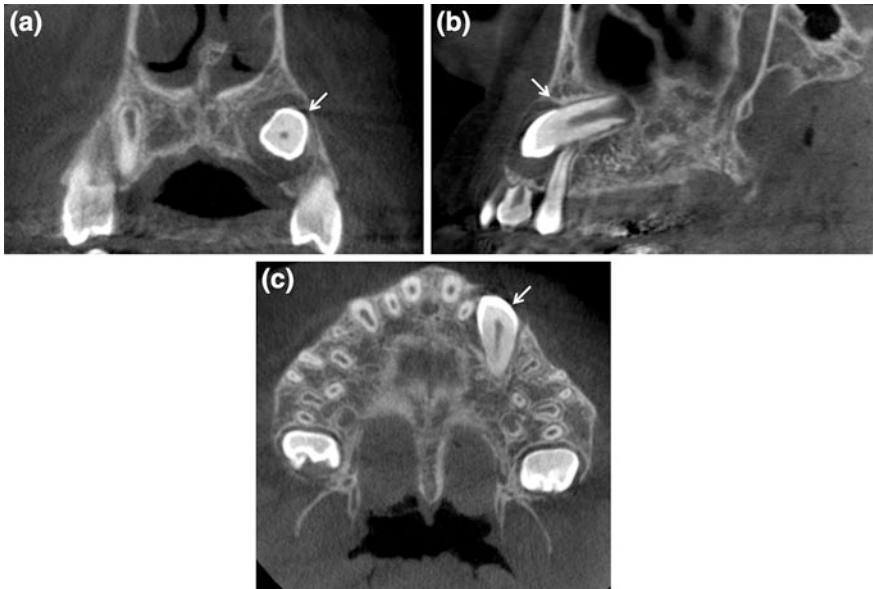
Fig. 6.22 CBCT coronal (**a**), sagittal (**b**) and axial (**c**) sections: the upper left canine is impacted and oriented with the axis of the tooth at a right angle to the dentition (vestibular manifestation) (*thin arrow*)
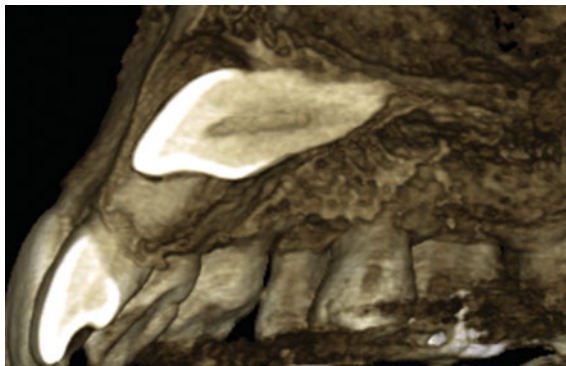
Fig. 6.23 CBCT 3D reconstruction image showing horizontally impacted upper left canine

Case No. 17
• 39-year-old male.
• CBCT required for the orthodontic study (Figs. 6.24 and 6.25).
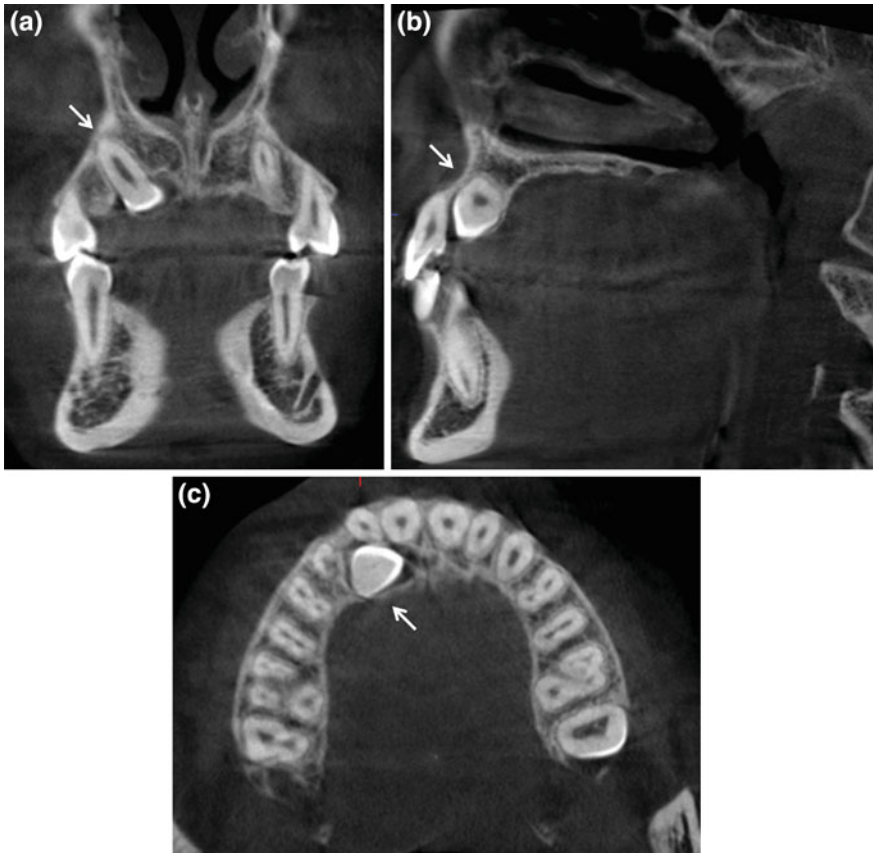
Fig. 6.24 CBCT coronal (**a**), sagittal (**b**) and axial (**c**) scans demonstrating the spatial relationship of upper right canine (*thin arrow*) to the dental arch: the impacted canine moves distal-buccally

Fig. 6.25 CBCT 3D reconstruction of 13 impacted canine

Case No. 18
- 16-year-old male.
- Clinical notes:
  – Asymptomatic patient
- CBCT required for planning orthodontic treatment (Figs. 6.26 and 6.27).
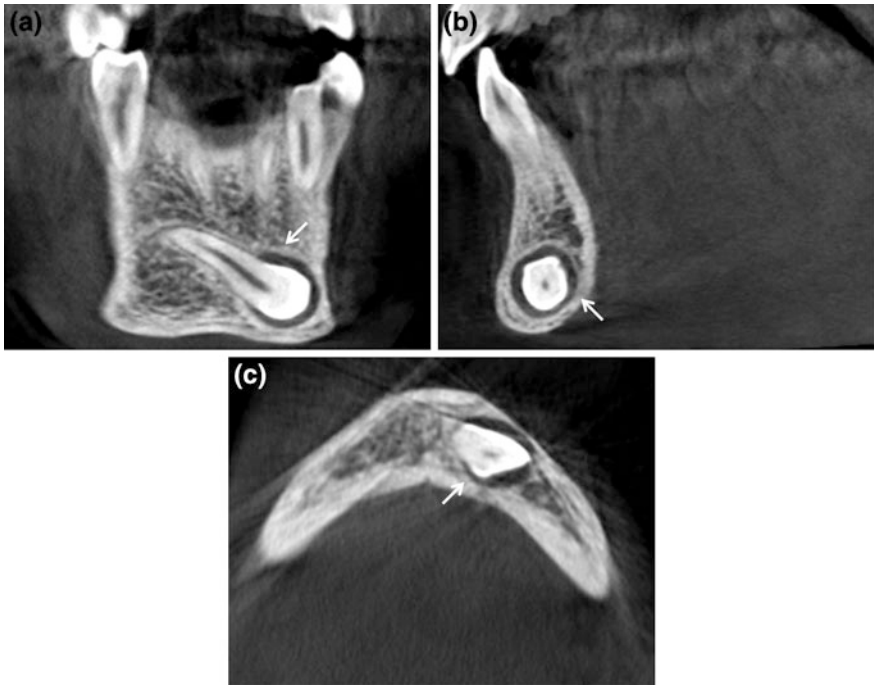
Fig. 6.26 CBCT coronal (**a**), sagittal (**b**) and axial (**c**) sections showing the right maxillary canine mesoangular impaction (*thin arrow*). Note the bone resorption around the impacted tooth

Fig. 6.27 CBCT 3D reconstruction of impacted lower right canine

Case No. 19
- 14-year-old female.
- Clinical notes:
  – Asymptomatic patient (Fig. 6.28 and 6.29).
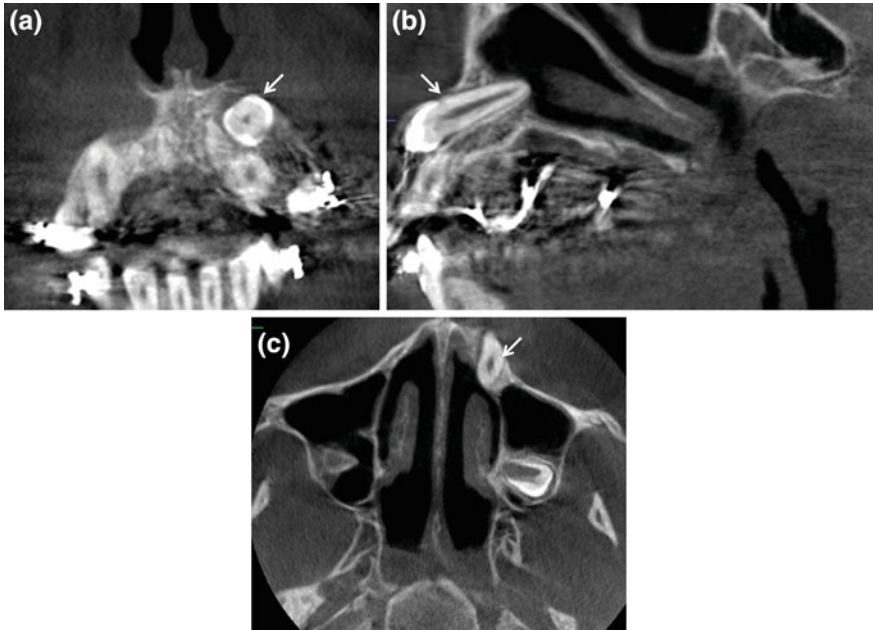
Fig. 6.28 CBCT coronal (**a**), sagittal (**b**) and axial (**c**) scans showing maxillary left canine (*thin arrow*) that is horizontal impacted without sign of root resorption
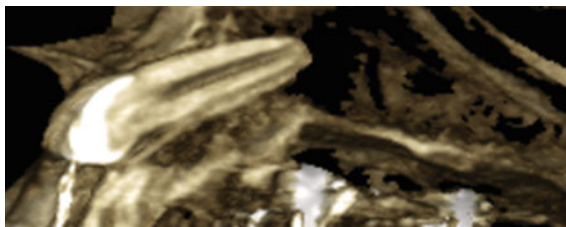
Fig. 6.29 CBCT 3D reconstructions of impacted 23 in vestibular position

Case No. 20

- 24-year-old female.
- CBCT required for orthodontic study (Figs. 6.30 and 6.31).
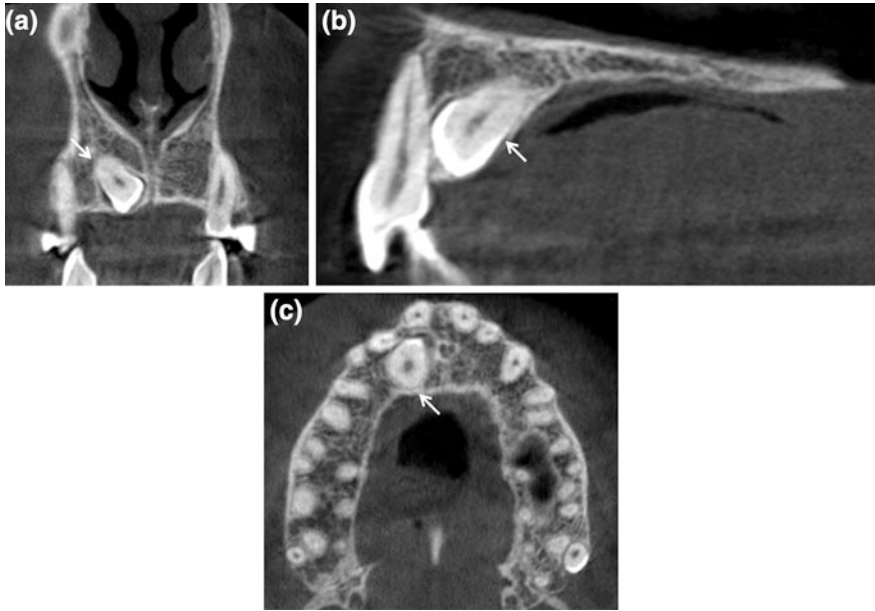
Fig. 6.30 CBCT coronal (**a**), sagittal (**b**) and axial (**c**) sections showing the mesoangular impacted maxillary right canine (*thin arrow*). Note the absence of root or bone resorption
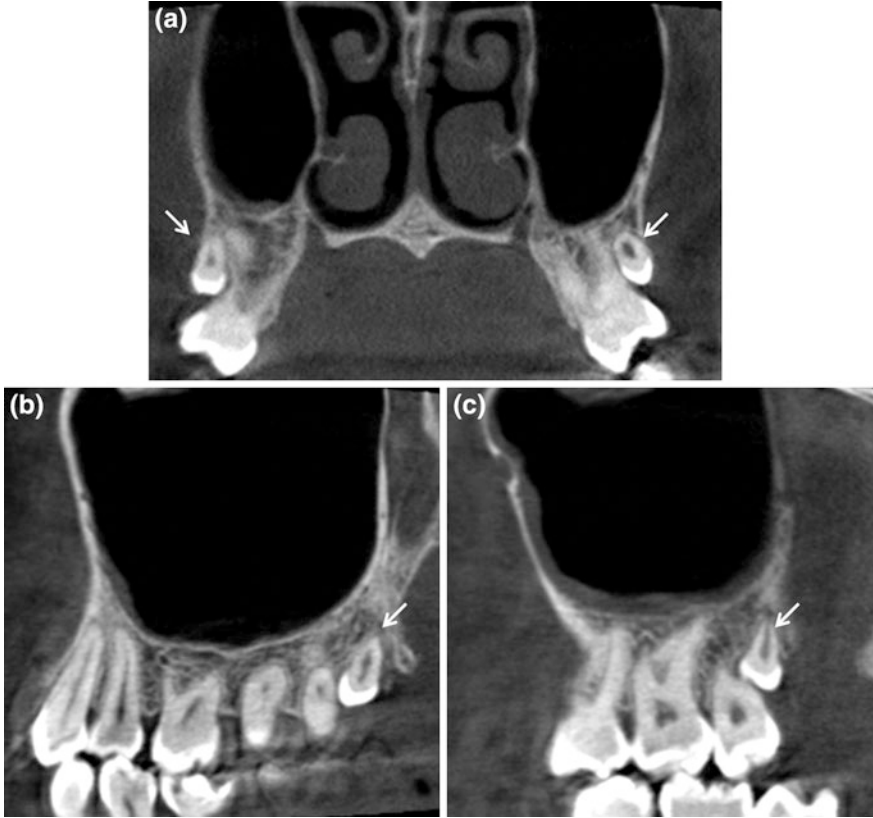
Fig. 6.31 CBCT coronal (**a**), sagittal (**b**) and axial (**c**) sections showing two vertically orientated small supernumerary teeth (*thin arrow*) close to the third upper molars.

Case No. 21
- 47-year-old male.
- CBCT required for planning orthodontic surgery (Figs. 6.32 and 6.33).
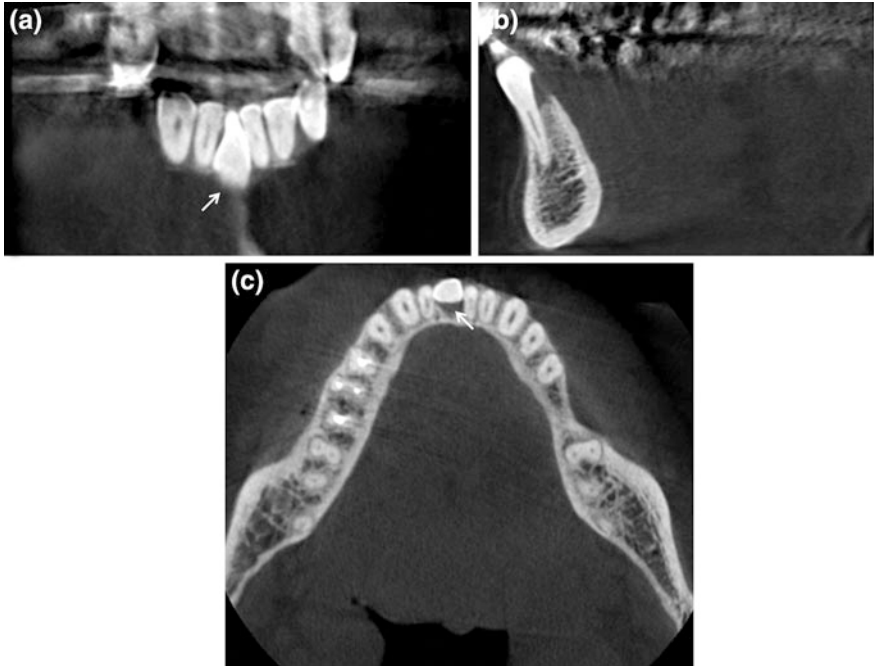
Fig. 6.32 CBCT coronal (**a**), sagittal (**b**) and axial (**c**) scans demonstrating an inverted supernumerary tooth (*thin arrow*) placed between mandibular central incisors

Fig. 6.33 CBCT 3D view of the mesodens
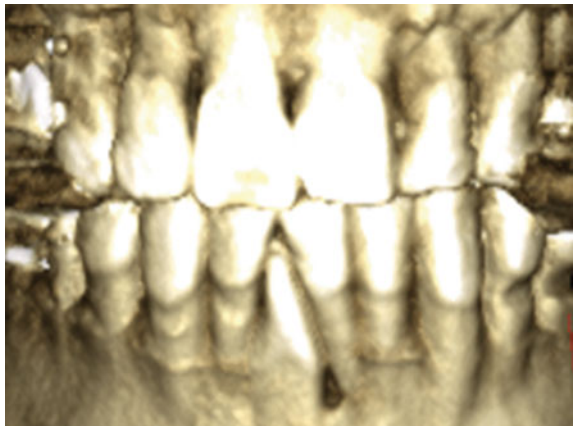
Case No. 22
- 44-year-old female.
- Clinical notes:
  – Recurrent pain as an electrical shock in that area of 38 element
  – Lynphonodal reaction at the base of the neck
- CBCT required for the extraction of element 38 (Figs. 6.34, 6.35 and 6.36).

Fig. 6.34 OPT shows the impaction of 28, 35, 38 (*). Note the conservative restoration 14, 15, 16, 17, 25, 26, 27
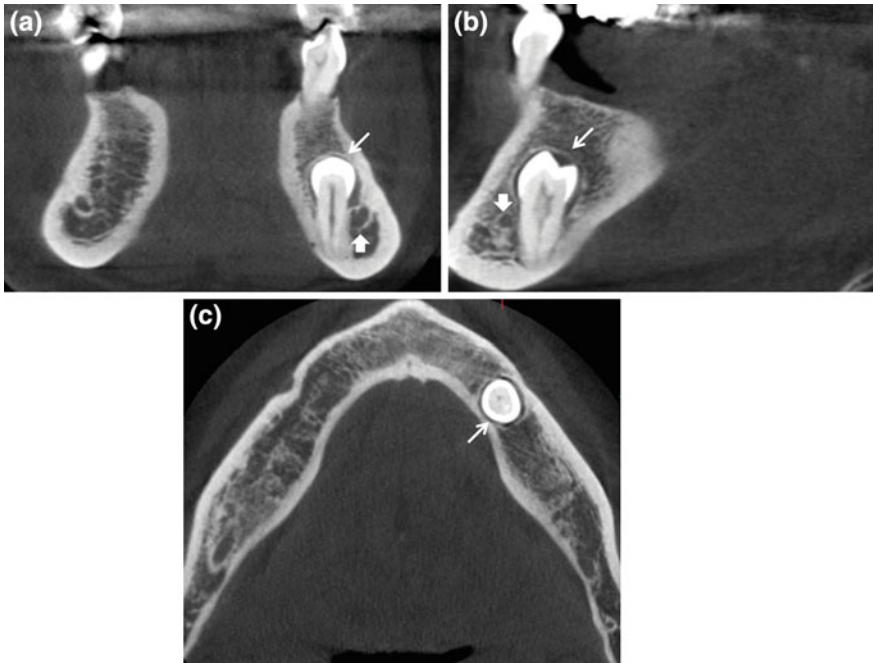
Fig. 6.35 CBCT coronal (**a**), sagittal (**b**) and axial (**c**) sections showing impacted 35 tooth (*thin arrow*). Note the vertical orientation and the thin radiopaque layer around the crown (follicular space). Impacted premolar is placed on the lingual side of the mandibular canal (*arrow*)
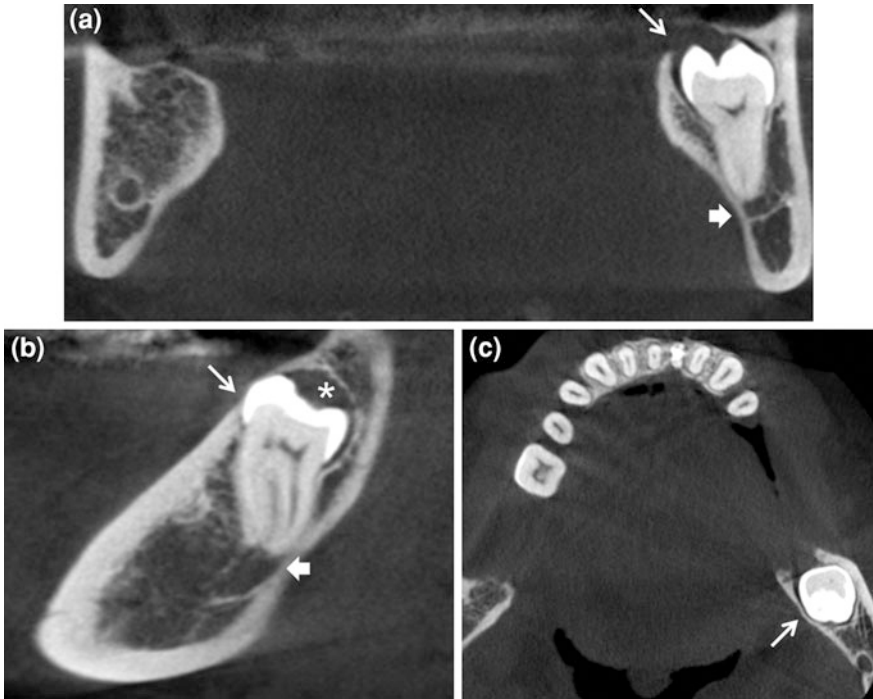
Fig. 6.36 CBCT coronal (**a**), sagittal (**b**) and axial (**c**) scans showing the left mandibular third molar that is vertically impacted (*thin arrow*). Note the mild enlargement of follicular space (*) (radiopaque layer around the crown). Impacted 38 is in relation with the superior wall of the mandibular canal (*arrow*)

6.5   Dental Implantology

Case No. 23
- 66-year-old female.
- Clinical notes:
    - Need to restore chewing function of superior dental arch
    - Pre-implant evaluation (Figs. 6.37, 6.38 and 6.39).
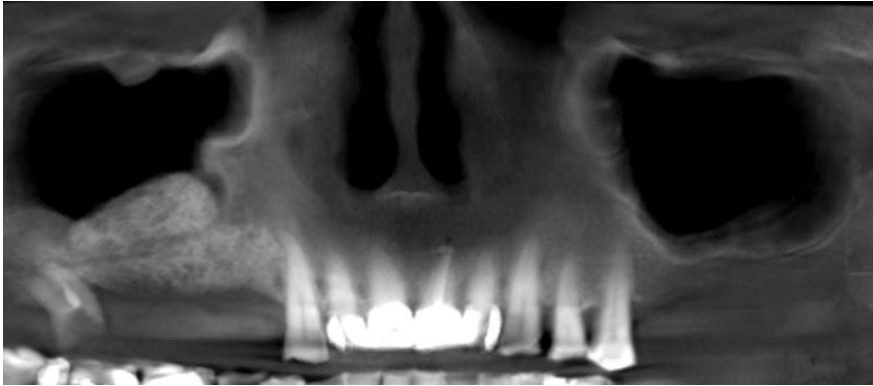
Fig. 6.37 CBCT "panorex" shows the region of interest for dental implant planning
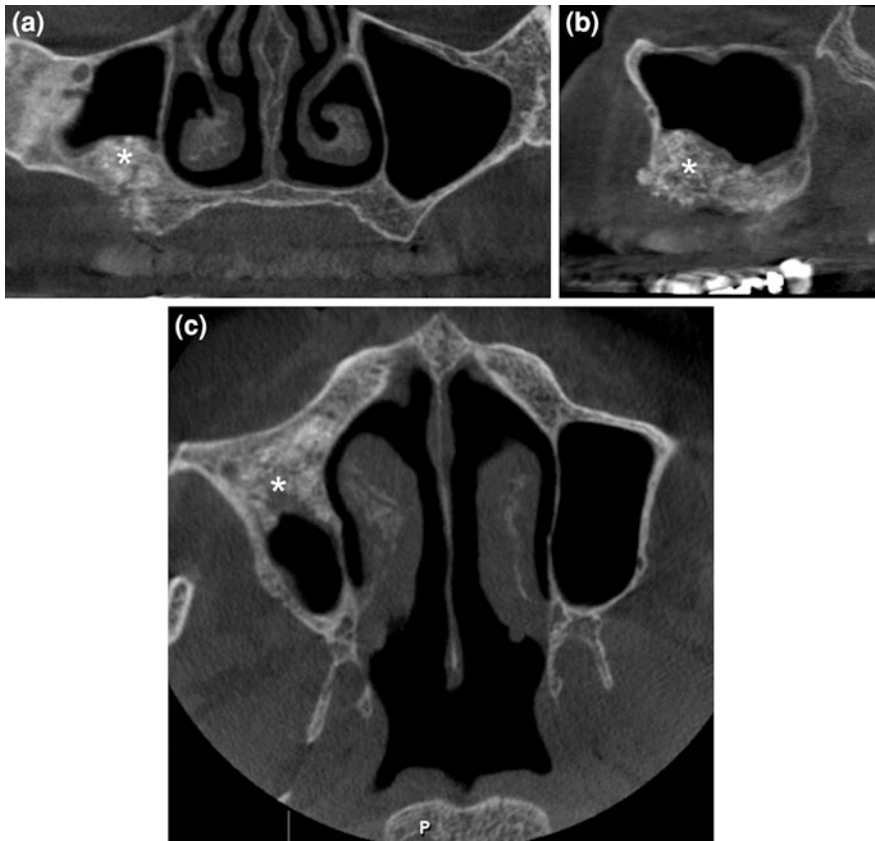
Fig. 6.38 CBCT coronal (**a**), sagittal (**b**) and axial (**c**) scans demonstrating the right sinus lift with bone graft (*) to provide enough bone to place the implant
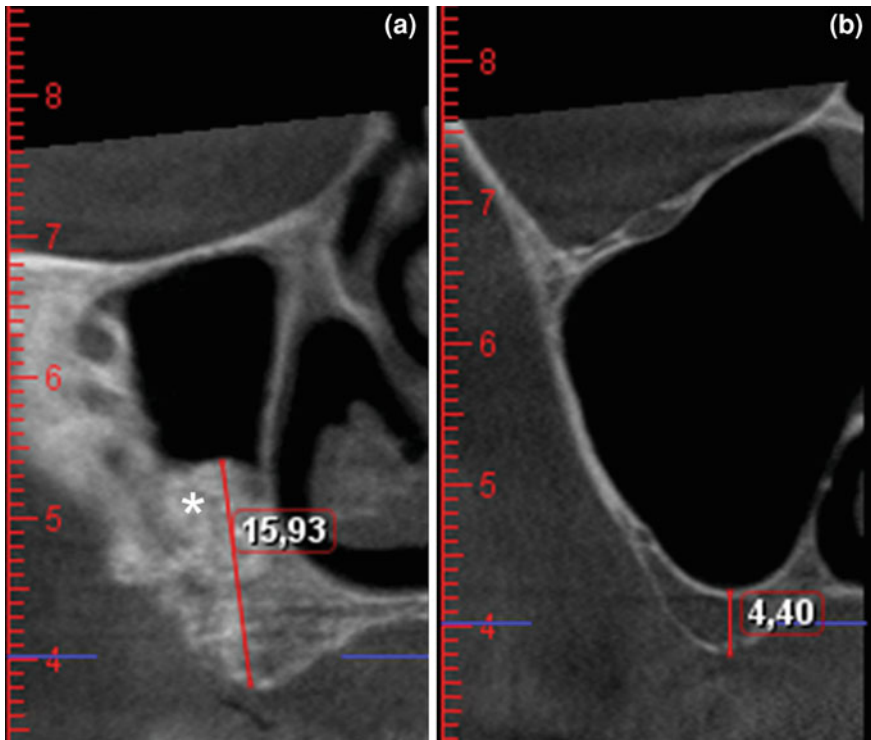
Fig. 6.39 CBCT cross-sections showing measurement of the distance between the floor of the right maxillary sinus and the alveolar crest in the molar region (**b**) and at level of bone graft (*) (**a**)

Case No. 24
- 65-year-old female.
- Clinical notes:
  - Generalised gingivitis
  - Periodontal pocket formation
- CBCT required for pre-implant evaluation (Figs. 6.40, 6.41, 6.42, 6.43 and 6.44).
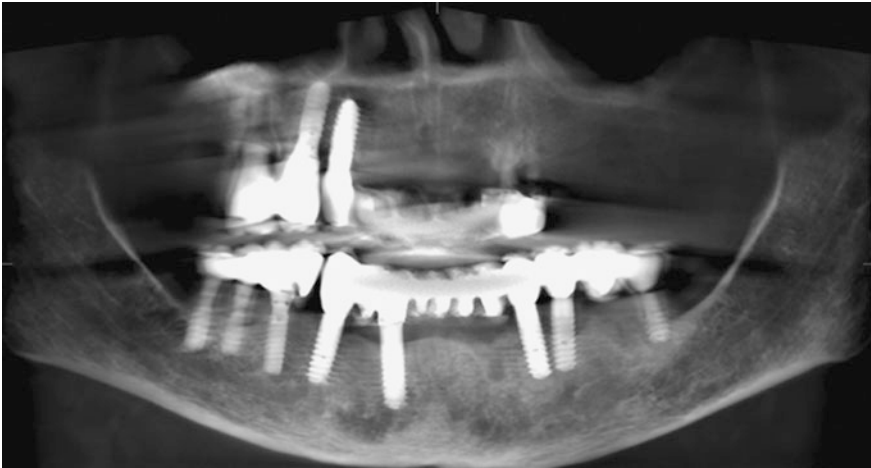
Fig. 6.40 CBCT pre-operative panorex shows the left edentulous maxilla
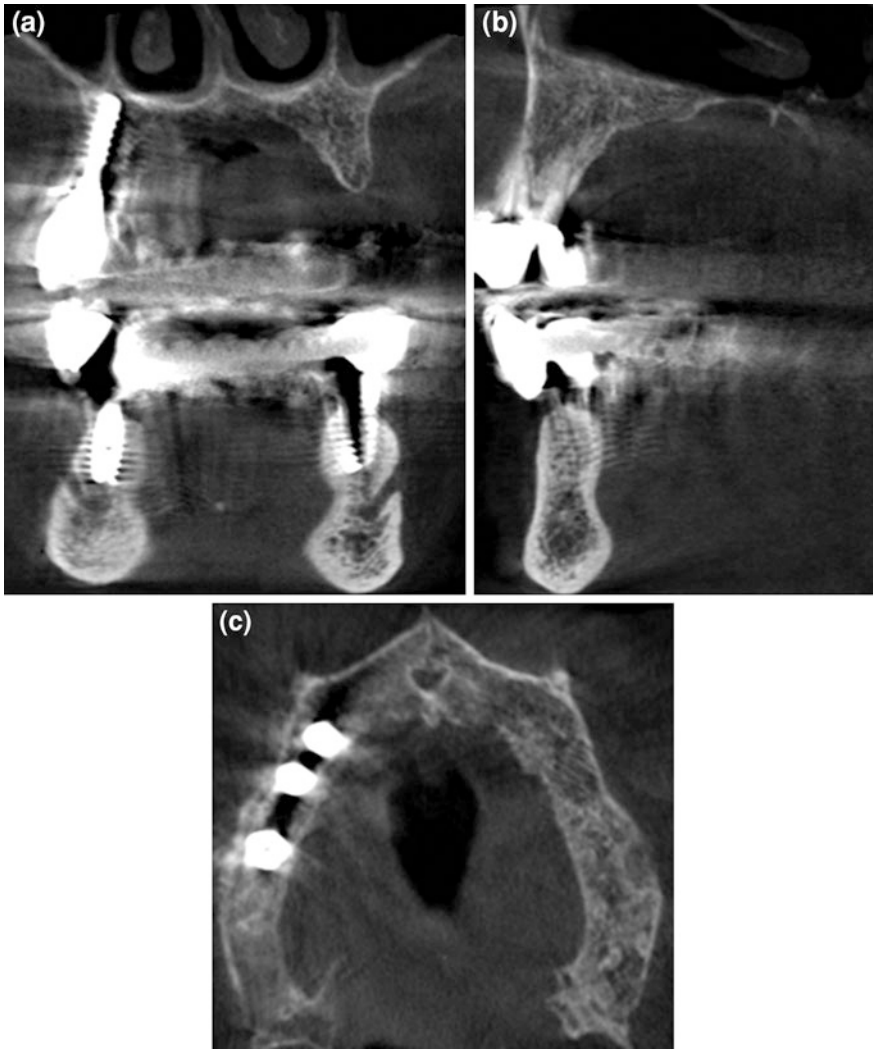
Fig. 6.41 CBCT coronal (**a**), sagittal (**b**) and axial (**c**) scans demonstrating the edentulous left maxillar region

Fig. 6.42 CBCT cross-section shows the distance between the floor of the maxillary sinus and the alveolar crest in the premolar region
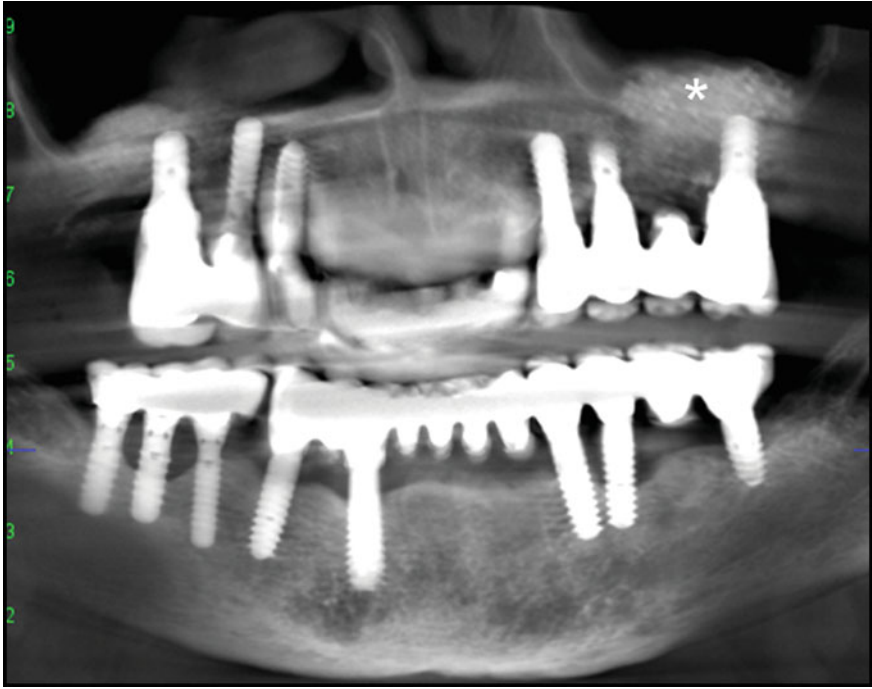
Fig. 6.43 CBCT post-implant panorex shows in the left maxilla three implants surrounded by osseous structure. Note the bone graft and the left sinus lift (*)
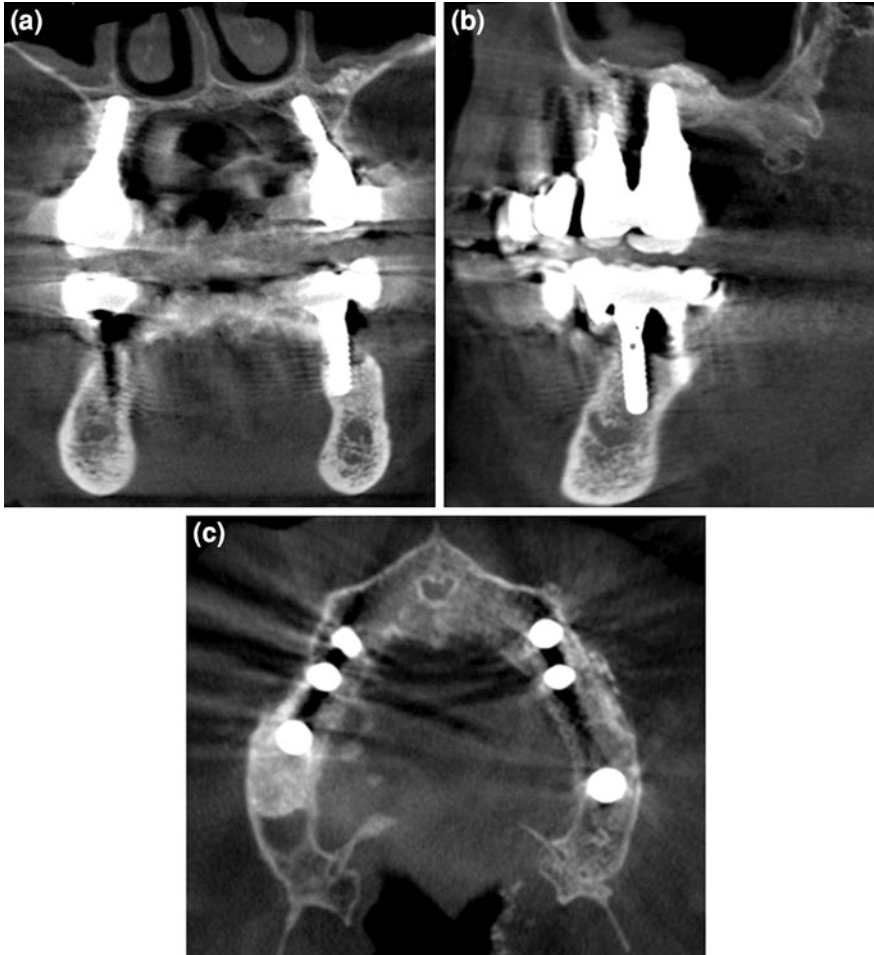
Fig. 6.44 CBCT coronal (**a**), sagittal (**b**) and axial (**c**) sections showing the post-operative maxillar region

Case No. 25
- 70-year-old female.
- Clinical notes:
  – Periodontal patient
- CBCT required for pre-implant evaluation (Figs. 6.45, 6.46 and 6.47).

Fig. 6.45 CBCT panorex: pre-operative panoramic image of edentulous maxilla and right branch of mandibular
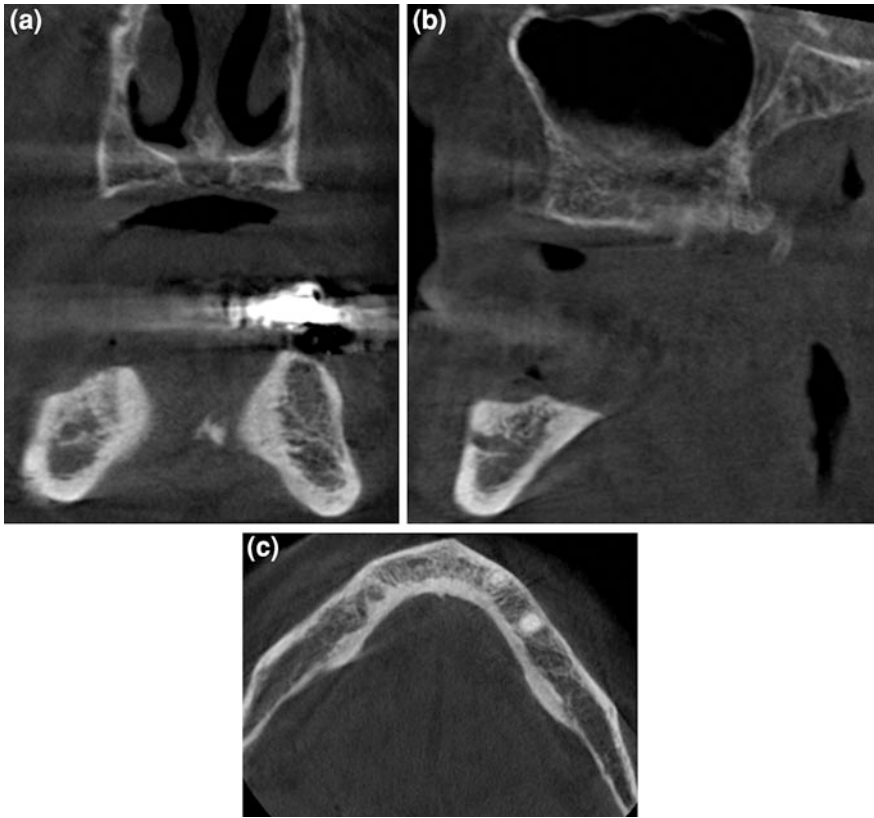
Fig. 6.46   CBCT coronal (**a**), sagittal (**b**) and axial (**c**) sections in the area of missing mandibular teeth for planning implant
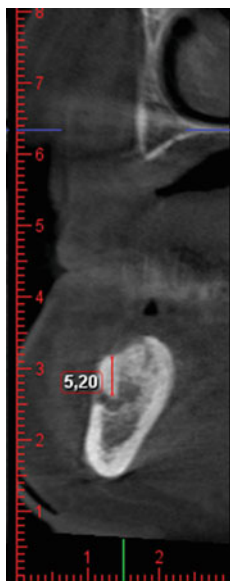
Fig. 6.47 CBCT cross-section showing the measurement from the roof of the mandibular canal to the alveolar crest

Case No. 26
- 60-year-old male.
- Clinical notes:
  – Continuous pain after implant surgery on II quadrant
  – The fixture has broken the vestibular cortical of the maxilla in II quadrant
- CBCT required for post-implant evaluation (Figs. 6.48, 6.49 and 6.50).
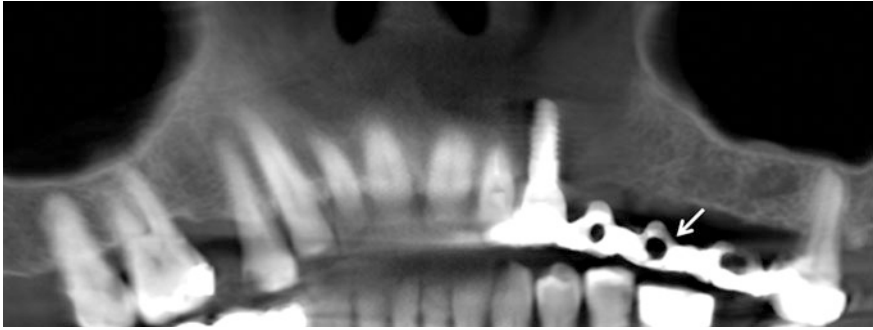
Fig. 6.48 CBCT panorex: note the implant screw in left maxilla with a fixed bridge (*thin arrow*)
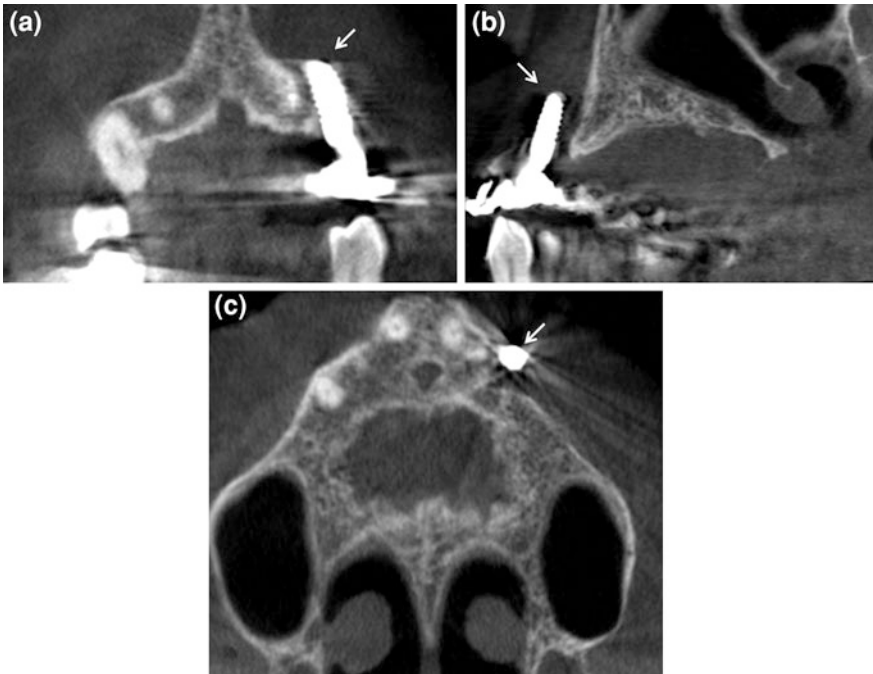
Fig. 6.49 CBCT coronal (**a**), sagittal (**b**) and axial (**c**) scans showing clearly the implant screw (*thin arrow*) has lost the relationship with the alveolar bone and moves to vestibular side
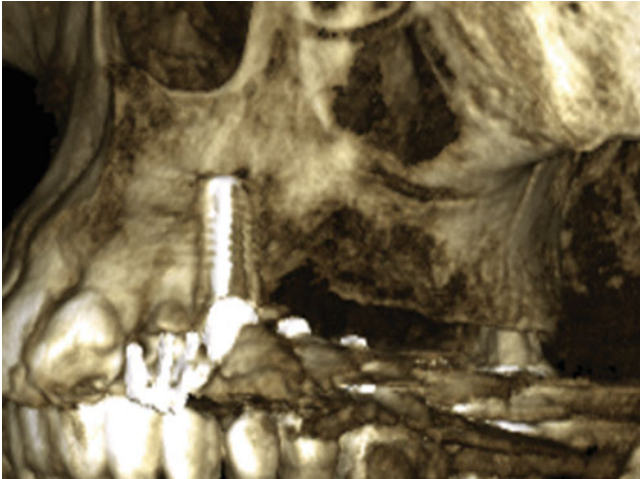
Fig. 6.50 CBCT 3D reconstruction of left maxillar implant

6.6   Miscellaneous Dental Diseases

Case No. 27
- 63-year-old female.
- Clinical notes:
  - Discomfort from TMJ
  - Clicking sounds in the jaw joint when opening or closing the mouth (Fig. 6.51).
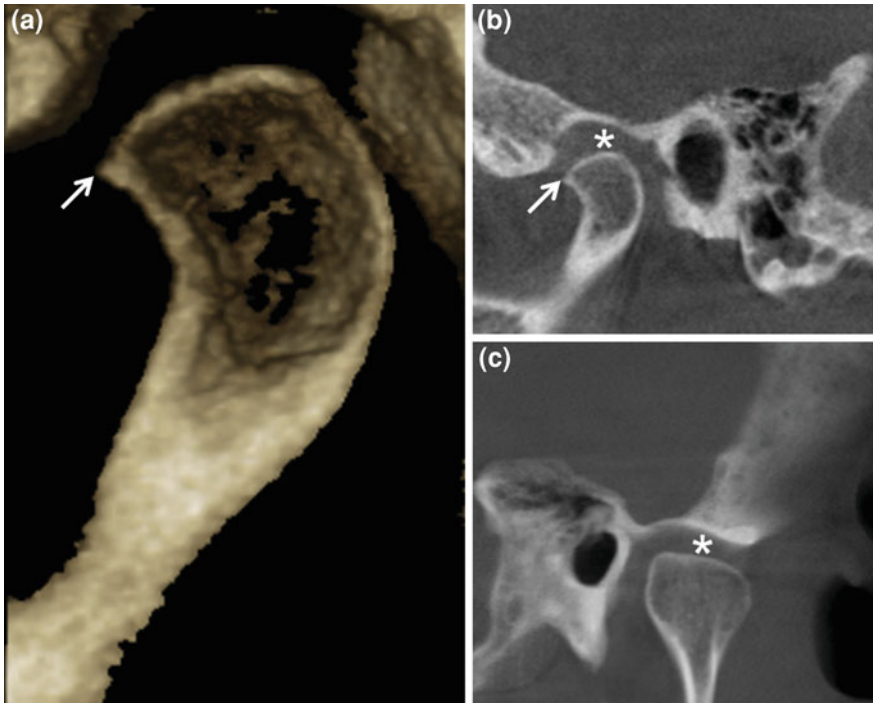
Fig. 6.51 CBCT sagittal (**b**) and coronal (**c**) scans and 3D reconstruction (**a**) of left condylar head. The joint space (*) is not reduced, but we can note a small degenerative ostheophyte (*thin arrow*) on the anterior surface of the condylar head

Case No. 28
- 13-year-female.
- Clinical notes:
  - Facial asymmetry (Figs. 6.52 and 6.53).
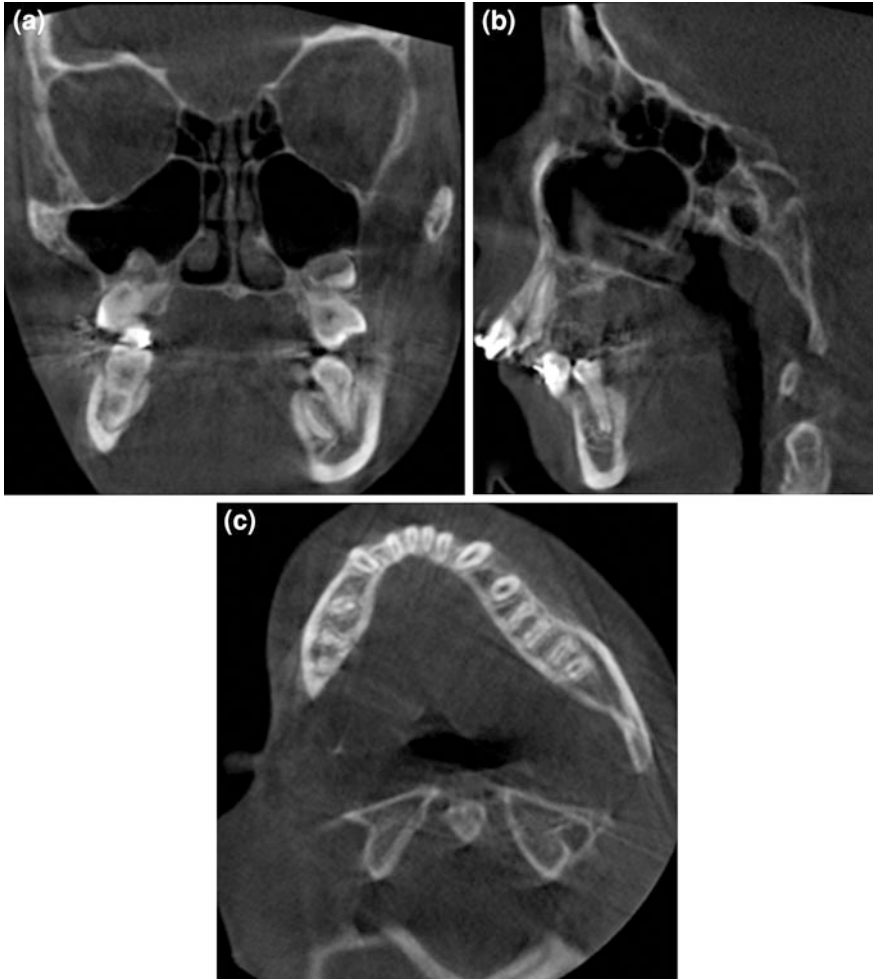
Fig. 6.52 CBCT coronal (**a**), sagittal (**b**) and axial (**c**) sections showing a significant asymmetry caused by a right hemifacial microsomia
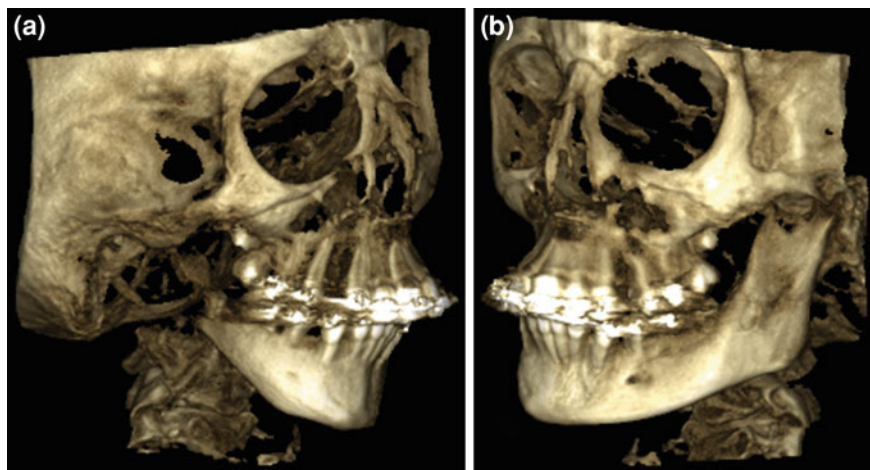
Fig. 6.53 CBCT 3D reconstruction of right (**a**) and left (**b**) hemifacial shows the evident mandibular asymmetry

Case No. 29
- 47-year-old female.
- Clinical notes:
  - Pain and mobility in the region of right mandibular incisor after a dental trauma (Fig. 6.54).
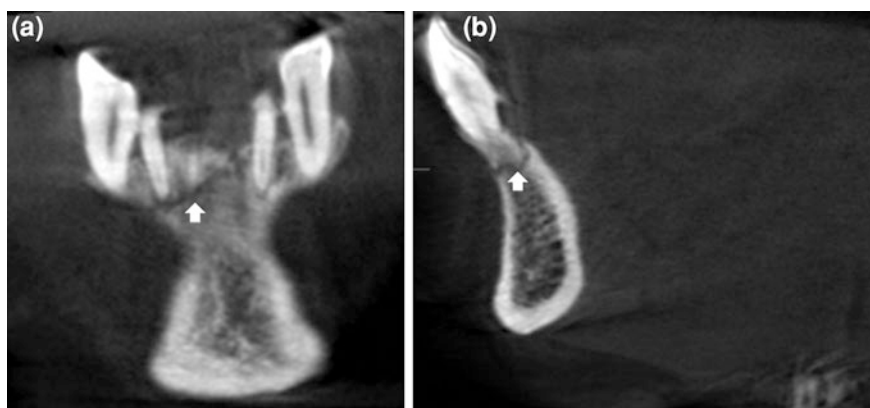
Fig. 6.54 CBCT coronal (**a**) and sagittal (**b**) scans demonstrating an oblique radiopaque fracture line (*arrow*) in the alveolar bone from 43 to 41. Note the area of low density periapical to right mandibular canine

Case No. 30
- 57-year-old male.
- Clinical notes:
  - Dental trauma
- CBCT required to evaluate the fracture of left maxillary incisor and to plan the treatment (Fig. 6.55).
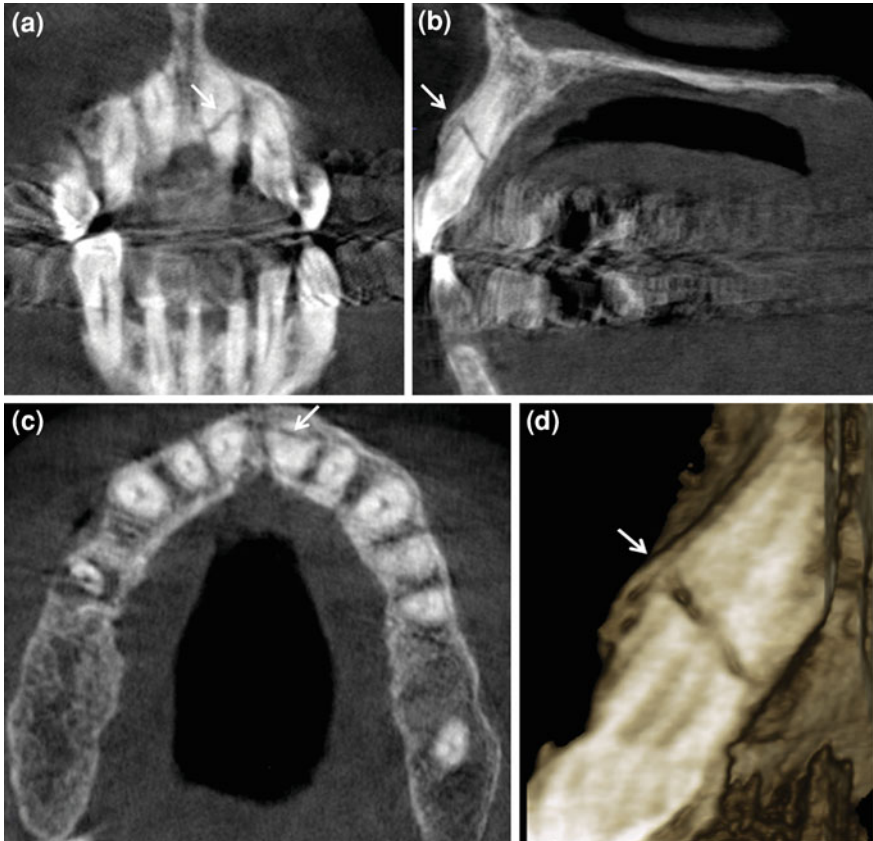
Fig. 6.55 CBCT coronal (**a**), sagittal (**b**) and axial (**c**) scans showing a horizontal fracture (*thin arrow*) in middle third of root of left maxillary central incisor. Note the 3D model of left central incisor (**d**)

Case No. 31
- 53-year-old male.
- Clinical notes:
  - Swelling in the anterior region of palate for the past 6 months
  - No detectable extraorally abnormality or lymphadenopathy (Fig. 6.56).
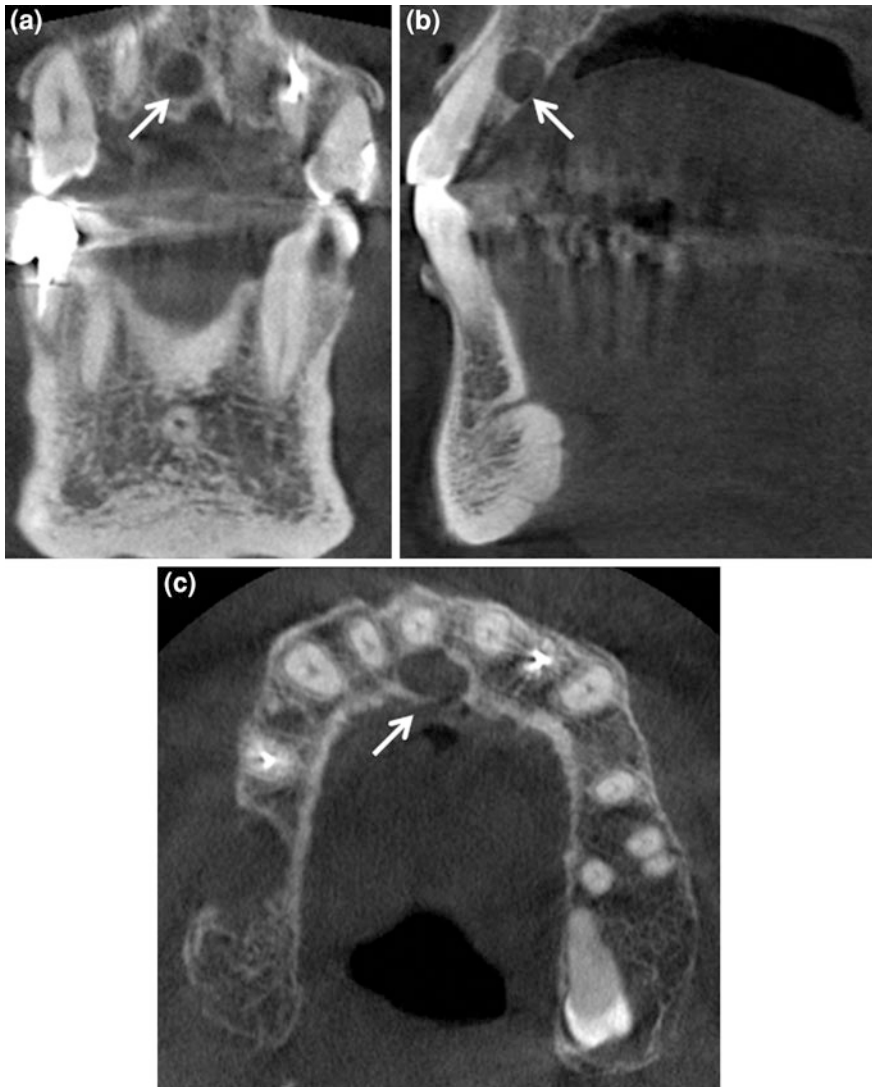
Fig. 6.56 CBCT coronal (**a**), sagittal (**b**) and axial (**c**) scans showing in the posterior maxilla a well-defined ovoid radiolucent area with discontinuity of the palatal cortical plates (*thin arrow*). It is a nasopalatine duct cyst

Case No. 32
- 57-year-old female.
- Clinical notes:
  - Treated with bisphosphonates for bone metastases from breast cancer
  - Pain, feeling of heaviness in the jaw
  - Loosening of teeth
  - Small initial exposed bone in the mandibular region (Figs. 6.57, 6.58, 6.59 and 6.60).
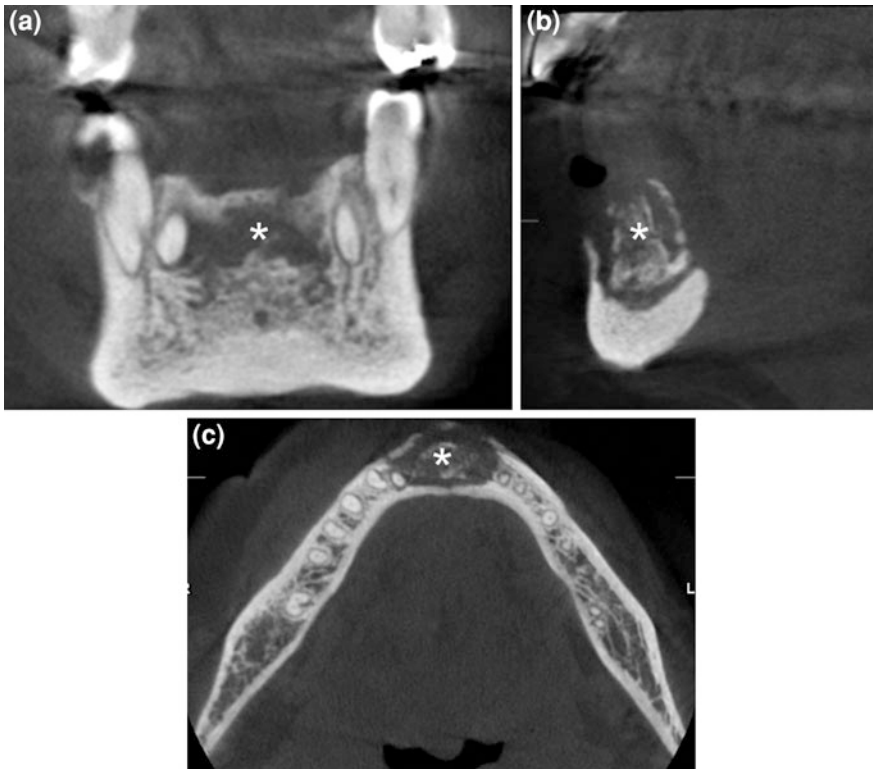
Fig. 6.57 CBCT coronal (**a**), sagittal (**b**) and axial (**c**) scans showing mandibular bone defect due to bisphosphonate-related osteonecrosis that appears like a radiolucent lesion with sclerotic margin (*)

Fig. 6.58 CBCT 3D
reconstruction of the bone
defect
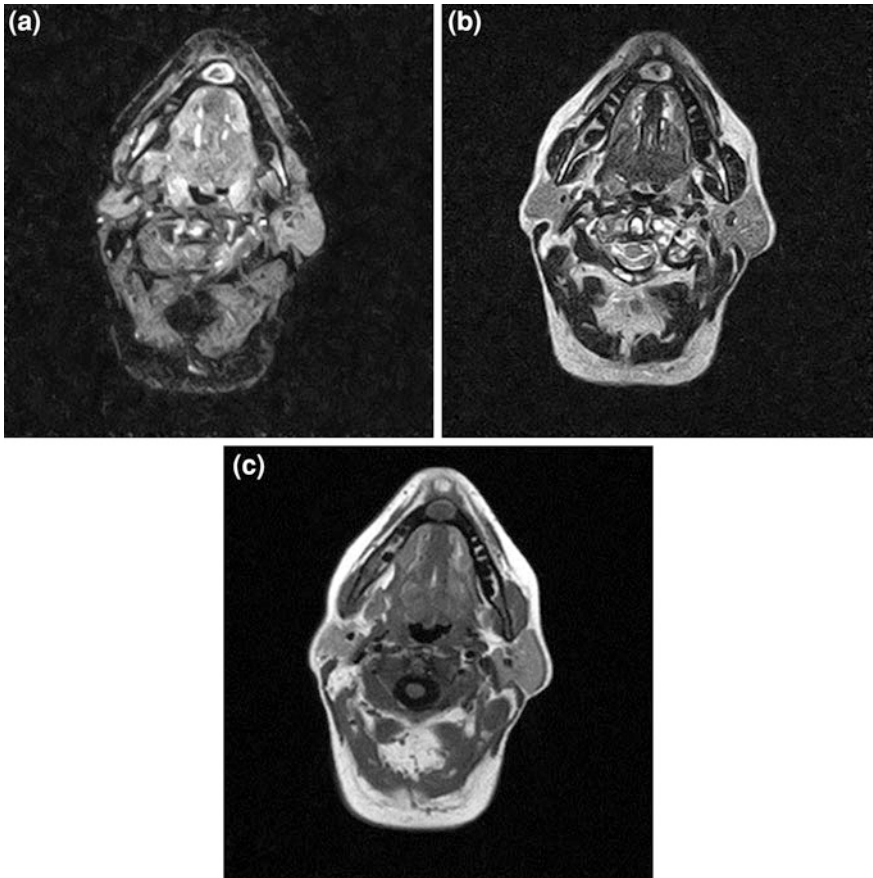
Fig. 6.59 MRI axial STIR (**a**) T2 (**b**) and T1 (**c**) weighted images demonstrating typical behavior of bisphosphonate osteonecrosis of mandibular bone (*thin arrow*)
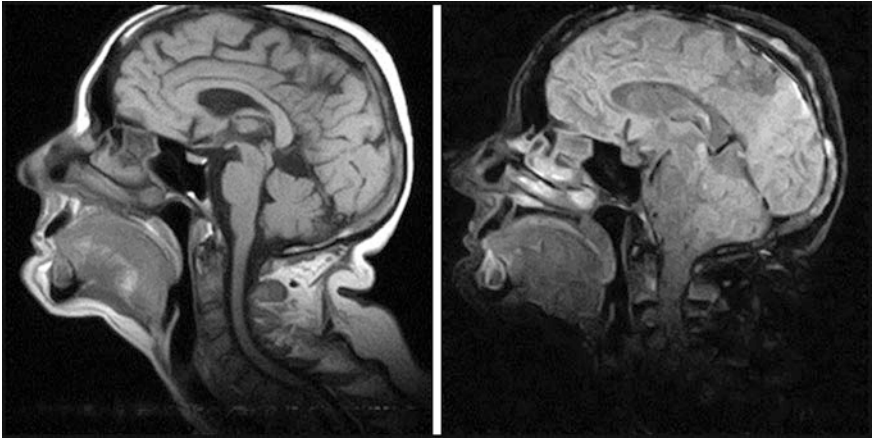
Fig. 6.60   MRI sagittal T1 and STIR weighted images showing focal lesion of osteonecrosis affecting mandibular branch (*thin arrow*)

Index